August 2022

Doctoral Thesis

Studies on the role of N^6-adenosine methyltransferase METTL3 as a critical regulator of tumorigenesis and targeted drug resistance

Chosun University Graduate School

Department of Pharmacy

Poshan Yugal Bhattarai

종양형성과 표적항암제 내성의 핵심 조절 인자로서 N^6-아데노신 메틸전이효소 METTL3 의 역할에 관한 연구

Studies on the role of N^6-adenosine methyltransferase METTL3 as a critical regulator of tumorigenesis and targeted drug resistance

2022 년 8 월 26 일

조선대학교 대학원

약 학 과

포산 유갈 밧타라이

Studies on the role of N^6-adenosine methyltransferase METTL3 as a critical regulator of tumorigenesis and targeted drug resistance

지도교수 최 홍 석

이 논문을 약학 박사학위신청 논문으로 제출함

2022 년 4 월

조선대학교 대학원

약 학 과

포산 유갈 밧타라이

포산 유갈 밧타라이의 박사학위 논문을 인준함

위원장	서울대학교	교수	강 건 욱 (인)
위 원	서울대학교	교수	오 원 근 (인)
위 원	조선대학교	교수	기 성 환 (인)
위 원	조선대학교	교수	이 금 화 (인)
위 원	조선대학교	교수	최 홍 석 (인)

2022 년 6 월

조선대학교 대학원

Contents

List of Figures

List of Abbreviations

M^6A	N^6-methyl adenosine
METTL3	Methyltransferase like -3
METTL14	Methyltransferase like -14
WTAP	Wilms tumor 1-associating protein
FTO	Fat mass and obesity-associated protein
PIN1	Peptidyl-prolyl cis-trans isomerase NIMA-interacting 1
TAZ	Transcriptional coactivator with PDZ-binding motif
EGFR	Epidermal growth factor receptor
MEK	MER/ERK Kinase
ERK	Extracellular signal-regulated kinase
MAPK	Mitogen activated protein kinase
GST	Glutathione S -transferase
Ni-NTA	Nickel Nitriloacetic acid
IP	Immunoprecipitation
meRIP	Methylated RNA immunoprecipitation
RT-PCR	Reverse transcriptase polymerase chain reaction
DMEM	Dulbecco's modified Eagle's Medium
RPMI	Roswell Park Memorial Institute Medium
PBS	Phosphate-buffered saline
SDS-PAGE	Sodium dodecyl sulfate-polyacrylamide gel electrophoresis
PVDF	Polyvinylidene difluoride

RIPA	Radioimmunoprecipitation assay buffer
SDS-PAGE	Sodium dodecyl sulfate-polyacrylamide gel electrophoresis
Ub	Ubiquitin
CHQ	chloroquine
CHX	Cycloheximide
DMSO	Dimethyl sulfoxide
Fluc	Firefly luciferase
Rluc	Renilla luciferase

국문 초록

종양 형성과 표적항암제 내성의 핵심 조절 인자로서 N^6-아데노신 메틸 전이 효소 METTL3 의 역할에 관한 연구

포산 유갈 밧타라이

지도교수: 최홍석

조선대학교 대학원약학과

포유동물 세포에서 methyltransferase-like 3(METTL3)는 mRNA 의 N6-메틸아데노신(m^6A) 수식을 담당하는 N^6-아데노신 메틸트랜스퍼라제 복합체의 catalytic subunit 이다. METTL3 는 여러 암에서 과발현 된다고 알려졌지만, 그 발현을 조절하는 분자생물학적 작용기전은 아직까지 알려지지 않았다. 본 연구는 METTL3 단백질 안정성과 mRNA 의 m^6A 수식의 조절과정에서 peptidyl prolyl cis-trans isomerase-interacting-1(PIN1)의 주요 역할을 규명하였다. PIN1 은 인산화 의존적 방식으로 METTL3 과 결합하여, 유비퀴틴 의존적으로 proteasome 또는 리소좀에 의한 단백질 분해작용을 억제하였다. PIN1 에 의하여 안정화된 METTL3 은 TAZ 및 EGFR mRNA 의 m^6A 수식을 증가시켜 단백질 번역의 효율성을 촉진하였다. PIN1 의 knockout 은 polysome 분획에서 TAZ 및 EGFR mRNA 을 감소시켰다. 또한 MEK1/2 과 PIN1 을 동시에 억제하였을 때 METTL3 단백질의 안정성을 감소시켰고, TAZ 와 EGFR 의 m^6A 의존적 단백질 번역이 감소되었으며, 그 결과 유방암 세포 성장이 억제되고 G0/G1 단계에서 세포 주기가 정지 되었다. PIN1 이 과발현된 MCF7 세포에 METTL3 을 knockout

시켰을 때, PIN1에 의해 증가된 콜로니 형성이 감소되었다. 동종이식 마우스 실험에서는 PIN1이 과발현 된 4T1 세포에서 증가된 종양이 METTL3 knockout에 의해 억제되었다. 임상적으로 PIN1 및 METTL3 발현은 유방암 조직에서 유의성 있게 증가하였으며, METTL3 발현은 유방암 형성의 단계 의존적으로 증가함과 동시에 PIN1 발현과도 유의성있는 양성 상관관계가 있었다. 종합적으로, 본 연구는 mRNA 번역과정에서 PIN1 의 새로운 역할을 규명하고, 나아가 PIN1/METTL3 신호전달과정이 유방암의 새로운 치료 표적이 될 수 있음을 시사한다.

악성흑색종 환자에서 후천적 내성획득은 BFAF(V600E) 키나제 억제제 PLX4032의 치료 효능을 감소시킨다. 최근 m^6A 수식에 의한 mRNA의 후전사적 변형은 악성흑색종 발병의 주요 원인으로 보고 되었다. 하지만 악성흑색종의 PLX4032 저항성 획득 기전에서 mRNA의 m^6A 수식과의 상관성을 아직 밝혀지지 않았다. 본 연구에서 A375 흑색종 세포와 비교하여 PLX4032 내성을 획득한 A375R 세포에서 METTL3 발현이 증가되었음을 규명하였다. 또한, METTL3 은 A375R 세포에서 EGFR mRNA의 m^6A 변형을 증가시켜 단백질 번역의 효율성을 촉진하였다. 나아가 EGFR 발현 증가는 RAF/MEK/ERK 경로의 리바운드 활성화를 촉진하여 A375R 세포에서 PLX4032 내성을 유도하였다. 하지만, A375R 세포에서 METTL3 knockout은 EGFR 단백질 발현을 감소시킴과 동시에 PLX4032에 대한 감수성을 회복시켰다. A375R 세포에서 METTL3 knockout 시킨 후 PLX4032 처리하였을 때 세포사멸을 유도하였고 콜로니 형성을 감소시켰으며, 또한 BALB/c nude 마우스에서 A375R 세포의 종양 성장을 감소시켰다. 종합적으로 악성흑색종 세포에서 METTL3 은 EGFR mRNA 의 m^6A 수식조절을 통한 단백질 발현의 증가와 이를 통한 RAF/MEK/ERK 신호전달의 리바운드 활성화를 유도하였으며, 그 결과 PLX4032 내성을 유도하였음을 알 수 있다. 이러한 결과는 METTL3에 의한 mRNA의 m^6A 수식이 발암과정과 항암제 내성의 주요 기전이고, 나아가 METTL3은 표적항암제의 중요한 후보 인자임을 제시한다.

I. Introduction

1. Epitranscriptomics: Introduction of m^6A modification

The ribonucleotides present in RNA molecules contain a diverse range of chemical modifications in the nitrogenous base and the ribose sugar. The "epitranscriptome" is a collective terminology to indicate all the chemical modifications found in RNA molecules. To date, more than 170 types of chemical modification are reported to occur in RNAs including messenger RNA (mRNA), ribosomal RNA (rRNA), transfer RNA (tRNA), and long noncoding RNA (lncRNA) (Kumar & Mohapatra, 2021). Some of the most common chemical modifications are shown in Figure A. N^6-methyladenosine (m^6A) is the most common internal chemical modification found in mRNA. M^6A modification is catalyzed by a nuclear methyltransferase complex consisting of methyltransferase like 3 (METTL3), METTL14, and Wilms's tumor-associated protein (WTAP) (Liu et al., 2014). Proteins with the YTH domain such as YTHDF1, F2, F3, C1, and C2 are known to specifically recognize and bind with the m^6A nucleotide (Zaccara et al., 2019). In contrast, RNA demethylases with Alk domain such as ALKBH5, and ALKBH9 (FTO) can remove the methyl group from m^6A (Zaccara et al., 2019). The reversible nature of m^6A modification results in the dynamic regulation of gene expression.

A

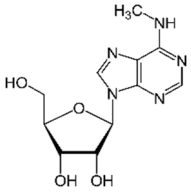

N^6-methyladenosine

(m^{6}A)

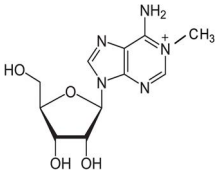

N^1-methyladenosine

(m^{1}A)

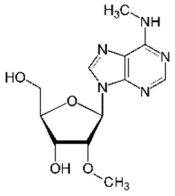

N^6,2′-O-

dimethyladenosine

(m^{6}Am)

G

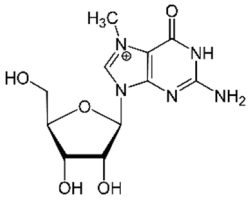

5-Methylguanosine

(m^{7}G)

C

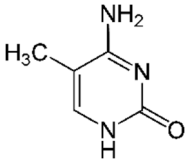

5-Methycytosine

(5mc)

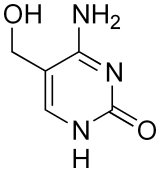

5-Hydroxymethylcytosine

(5hmc)

U

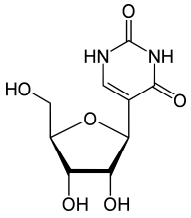

Pseudouridine(Ψ)

Figure A. Common nucleotide modifications found in RNA molecules

2. M^{6}A-related proteins

M^{6}A-related proteins are categorized into three groups based on their ability to install, recognize, and remove the m^{6}A modification.

2.1 Writers

M6A writers include the proteins involved in the N^6-adenosine methyltransferase reaction. The reaction is catalyzed by a complex, called methyltransferase complex (MTC), composed of three core proteins: METTL3, METTL14, and WTAP. Among the core proteins, METTL3-METTL14 forms a dimer which is responsible for m^{6}A modification (Liu et al., 2014). In contrast, WTAP recruits the METTL3-METTL14 dimer to the nuclear speckles, the principal sites of m^{6}A deposition, located in the cell nucleus (Ping et al., 2014). Recent crystallographic studies have shown that METTL3 is the sole catalytic subunit of the MTC (P. Wang et al., 2016; X. Wang et al., 2016). In contrast, METTL14 provides allosteric support to recognize the RNA substrate and helps to stabilize the MTC (X. Wang et al., 2016). As METTL3 and METTL14 contain the methyltransferase (MTase) domain, either of these purified proteins can catalyze the methyltransferase reaction in vitro (Bokar et al., 1997). However, the rate of catalysis is significantly increased for the METTL3-METTL14 dimer complex (Bokar et al., 1997).

2.2 Readers

M^{6}A Readers include the proteins which recognize and bind with the m^{6}A nucleotide. Reader proteins are broadly classified into either direct readers or indirect readers (Zaccara et al., 2019). The direct reader includes a protein that can directly recognize the m^{6}A nucleotide. The ability to recognize the m^{6}A is attributed to the YT521-B homology (YTH) domain. Proteins with the YTH domain share significant homology with other RNA binding domains. The role of the YTH domain-containing proteins as m^{6}A readers were reinforced by the finding that an m^{6}A probe pulls down YTH protein from the cell lysate (Dominissini et al., 2012). The human genome

encodes 5 proteins with the YTH domain: YTHDF1, DF2, DF3, DC1, and DC2. The YTHDF1-DF3 are located mostly in the cytosol, DC1 is localized in the nucleus, whereas YTHDC2 is ubiquitous (Zaccara et al., 2019). Indirect readers recognize the structural deformation in mRNA caused by m^6A. Given that m^6A has a lower ability to base-pair with Uracil, compared to adenosine, the presence of m^6A base in mRNA tends to form a linear, unfolded structure around its location (Roost et al., 2015). Structural change in mRNA caused by m^6A is known as 'm^6A structural switch' (Liu et al., 2015). Indirect m^6A readers recognize the m^6A switch and include two well-known proteins: heterogenous nuclear ribonucleoprotein G (HNRNPG) and A2B1 (HNRPA2B1) (Zaccara et al., 2019). The indirect readers have a lower binding affinity to the unmethylated mRNA compared to the m^6A modified mRNA (Zaccara et al., 2019).

2.3 Erasers

M^6A Eraser includes the proteins involved in demethylation reaction, converting m^6A into A. The presence of m^6A erasers in the human genome suggests that m^6A modification is a dynamic event, which can be regulated by cell signaling pathways, in response to the extracellular environment. M^6A erasers are characterized by their sequence homology to the ALKB family of dioxygenases (Gerken et al., 2007). ALKBH5 is a major example of m^6A eraser protein. In addition, Fat mass and obesity-associated protein (FTO), also known as ALKBH9, was previously recognized as an m^6A eraser. However, recent studies indicate that FTO has a poor affinity towards m^6A instead, it is a strong eraser of m^6Am modification (Mauer et al., 2017).

3. Effect of m^6A modification in mRNA processing

3.1. Translation efficiency

Studies have shown that increased m^6A modification of specific mRNAs in cancer cells promotes their translation efficiency. The ability of m^6A to promote translation efficiency lies in the recruitment of m^6A reader proteins such as YTHDF1 and eukaryotic initiation factor 3 (eIF3)

complex to the translating mRNA. M^6A located around the stop codon is recognized by YTHDF1 protein, which in turn binds with the eIF3b subunit of the eIF3 complex (Wang et al., 2015). Given that the eIF3 complex recruits a small ribosomal subunit (40S) for the initiation of translation, m^6A -YTHDF1-eIF3 axis facilitates the translation initiation step to enhance translation. Apart from YTHDF1, cytosolic METTL3 also serves as an m^6A reader and promotes translation through a mechanism that is similar to YTHDF1 (Lin et al., 2016). In addition, m^6A nucleotide can directly bind with the eIF3 complex. Specifically, the m^6A nucleotide located in 5' UTR of mRNA can recruit the eIF3 complex to initiate cap-independent translation during stressful conditions such as viral infection or heat shock stress (Kate D. Meyer et al., 2015). In addition, METTL3 bound in the 3'UTR region of an mRNA could also interact with eIF3h to form an mRNA loop (Choe et al., 2018). Increased loop formation, in turn, promotes translation efficiency via enhanced ribosome recycling and polysome formation. METTL3-eIF3h interaction plays a crucial role in the enhanced translation and neoplastic transformation (Choe et al., 2018). The mechanism of m^6A-dependent translation allows the cancer cells to enhance the translation efficiency of specific mRNAs to drive tumorigenesis and resistance to anticancer drugs (Cai et al., 2021; Zeng et al., 2020).

3.2. mRNA stability

One of the major aspects of RNA biology regulated by m^6A modification is the regulation of mRNA half-life. Studies have shown that ability of m^6A to regulate mRNA stability lies in the recruitment of YTHDF2 (Wang et al., 2014). YTHDF2 relocates the mRNA from the ribosome to the mRNA decay sites such as processing bodies to facilitate mRNA degradation (Wang et al., 2014). In addition, YTHDF2 recruits endoribonuclease such as HRSP12 or the deadenylate complex CCR4-NOT to facilitate mRNA degradation (Du et al., 2016; Park et al., 2019).

3.3. Alternative splicing

Precursor mRNAs from almost 95% of the genes undergo alternative splicing to produce a large number of transcript variants in humans (Pan et al., 2008). The role of m^6A modification in mRNA splicing comes from early evidence which showed that m^6A present within the intron region affects the splicing of *sxl* mRNA, a gene crucial to sex determination in *Drosophila melanogaster* (Kan et al., 2017). Recent studies have shown that nuclear m^6A reader YTHDC1 facilitates the splicing of pre-mRNA via binding with m^6A nucleotide (Xiao et al., 2016). YTHDC1 is known to bind with several splicing factors including SRSF1, SRSF3, SRSF7, SRSF9, and SRSF10 (Xiao et al., 2016). Moreover, YTHDC1 promoted exon inclusion in specific mRNAs via the recruitment of SRSF3 (Xiao et al., 2016). Similarly, m^6A reader HNRPG simultaneously interacted with the m^6A-modified nascent pre-mRNA and c-terminal domain (CTD) of RNA polymerase II to regulate alternative splicing (Zhou et al., 2019).

4. The role of METTL3-induced m^6A modification in cancer progression

Several studies have shown that METTL3 expression is deregulated in various human cancer which is involved in the progression of tumors. The expression of METTL3, specific mRNA substrates, the effect of m^6A modification on mRNA biology, and cancer phenotypes resulting from aberrant m^6A modification in some representative human cancers are shown in Table 1.

Table 1. The role of METTL3 in various human cancers

Cancer Type	METTL3 expression	mRNA substrate	Biological function	Phenotype	Ref
Lung cancer	Increased	*EGFR, BRD4, MGMT, TIMP1*	Translation ↑	Tumorigenesis	(Choe et al., 2018)
Glioma	Increased	*SOX2*	mRNA stability ↑	Stem-like cell maintenance, radio resistance	(Visvanathan et al., 2018)
Leukemia	Increased	*c-Myc BCL2 PTEN*	Translation ↑	Inhibits differentiation, Increases cell growth	(Vu et al., 2017)
Leukemia	Increased	*SP1, SP2*	Translation ↑	Cell proliferation, Differentiation	(Barbieri et al., 2017)
Colorectal cancer	Increased	*SOX2*	mRNA stability ↑	Self-renewal, stem cell frequency and migration	(Li et al., 2019)
Ovarian cancer	Increased	*AXL*	Translation ↑	promotes the proliferation, invasion, and tumor formation	(Hua et al., 2018)
Melanoma	Increased	*MMP2*	Translation ↑	Promotes invasion	(Dahal et al., 2019)
HCC	Increased	*SOCS2*	mRNA stability ↑	Cell proliferation, migration, and colony formation	(Xu et al., 2020)
Breast	Increased	*BCL2 EZH2*	mRNA stability ↑ Translation ↑	Promotes proliferation, Inhibits apoptosis	(Hu et al., 2022; Wang et al., 2020)

5. Regulatory role of PIN1 in METTL3-induced m^{6}A modification and mRNA processing

The *cis-trans* conformational change of proline, which is induced by peptidyl-prolyl *cis-trans* isomerase (PPIase), regulates the conformations of proteins in cells (Chen et al., 2018). The human genome encodes approximately 30 PPIases belonging to three families: cyclophilin, FK506-binding protein (FKBP), and Parvulin (Lu et al., 2007). PPIases act as molecular chaperones and play a crucial role in the assembly and disintegration of macromolecular structures, including messenger ribonucleoprotein complexes, mRNA complexes, and RNA-binding proteins (Thapar, 2015). The proper packaging of mRNAs into ribonucleoprotein complexes is essential for various post-transcriptional events, including epitranscriptomic modifications, alternative splicing, nuclear export, mRNA degradation, and translation (Keene, 2001). Several PPIases have been identified as intrinsic components of the spliceosome and mRNA degradation machinery (Thapar, 2015). Among these PPIases, peptidyl-prolyl *cis-trans* isomerase NIMA-interacting 1 (PIN1) is the only member that binds to and isomerizes specific phosphorylated serine/threonine-proline (pSer/Thr-Pro) motifs in proteins(Lu et al., 2007). The expression of PIN1 is increased in several types of cancers, including breast cancer (Khanal et al., 2013; Rustighi et al., 2017). PIN1-induced conformational changes regulate the functions of several transcription factors and epigenetic modifiers, including p53, c-Myc, nuclear factor kappa B, β-catenin, hypoxia-inducible factor 1α, signal transducer and activator of transcription 3, and SUV39H1, to promote breast tumorigenesis (Rustighi et al., 2017). High-throughput sequencing of the transcriptome has shown a strong correlation between the expression of PIN1 and the genes involved in mRNA splicing, translation, and ribosome biogenesis (Farrell et al., 2013). This has triggered interest in the study of PIN1 as a regulator of RNA processing events. The regulatory role of PPIase in RNA processing has been supported by several lines of evidence.

For instance, parvulin 14 has been found to facilitate the splicing of pre-rRNA to 18 and 28S rRNA (Fujiyama-Nakamura et al., 2009). Furthermore, PIN1 has been shown to regulate the stability of mRNAs containing AU-rich elements (ARE) through the prolyl isomerization of ARE-binding proteins (Shen & Malter, 2015). Similarly, PIN1 was found to regulate the stability of parathyroid hormone mRNA levels in a rat model of secondary hyperparathyroidism (Nechama et al., 2009). The interest in studying the role of PPIase in mRNA translation is based on an early discovery in which the immunosuppressive drug rapamycin bound to the prolyl isomerase FKBP12 and suppressed protein synthesis via the inhibition of the mechanistic target of rapamycin complex (Choi et al., 1996). Further studies have shown that PIN1 directly binds to and promotes the phosphorylation of ribosomal S6 kinases, which can facilitate protein synthesis, in mouse embryonic fibroblast cells (Lee et al., 2009). A notable role of PIN1 in mRNA translation was further uncovered during a study of cytoplasmic polyadenylation element-binding proteins (CPEB) in *Xenopus* oocytes. CPEB prevents the translation of mRNAs involved in cell cycle progression, such as *cyclin B1*, by blocking the cap-binding protein eIF4E. However, PIN1 facilitates the ubiquitination of CEBP, which restores the normal translation of cyclin B1 mRNA, thereby allowing the cell cycle to function (Nechama et al., 2013). In contrast, the inhibition of PIN1 enhances protein synthesis in dendritic termini via eIF4E and 4EBP1/2 (Westmark et al., 2010). PPIases, including PIN1, therefore act as crucial regulators of RNA splicing, mRNA stability, and translation to regulate physiological processes. Most studies have been performed in non-cancerous models, however, rendering the role of PIN1 in RNA processing during carcinogenesis unclear.

Recently, epitranscriptomic modifications of mRNA, such as N^6-methyladenosine (m^6A), have emerged as critical factors in regulating the post-transcriptional processing of mRNAs in human

cancers, including breast cancer (Pan et al., 2021; Wang et al., 2020; Wu et al., 2019). M^6A modification is mediated by a nuclear methyltransferase complex comprising three core proteins: methyltransferase-like protein 3 (METTL3), METTL14, and Wilms tumor 1-associated protein (WTAP) (Zaccara et al., 2019). Among these core proteins, METTL3 is the sole catalytic subunit of the methyltransferase complex. Studies have shown that METTL3-induced m^6A modifications regulate mRNA stability and translation efficiency to promote carcinogenesis (Cai et al., 2021). For instance, the enhanced m^6A modification of transcriptional co-activator with PDZ-binding motif (*TAZ*) and epidermal growth factor receptor (*EGFR*) mRNA has been found to promote their translation efficiency to promote lung tumorigenesis (Lin et al., 2016). Notably, the expression of TAZ and EGFR is frequently upregulated in breast cancer patients and is associated with poor prognoses (Cordenonsi et al., 2011; Masuda et al., 2012). Interestingly, PIN1 is known to increase the protein expression of TAZ and EGFR in various human cancers, including breast cancer, melanoma, lung cancer, and ovarian cancer, through poorly defined mechanisms (Beretta et al., 2016; Khanal et al., 2019; KIM et al., 2019). These observations have led to the question of whether PIN1 regulates the protein abundance of specific oncogenes, such as TAZ and EGFR, via the regulation of m^6A-related mRNA processing. However, to uncover the role of PIN1 in m^6A-dependent mRNA processing, it is essential to examine protein-protein interactions between PIN1 and proteins involved in m^6A modifications. In this study, we identified the novel METTL3-PIN1 interaction with important implications in the regulation of m^6A-dependent mRNA translation. Our results indicate that the PIN1/METTL3 axis may be a potential therapeutic target for patients with breast cancer.

6. Role m^{6}A-dependent translation in targeted drug resistance

Emerging evidence indicates that aberrant deposition of m^{6}A on specific mRNAs plays a crucial role in the pathogenesis of melanoma (Huang et al., 2020; Jiang et al., 2021). Specifically, m^{6}A modification of mRNA promotes the invasiveness of melanoma cells and reduces their sensitivity to immunotherapy (Dahal et al., 2019; Yang et al., 2019). However, the roles of epitranscriptomic modifications in the development of acquired resistance to chemotherapy, known to often require permanent genetic and epigenetic changes,(Nyce et al., 1993; Vasan et al., 2019) remain to be explored.

M^{6}A modifications are catalyzed by a methyltransferase complex consisting of three core proteins: methyltransferase-like protein 3 (METTL3), METTL14, and Wilms tumor 1-associated protein (WTAP) (Huang et al., 2020). Crystallographic studies have identified METTL3 as the catalytic subunit, whereas METTL14 and WTAP provide structural support and are indispensable for m^{6}A deposition (P. Wang et al., 2016; X. Wang et al., 2016). The expression of METTL3 is deregulated in several types of cancer such as lung cancer, breast cancer, colorectal cancer, acute myeloid leukemia, and glioma (Zheng et al., 2019). Concomitant changes in the levels of mRNA m^{6}A modification are associated with different aspects of cancer cell biology including cell transformation, cell proliferation, apoptosis, invasion, metastasis, renewal of cancer stem cells, and drug resistance (Zheng et al., 2019). Notably, METTL3-mediated m^{6}A modification regulates the translation and stability of a specific cluster of mRNAs that encodes proteins associated with apoptosis, autophagy, cell cycle, DNA repair, and metabolism, thereby facilitating the development of chemoresistance in several cancers (Xiang et al., 2020). For example, METTL3 has been reported to promote tamoxifen and adriamycin resistance in breast cancer cells (X. Liu et al., 2020; Pan et al., 2021), cisplatin resistance in seminoma (Wei et al., 2020), gefitinib and cisplatin resistance in non-small cell lung cancer (Jin et al., 2019; S. Liu et

al., 2020), gemcitabine, 5-fluorouracil, and cisplatin resistance in pancreatic cancer (Taketo et al., 2018), and sorafenib resistance in liver cancer (Lin et al., 2020). In particular, METTL3 promotes chemo- and radioresistance in pancreatic cancer cells through activation of mitogen-activated protein kinase (MAPK) cascades (Taketo et al., 2018). However, it remains unknown whether METTL3 contributes to the rebound activation of MAPK cascades, including the RAF/MEK/ERK pathway, which constitutes the most commonly implicated mechanism in the development of PLX4032-resistant melanoma.

BRAF-V600E constitutes the most common mutation found in patients with melanoma (Sullivan & Flaherty, 2011). PLX4032 specifically inhibits BRAF kinase (V600E) and prevents melanoma tumorigenesis; however, the development of acquired resistance limits its clinical efficacy (Lito et al., 2013). As the underlying mechanism of PLX4032 resistance often involves rebound activation of the RAF/MEK/ERK pathway (Flaherty, 2011; Sullivan & Flaherty, 2011). MEK inhibitors such as trametinib have been approved in combination with PLX4032 to overcome chemoresistance. Nevertheless, the efficiency of combinatorial therapy remains limited owing to associated toxicity and frequent relapse of tumors (Villanueva et al., 2011). Receptor tyrosine kinases, including epidermal growth factor receptor (EGFR) and human epidermal growth factor receptor 3 (HER3), represent alternative therapeutic targets as these are upregulated at the protein level, albeit not necessarily at the transcriptional level, and constitute strong predictors of PLX4032 resistance in melanoma cells (Carroll et al., 2019). In particular, EGFR promotes rebound activation of the RAF/MEK/ERK pathway to induce PLX4032 resistance (Dratkiewicz et al., 2020). However, the mechanism underlying the enhanced expression of EGFR protein in PLX4032-resistant tumors remains elusive.

In this study, we evaluated the relationship between METTL3 expression at the protein level in PLX4032-resistant melanoma cells and m^6A modification of *EGFR* mRNA. In addition, we

clarified whether m^6A deposition promotes the translation efficiency of EGFR, resulting in reactivation of the RAF/MEK/ERK pathway and consequent PLX4032 resistance. Our study highlights the regulatory role of METTL3 in the development of PLX4032 resistance and suggests a novel strategy to restore PLX4032 sensitivity via METTL3 inhibition.

II. Materials & Methods

Cell culture and establishment of stable cell lines

MCF7 and HEK293 cells purchased from the American Type Culture Collection (ATCC) were maintained in Dulbecco's modified Eagle's medium (DMEM) supplemented with 10% fetal bovine serum (FBS) at 37 °C in humidified air containing 5% CO2. 4T1 cells obtained from the ATCC were maintained in RPMI medium supplemented with 10% FBS. To establish MCF7 and 4T1 cells stably overexpressing PIN1, cells were transfected with the pcDNA4-His/XP-PIN1 vector and selected with Zeocin (300 μg/mL for MCF7 and 250 μg/mL for 4T1) for several weeks until resistant colonies were formed. The cells from the resistant colonies were pooled together and maintained in the respective media for each cell line. A375 cells, purchased from the American Type Culture Collection (ATCC), were maintained in Dulbecco's modified Eagle's medium (DMEM) supplemented with 10% fetal bovine serum (FBS) at 37 °C in humidified air containing 5% CO2. HMCB cells obtained from ATCC were maintained in RPMI medium supplemented with 10% FBS. The A375R cell line was established as described in our previous study with a slight modification: A375R cells were briefly challenged with 5 μM PLX4032 and maintained in DMEM supplemented with 10% FBS and 5 μM PLX4032.1

Antibodies and reagents

Antibodies against METTL3 (96391, WB 1:1000, IP 1 μL), TAZ (8418, WB 1:1000), p-MEK1/2 (9154, WB 1:1,000), p-ERK1/2 (4377, WB 1:1,000), p-RAF1 (9427, WB 1:1,000), cleaved caspase-3 (9661, WB 1:1,000), METTL3 (96391, WB 1:1000), METTL14 (51104, WB 1:1000), WTAP (56501, WB 1:1,000), and FTO (31687, WB 1:1,000) were purchased from Cell Signaling Technology Inc. (Danvers, MA, USA). The antibody against METTL3 (195352, IHC 1:500) was purchased from Abcam (Cambridge, USA). Antibodies against EGFR (sc-373746 WB 1:1,000;

IP 1 μg), eIF3b (sc-137124, WB 1:1000), eIF4E (sc-9976, WB 1:1000), PIN1 (sc-46660, WB 1:5000; IP 1 μg; IHC 1:500), and GFP (sc-8334 WB 1:5000) were purchased from Santa Cruz Biotechnology (Dallas, TX, USA). Anti-β-actin (A1987, 1:10,000) and anti-FLAG (F3165, 1:5,000) antibodies were purchased from Sigma-Aldrich (St. Louis, MO, USA). Anti-m^{6}A antibody (dot blot 1:1,000; IP 1 μg) was obtained from Synaptic Systems (Goettingen, Germany). Antibodies against puromycin (MABE343, WB 1:5,000) were purchased from Merck Millipore (Burlington, MA, USA). PD98059 (513000) was purchased from Calbiochem (San Diego, CA, USA). Trametinib (HY-10999) was purchased from MedChemExpress (NJ, USA). ATRA (R2625) was purchased from Sigma-Aldrich. PLX 4032 was obtained from Advanced ChemBlock (San Diego, CA) The EpiQuik m^{6}A RNA Methylation Quantification Kit (Colorimetric) was obtained from Epigentek (P-9005-96). The jetPEI® transfection reagent was obtained from Polyplus-transfection (Illkrich, France). Lipofectamine 3000 transfection reagent was purchased from Invitrogen (Carlsbad, CA, USA).

CRISPR/Cas9 knockout and mammalian expression vectors

To knockout genes using the CRISPR/Cas9 system, guide RNAs targeting human METTL3 (1st, 5'-GAGTTGATTGAGGTAAAGCG-3'; 2nd, 5' GTATCTCCAGATCAACATCTG-3'), human PIN1 (1st, 5'- GATGAGCGGGCCCGTGTTCA-3'; 2nd, 5'-GAAGATCACCCGGACCAAGG-3'), mouse Mettl3 (1st, 5'-GAGTTGATTGAGGTAAAGCG-3'; 2nd 5'-GGGCAAATTTGCAGTTGTGA-3'), and EGFR (1st, 5'-GAGAACCTAGAAATCATACG-3'; 2nd, 5'-GTGGAGCCTCTTACACCCAG-3') were designed using the Broad Institute CRISPick portal (https://portals.broadinstitute.org/gppx/crispick/public) and cloned into the BbsI site of the peSpCas9(1.1)-T2A-puro vector (a gift from Andrea Nemeth, Addgene #101039). Plasmid DNAs were transfected into cells using Lipofectamine 3000 reagent. At 48 h following the

transfection, cells were harvested and used for the experiment without single-cell isolation. To establish METTL3 KO stable cells (Figure 4h), cells transfected with sgMETTL3 were selected with 2 μg/mL puromycin for 48 h. The surviving cells were passaged three times before being used for the experiment. pcDNA3-Flag-METTL3 (Addgene plasmid #53739) and pcDNA3-Flag-METTL14 (Addgene plasmid #53740) were gifted by Chuan He. pBiFC-VN173 (Addgene #22010) and pBiFC-VC155(Addgene #22011) were gifts provided by Chang-Deng Hu. The pRSTF-tagged cap (Addgene #35572) and pQCXIP-MS2-HB (Addgene #35573) were gifts from Marian Watermen. pCMV-FLAG-TAZ (Addgene #24809) was gifted by Jeff Wrana. The pACT, pBIND, and pG5-luc plasmids were obtained from Promega (Madison, WI, USA). psiCHECK3 was a gift from Anthony Leung (Addgene, #136010). The construction of pcDNA4-His/XP-PIN1, GST-PIN1(WT), GST-PIN1(WW), and GST-PIN1 (PPIase) has been previously described (Khanal et al., 2012). To construct pACT-PIN1, the PIN1 open reading frame (ORF) was PCR-amplified from pcDNA4-His/XP-PIN1 and cloned into the Sal/NotI site of the pACT vector. The ORFs were PCR-amplified from pcDNA3-Flag-METTL3, pCDNA3-Flag-METTL14, pcDNA3-Flag-WTAP, and pGEM-WTAP (Sinobiological #HG12018-G), and cloned into the SalI/NotI sites of the pBIND vector. The pBIND-SGK1 plasmid was a gift from Zigang Dong (Hormel Institute). To construct pBiFC-VN-METTL3 and pBiFC-VC-PIN1, the ORFs of METTL3 and PIN1 were PCR-amplified from the pcDNA3/Flag-METTL3 and pcDNA4-His/XP-PIN1 vectors and cloned into the HindIII/XbaI and EcoRI/XhoI sites, respectively. To construct pcDNA3-Myc-EGFR, the ORF of EGFR (NM_005228.5) was PCR-amplified from cDNA prepared from HEK293 cells using Phusion High-Fidelity DNA polymerase (Thermo Fisher Scientific, Waltham, MA) and cloned into the HindIII/XbaI site of the pcDNA3.1-myc-HisA vector. To design the psiCHECK3-EGFR, the putative m^6A modification site of EGFR (NM_005228.5, nucleotides 3736–3900) was PCR-amplified from

HEK293 cDNA and cloned into the 3'-UTR of the Renilla luciferase gene at the XhoI site of the psiCHECK3 vector (a gift from Anthony Leung, Addgene plasmid # 136010). To construct the psiCHECK3-TAZ, a putative m^6A modification site of TAZ (NM_015472.6, nucleotides 1245–1467) was PCR-amplified from cDNA prepared from MCF7 cells and cloned into the XhoI site of the psiCHECK3 vector. To construct the pcDNA3-4X(MS2) vector, the MS2 hairpin loop was PCR-amplified from the pRSTF-MS2-tagged cap vector and cloned into the BbsI site located at the 3' UTR of the pcDNA3.1-Myc/HisA vector. To construct pcDNA3-myc-EGFR-4x(MS2) and pcDNA3-Flag-TAZ-4x(MS2), pcDNA3-Myc-EGFR and pCMV5-Flag-TAZ vectors were digested with MluI/XbaI and KpnI/EcoRI, and the ORF was subcloned into the pcDNA3-4X(MS2) vector. Mutagenesis was performed using the Quick-change II kit (Agilent, Santa Clara, CA, USA) according to the manufacturer's instructions.

Immunohistochemistry

Informed consent was obtained from all of the patients. All research protocols were approved by the ethics committee of the Chosun University Hospital. Tissues from 30 patients with invasive breast carcinoma were collected. IHC staining was performed as previously described (Choe et al., 2018). For METTL3, each sample was scored as the percentage of positively stained cells (percentage score: 1–5) and the staining intensity (intensity score: 1–5). The IHC score was calculated by multiplying the percentage and intensity scores. For PIN1, IHC stain was scored based on the percentage of positively stained cells (score range: 0-3).

Mammalian Two-Hybrid Assay

pACT-PIN1 and pBIND vectors were combined with pG5-luc vectors in equal molar ratios. DNA (100 ng) was transfected into HEK293 cells cultured in 48-well plates using jetPEI reagent. After 48 h, cells were lysed in passive lysis buffer (Promega, Madison, WI, USA). Firefly and Renilla luciferase activities in the cell lysates were measured using the Dual-Luciferase Reporter Assay

System (Promega). Renilla activity was used to normalize the transfection efficiency.

GST Pulldown Assay

For the GST pulldown assays, the cells were transfected with the indicated plasmid DNA. After 48 h of transfection, cells were lysed in NET-NL buffer containing 50 mM Tris-HCl (pH 7.5), 150 mM NaCl, 0.5% NP-40, 1 mM ethylenediaminetetraacetic acid, 1 mM dithiothreitol, 0.2 mM phenylmethylsulfonyl fluoride, protease inhibitor cocktail (Roche Life Sciences, Indianapolis, IN, USA), and phosphatase inhibitor cocktail (Thermo Fisher Scientific), and the lysate was incubated with glutathione-sepharose beads (GE Healthcare, Chicago, IL, USA) containing GST or GST-PIN1 at 4 °C for 4 h. The precipitated proteins were resolved using sodium dodecyl sulfate-polyacrylamide gel electrophoresis (SDS-PAGE) and detected by immunoblotting.

Ni-NTA Pulldown Assay

HEK293 and MCF7 cells were lysed in His-lysis buffer (50 mM Tris-HCl pH 8.0, 150 mM NaCl, 0.5% NP-40, 0.1 mM ethylenediaminetetraacetic acid, 1 phenylmethylsulfonyl fluoride, 25 mM imidazole). The lysate was incubated with His-Pur resin (ThermoScientific, Waltham, MA, USA) for 1 h at 4 °C, followed by washing with His-lysis buffer or high-salt buffer (His lysis buffer with 500 mM NaCl). The precipitated proteins were resolved using SDS-PAGE and detected by immunoblotting.

Protein Immunoblotting and Immunoprecipitation

For immunoblotting, cells grown in monolayers were harvested, washed in PBS, and lysed in RIPA buffer containing 150 mM NaCl, 50 mM Tris-HCl (pH 7.4), 0.25% sodium deoxycholate, 1 mM ethylenediaminetetraacetic acid, 1% NP40, 1 mM NaF, 0.2 mM phenylmethylsulfonyl fluoride, 0.1 mM sodium orthovanadate, and protease/phosphatase inhibitor cocktail. Protein samples (10–30 μg) were resolved using SDS-PAGE, blotted onto polyvinylidene fluoride

membranes, and probed using the indicated antibodies. For co-immunoprecipitation, cells were harvested and lysed in NET-NL buffer. The lysate was immunoprecipitated with the indicated antibodies and immunoblotted. The immunoblots were visualized using SuperSignal West Femto chemiluminescence substrate (Thermo Fisher Scientific) and Amersham Imager 680 (GE Healthcare, Chicago, IL, USA).

Bimolecular Fluorescence Complementation (BiFC) and Immunofluorescence Microscopy

MCF7 cells were seeded onto coverslips and transfected with the indicated BiFC plasmids. Cells were fixed using 4% formaldehyde, washed with phosphate-buffered saline (PBS), mounted on slides using ProLong Gold Antifade mountant with DAPI (Thermo Fisher Scientific), and examined under a fluorescence microscope using a GFP filter. To assess immunofluorescence with puromycin labeling, MCF7 cells transfected with sgCtrl or sgPIN1 plasmids were treated with puromycin (2 μg/mL) for 1 h at 37 °C, fixed with Cytofix/Cytoperm™ reagent (BD Biosciences, San Diego, CA, USA), and probed with anti-puromycin antibody followed by anti-mouse IgG-Texas Red antibody (Thermo Fisher Scientific). The coverslips were mounted on slides using ProLong Gold Antifade mountant with DAPI and examined under a fluorescence microscope. A375 and A375R cells were seeded on coverslips, fixed using Cytofix/Cytoperm™ reagent, and then probed with anti-m^6A antibody followed by anti-mouse IgG-Alexa Fluor 647 antibody (Thermo Fisher Scientific). The coverslips were mounted on slides using ProLong Gold Antifade mountant with DAPI and examined using a confocal microscope (Nikon, Minato, Japan). Fluorescence intensity was measured using the Fiji program (downloaded from https://fiji.sc/). In brief, the fluorescence intensity was calculated as the corrected total cell fluorescence (CTCF) using the following formula: CTCF = integrated density − (area of selected cell × mean fluorescence of background readings). The fluorescence intensity of cells (N = 6) from each group was calculated using the above formula. To minimize the variations in intensity

arising from the imaging conditions, fluorescence microscopy images were captured simultaneously, and the exposure times remained constant.

Puromycin labeling and immunoprecipitation

MCF7 cells were treated with 2 μg/mL puromycin for 1 h at 37 °C. The cells were harvested and lysed in NET-NL buffer containing 50 mM Tris-HCl (pH 7.5), 150 mM NaCl, 0.5% NP-40, 1 mM ethylenediaminetetraacetic acid, 1 mM dithiothreitol, 0.2 mM phenylmethylsulfonyl fluoride, protease inhibitor cocktail (Roche Life Sciences, Indianapolis, IN, USA), and phosphatase inhibitor cocktail (Thermo Fisher Scientific). The lysate was immunoprecipitated using an anti-puromycin antibody, followed by immunoblotting. A375 and A375R cells were treated with 1 μg/mL puromycin for 1 h at 37 °C. Cells were harvested and lysed in NET-NL buffer. The lysate was immunoprecipitated with an anti-EGFR antibody followed by immunoblotting with a puromycin antibody.

Poly(A) RNA dot blotting

Dot blotting was performed as described previously.3 Total RNA was isolated from A375 and A375R cells using TRIzol reagent (Invitrogen). Then, poly(A) RNA was purified from total RNA using the Oligotex mRNA mini kit (Qiagen, Hilden, Germany). Poly(A) RNA (100 ng) was crosslinked onto a Hybond N+ membrane using a UV crosslinker. The membrane was probed using an anti-m^6A antibody and the blots were visualized using a SuperSignal West Femto chemiluminescence substrate with the Amersham Imager 680.

meRIP-PCR (m^6A-RIP-PCR)

Total RNA (100 μg) was pre-cleared by incubation with 20 μL of recombinant protein G sepharose bead suspension (Invitrogen) in meRIP buffer (10 mM Tris pH 7.5, 150 mM NaCl, 0.1% NP-40, 2 mM ribonucleoside vanadyl complexes, and 200 U/mL RNasin) for 1 h at 4 °C. The precleared RNA solution was incubated with 1 μg of anti-m^6A antibody for 4 h at 4 °C.

Recombinant protein-G sepharose beads (50 μL) were blocked using 0.5 mg/mL bovine serum albumin in meRIP buffer for 1 h at 4 °C. The RNA–antibody mixture was added to the precleared beads and incubated for 2 h at 4 °C. The beads were washed five times with meRIP buffer, then the mRNA bound to the beads was eluted by incubation with 100 μL of elution buffer (meRIP buffer supplemented with 6.7 mM N6-methyladenosine base; Selleckchem, Houston, TX) at 4 °C for 1 h. The eluted RNA was purified using an RNeasy mini kit (Qiagen). Purified eluate (5 μL) was reverse transcribed into first-strand cDNA using TOPscript™ RT DryMIX dT18 plus (Enzynomics, Daejeon, Republic of Korea). The reverse transcription product was diluted in nuclease-free water at a ratio of 1:10 and used for real-time PCR or semi-quantitative endpoint PCR. Real-time PCR was performed using the Fast SYBR Green master mix on a StepOne Real-Time PCR system (both Thermo Fisher Scientific). Semi-quantitative endpoint PCR was performed using AccuPower PCR premix (Bioneer, Daejeon, Republic of Korea).

MS2-Tagged RNA Pulldown Assay

Pulldown was performed as previously described 5 with some modifications. In brief, MCF7 cells transfected with the indicated plasmids were cross-linked using UV irradiation (400 mJ/cm2). The cells were lysed in the lysis buffer (25 mM Tris-HCl pH 8.0, 300 mM NaCl, 25 mM imidazole, 10 mM Ribonucleoside Vanadyl complex, protease inhibitor cocktail), and the lysate was incubated with HisPur resin for 1 h at 4 °C. The precipitated proteins were detected by immunoblotting after RNA was digested with RNase A. To perform RT-PCR, the proteins in the precipitate were digested with proteinase K, and the RNA was purified using TRIzol Reagent. The purified RNA was converted into cDNA using a random hexamer primer and analyzed by PCR.

Luciferase assay

Renilla luciferase activity in cell lysates prepared from MCF7, A375 and A375R cells transfected

with psiCHECK3 vectors was measured using the Dual-Luciferase Reporter Assay System (Promega, Madison, WI). Firefly luciferase activity generated by this vector was used to normalize the results for transfection efficiency.

Polysome Fractionation

Polysome fractionation was performed as previously described2 with some modifications. In brief, MCF7 cells transfected with sgCtrl or sgPIN1 were treated with 100 μg/mL cycloheximide for 10 min at 37 °C. Cells were harvested and lysed in polysome lysis buffer (20 mM HEPES pH 7.6, 5 mM MgCl2, 125 mM KCl, 1% NP-40, 2 mM EDTA, 100 μg/mL cycloheximide, EDTA-free protease inhibitors, and RNAsin). An equal amount of lysate was layered onto 10 mL of 17.5–50% sucrose gradient and centrifuged at 31,000 rpm in a Beckman SW-41Ti rotor for 3 h at 4 °C. The gradients were fractionated and monitored at an absorbance of 254 nm. The collected fractions were analyzed by immunoblotting or RT-PCR.

Cell Proliferation Assay (BrdU Incorporation)

Cell proliferation was assessed using a cell proliferation ELISA kit (Roche Life Sciences, Penzberg, Germany), according to the manufacturer's instructions. In brief, MCF7 cells were seeded (5,000 cells per well) in 96-well plates in 100 μL medium supplemented with 10% FBS. After 24 h, the cells were treated with PD98059 and ATRA for 24 h in serum-free media, labeled with 10 μL/well BrdU-labeling solution, and incubated for an additional 4 h at 37 °C in 5% CO2. The medium containing the BrdU-labeling reagent was aspirated, and FixDenat solution was added to each well. The plate was incubated at room temperature (RT) for 30 min and the solution was removed. Anti-BrdU-POD working solution was then added to each well and incubated for an additional 90 min at RT. The cells were washed three times with washing solution, followed by the addition of 100 μL of substrate solution to each well, and incubated for another 30 min. Cell proliferation was estimated by measuring absorbance at 370 nm.

Sub-G1 assay and cell cycle measurements using flow cytometer

Cells were seeded and transfected with indicated plasmids followed by treatment with the indicated chemical for 24 h. The cells were washed, fixed with 70% ethanol, and then 200 μL of Muse™ Cell cycle reagent (Merck Millipore) was added. Then, cells were incubated at 25 °C for 30 min in the dark. The cell cycle was analyzed using a Muse Cell Cycle Assay kit (Merck Millipore).

Ki67 staining

Cells stained with Ki67 were analyzed using the Muse® Ki67 Proliferation Kit according to the manufacturer's instructions. In brief, formaldehyde-fixed MCF7 cells were stained with either Ki67 antibody conjugated with phycoerythrin (PE) or normal IgG-PE and analyzed using a Muse cell analyzer.

Cell viability assay

MTT assays were performed to ascertain cell viability using the EZ-Cytox Cell viability assay kit (Daeli Lab Service, Seoul, Republic of Korea). In brief, 5,000 cells were seeded in 96-well plates with 100 μL of cell suspension in each well and incubated at 37 °C in humidified air containing 5% CO2. After 24 h in culture, cells were incubated with different concentrations of PLX4032 for 24 h. The cells were then treated with 10 μL of tetrazolium salt and incubated for 4 h. The absorbance of purple formazan formed by live cells was measured at 450 nm using a microplate reader (Molecular Devices, San Jose, CA).

TUNEL assay

Apoptosis induction was assessed by TUNEL staining and detected using an in-situ cell death detection kit (Roche Life Science), according to the manufacturer's instructions. Briefly, 2 × 104 cells were seeded onto coverslips placed inside a 24-well plate and incubated for 24 h. The cells were transfected with indicated plasmids using Lipofectamine 3000 reagents. At 24 h following

transfection, cells were treated with indicated chemicals for the next 24 h. For TUNEL staining, cells were washed with phosphate-buffered saline and fixed using Cytofix/Cytoperm™ reagent at 4 °C for 20 min. Cells were stained with 50 μL TUNEL solution at 37 °C for 1 h, then washed twice with phosphate-buffered saline. DNA fragmentation was detected using an Axiovert 200 M fluorescence microscope equipped with a FITC filter.

Anchorage-independent cellular transformation assay (soft agar assay)

Briefly, 8,000 cells transfected with indicated plasmids were exposed to the indicated drug in 1 mL of 0.3% Eagle's basal medium supplemented with 10% FBS. The cultures were maintained at 37 °C in a 5% CO2 incubator for 14 days. Resultant cell colonies were scored using an Axiovert 200M microscope and Axio Vision software (Carl Zeiss, Oberkochen, Germany). A total of six images were captured for each group. The colony size and number were measured using Image J (NIH, Bethesda, MD).SubG1 assay

Mouse orthotopic model

Female BALB/c mice (6 weeks old) were obtained from OrientBio (Seongnam, Republic of Korea) and maintained in cages in light- and temperature-controlled rooms. The animals were fed commercial rat chow (OrientBio, Co., Seongnam, Korea) and had access to water ad libitum. The mice were randomly divided into four groups, with the indicated number of mice in each group. Cells (4T1-mock or 4T1-XP-PIN1 stable cells) transfected with sgCtrl, sgMettl3-1, or sgMettl3-2 knockout plasmids were then injected into the abdominal mammary glands (2 × 106 cells in 100 μL volume) of the mice and allowed to grow until tumor formation (16 d). The mice were observed daily for tumor growth. Tumor volume was calculated using the following formula: Volume = 0.5 × [(large diameter) × (small diameter)2]. This study was approved by the Animal Experiments Committee of Chosun University (CIACUC 2020-S0022).

Mouse xenograft model

Male BALB/c nude mice (6-week-old) were obtained from OrientBio (Seongnam, Republic of Korea) and maintained in cages in light and temperature-controlled rooms. A375 or A375R cells transfected with indicated CRISPR/Cas9 knockout plasmids were subcutaneously injected (2 × 106 cells/100 μL/mice) into mouse flanks. After five days, mice were divided into indicated groups and intraperitoneally injected three times weekly with dimethyl sulfoxide (n = 8) or PLX4032 (20 mg/kg, n = 12). Mice were euthanized 25 days after the first injection and tumor volume and weight was calculated in all groups. Tumors were fixed using 4% formaldehyde, sectioned, mounted on glass slides, and stained with hematoxylin and eosin (H&E). The tumor diameter was measured using calipers (Mitutoyo, Kawasaki, Japan) and tumor volumes were calculated as follows: tumor volume = 0.5 × [(large diameter) × (small diameter)2]. The study was conducted according to the ARRIVE guidelines and approved by the Animal Experiments Committee of Chosun University (CIACUC 2020-S0022).

Bioinformatics analyses

Bioinformatics analyses were performed using the data available in the DepMap portal (retrieved from https://depmap.org/portal/) and TCGA (retrieved from https://www.cbioportal.org/). The data were processed in R (Version 4.1) using the dplyr, tidyr, and ggVennDiagram packages. To analyze the m^6A-seq data (Figure 5a), sequence read archive (SRA) files were downloaded from the Gene Expression Omnibus (GSE37003) using the SRA toolkit (version 2.11.1) and analyzed as previously described (Dominissini et al., 2013) in the Linux operating system (Ubuntu 22.04 LTS). For drug sensitivity screening, Pearson correlation analysis was performed between PLX4032 (CTRP: 649420) drug sensitivity AUC from the cancer target discovery and development (CTD2) screening against the proteomics dataset (Figure. 8d) or protein array dataset (Figure. 9b). To examine the correlation between METTL3 mRNA level and the expression level of oncogenic proteins (Figure 9a), the Expression 21Q2 public dataset was

compared against the protein array dataset. Each analysis was run on a panel of melanoma cell lines (lineage: skin, lineage subtype: melanoma, n = 102). The actual number of cell lines used for each analysis, which depends on the availability of proteomic, protein array, and drug sensitivity AUC data for the particular cell line, is indicated in the figure legend.

Statistical analysis

Statistical analyses were performed using Prism 8 (GraphPad Software, San Diego, CA). Venn diagrams were constructed using R software (version 4.0.5; http://www.r-project.org) with the ggVennDiagram package. Two-tailed Student's t-test was used to assess comparisons between two independent groups. One-way analysis of variance (ANOVA) followed by Tukey's multiple comparison test was used for multiple comparison analyses. $P < 0.05$ was considered statistically significant.

III. Results

Part I: Stabilization of METTL3 by PIN1 promotes breast tumorigenesis via enhanced m^{6}A-dependent translation

1. Increased PIN1 expression in breast cancer is associated with METTL3 overexpression

Given that PIN1 expression is significantly increased in breast cancer, we examined the correlation between the expression of several genes with PIN1 in The Cancer Genome Atlas (TCGA) Pan-Cancer Atlas. We then performed the functional classification of the most significant hits ($p > 0.5$, q-value < 0.1) using the Database for Annotation, Visualization, and Integrated Discovery (DAVID) (https://david.ncifcrf.gov/, version 6.8). The genetic correlation data produced by DAVID showed that genes involved in RNA processing, splicing, and translation were significantly correlated with PIN1 expression in breast cancer patients, along with genes involved in transcription, apoptosis, and protein transport (Figures 1a and b). As epitranscriptomic modification via RNA methylation has emerged as a crucial regulator of RNA processing, we examined the correlation between the protein expression of several RNA methyltransferases and *PIN1* in the TCGA Pan-Cancer Atlas. The protein expression of METTL3 was most significantly correlated with *PIN1* expression (Figures 1c and d). A negative CERES dependency score revealed that both METTL3 and PIN1 were essential for the survival of breast cancer cells, indicating their function as oncogenes (Figure 1e). The immunohistochemistry (IHC) staining of tumor samples from breast cancer patients and normal adjacent tissue revealed that PIN1 and METTL3 expression were significantly increased in breast tumors compared to normal tissue (Figure 1f–h). Furthermore, METTL3 expression increased with tumor progression (Figure 1i). The linear trend between the IHC scores of PIN1 and METTL3 was positively correlated with the expression of METTL3 and PIN1 in the breast cancer tissue (Figure 1j). Together, these data indicate that increased PIN1 expression in breast cancer is associated with the overexpression of METTL3.

Figure 1 (a-b)

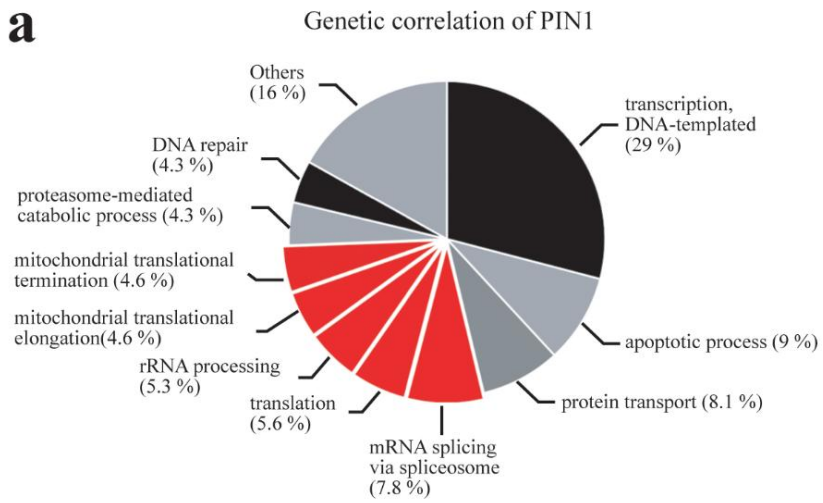

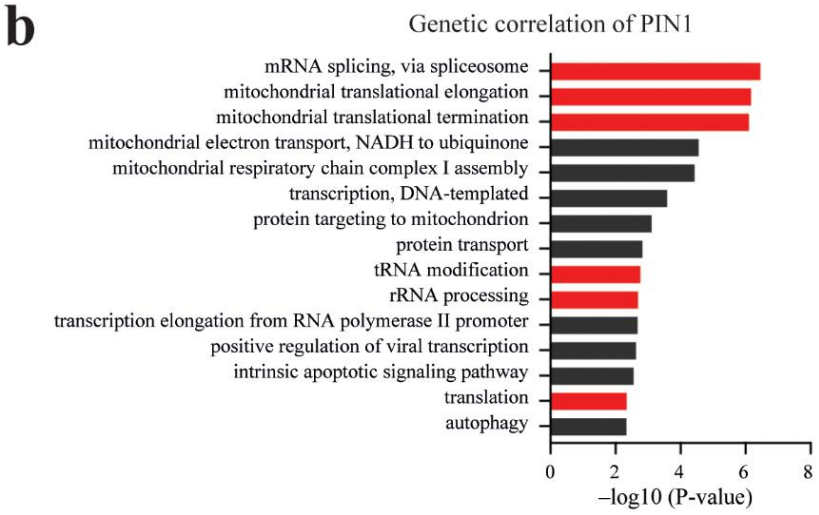

Figure 1 (c-e)

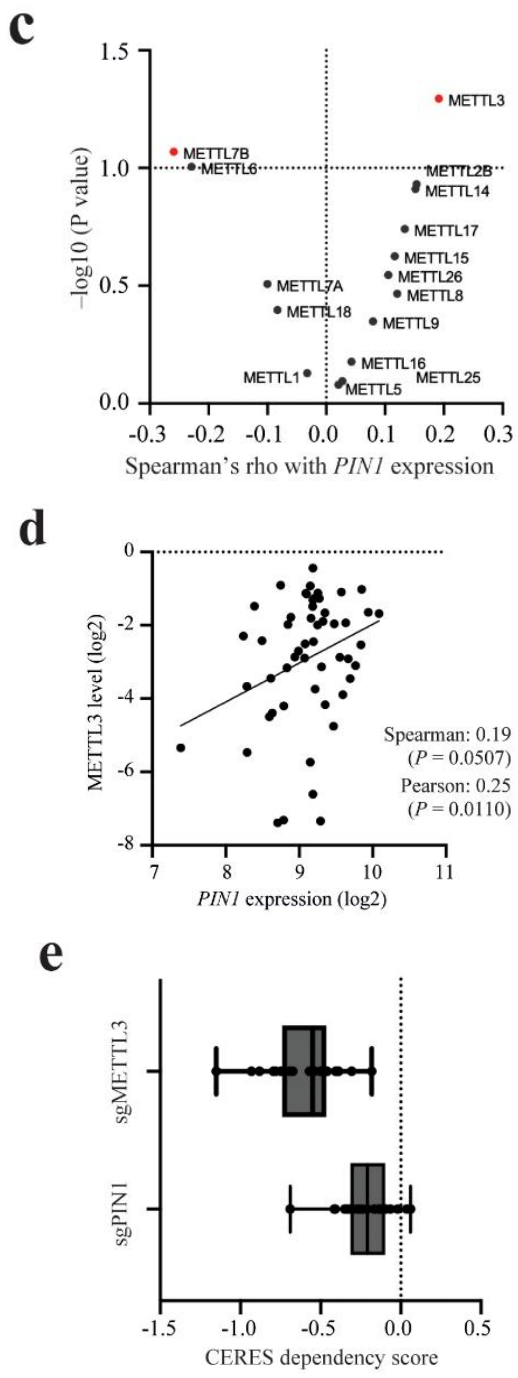

Figure 1 (f-j)

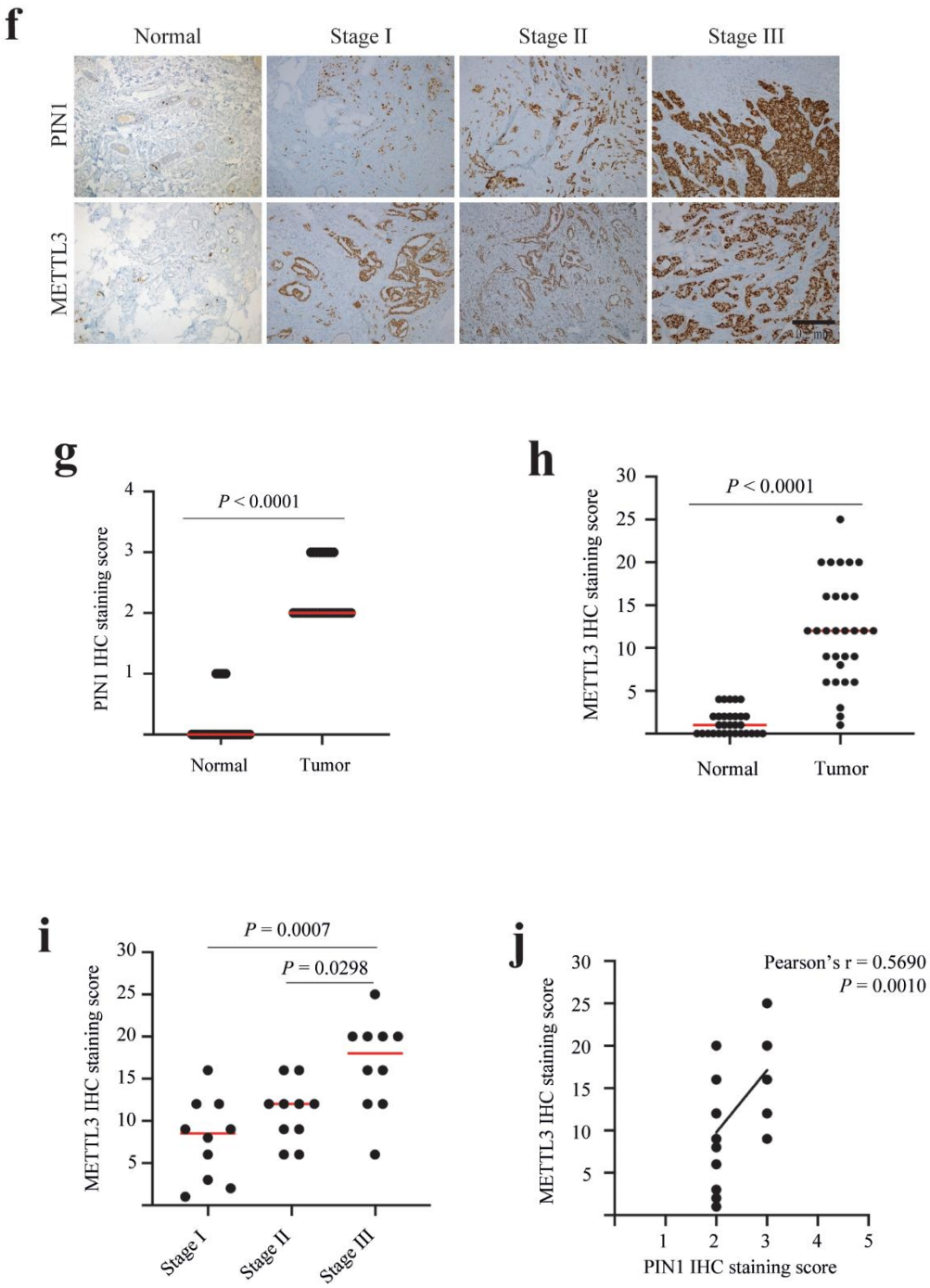

Figure 1. PIN1 expression is elevated and positively correlated with METTL3 abundance in human breast cancer

a, b Gene ontology (GO) enrichment analysis of genes significantly correlated ($p > 0.5$ and q-value < 0.1) with *PIN1* expression in breast cancer patients obtained from the TCGA Pan-Cancer Atlas. Proportions of significantly correlated genes based on biological processes (**a**), and the statistical significance of highly correlated biological processes (**b**). N = 1082 samples. The categories related to RNA processing and translation are highlighted in red. **c, d** METTL3 protein expression was significantly correlated with *PIN1* expression in breast cancer patients. Volcano plot showing the protein expression of several RNA methyltransferases and their correlation with *PIN1* mRNA expression in breast cancer patients as determined from the TCGA Pan-Cancer Atlas (**c**). N = 105 tumor samples. Significant correlations ($p < 0.05$) are shown in red. Protein expression was determined using quantitative mass spectrometry. Expression correlation between *PIN1* mRNA and METTL3 protein in breast cancer patients obtained from TCGA Pan-Cancer Atlas (**d**). Each dot represents a tumor sample. The correlation coefficients and significance (*p*-values) are shown in the graph. N = 105 samples. **e** Dependency of breast cancer cells on PIN1 and METTL3. Box plot showing the effect of the CRISPR-mediated depletion of METTL3 or PIN1 in a panel of breast cancer cell lines determined using the CERES project of DepMap. A negative dependency score indicated that the gene was essential for the survival of cancer cells. N = 25 cell lines. **f–i** Immunohistochemical (IHC) analysis of primary invasive breast carcinoma and adjacent normal tissue. Representative images of IHC staining of tumors and adjacent normal tissues using anti-PIN1 and anti-METTL3 antibodies (**f**). IHC scoring of PIN1 (**g**) and METTL3 (**h**) in normal and tumor tissues. Values are presented as mean ± standard deviation (SD), N = 30. Unpaired *t*-test. *p*-values are indicated in each figure. IHC scoring of METTL3 according to tumor stage (**i**). Values are presented as mean ± SD. N = 10. One-way analysis of variance (ANOVA). The *p*-value is indicated in the figure. Correlation

between METTL3 and PIN1 IHC scores in tumors at all stages (**j**). N = 30. Pearson's correlation coefficient (r) and *p*-value are indicated in the figure.

2. PIN1 interacts with METTL3 in a phosphorylation-dependent manner

To identify the m^{6}A-related proteins that may be associated with PIN1, we screened for interactions between PIN1 and m^{6}A writers and erasers using a mammalian two-hybrid (M2H) analysis. The relative luciferase activity resulting from hybridization was significantly increased between PIN1 and m^{6}A writer proteins, but not with the m^{6}A demethylase fat mass- and obesity-associated protein. METTL3 exhibited the strongest hybridization **(**Figure 2a**)**. As m^{6}A writer proteins are often present in the form of a methyltransferase complex, we performed an *in vitro* nickel-nitrilotriacetic acid (Ni-NTA) pulldown assay to identify the direct binding partners of PIN1. METTL3, but not METTL14 or WTAP, physically interacted with PIN1 (Figure 2b). To further verify this interaction, we performed an *in vitro* binding assay. The co-transfection of FLAG-METTL3 and XP-PIN1 into HEK293 cells followed by immunoprecipitation revealed that PIN1 co-immunoprecipitated with METTL3 and vice versa (Figure 2c). To map the PIN1 domain that interacts with METTL3, we performed a glutathione S-transferase (GST) pulldown assay using GST-PIN1 as the bait protein. The PPIase domain of PIN1, but not the WW domain, interacted with METTL3 (Figure 2d). As phosphorylation at the serine/threonine-proline (S/T-P) motif of the substrate protein was essential for its interaction with PIN1, we performed a GST pulldown assay after dephosphorylating METTL3 with alkaline phosphatase. Dephosphorylation abolished the binding of METTL3 to PIN1, indicating a phosphorylation-dependent interaction (Figure 2e). To further verify this interaction, serum-starved MCF7 cells were treated with 10% fetal bovine serum (FBS) to induce global protein phosphorylation. The lysate was used for the GST pulldown assay using GST-PIN1 as bait. The FBS stimulation increased the interaction of METTL3 with PIN1 in a time-dependent manner, indicating that the METTL3-PIN1 interaction is dependent on the FBS-induced phosphorylation of METTL3 (Figure 2f). To identify the METTL3 phosphorylation sites critical for binding with PIN1, S or T residues followed by a P were replaced with alanine (A) (denoted as S43A, S50A, T106A, T348A, and S525A). A Ni-NTA pulldown assay was performed with His-PIN1. The S525A mutation abolished the

interaction of METTL3 with PIN1, indicating that the SP site located at S525 in METTL3 is essential for its interaction with PIN1 (Figure 2g). Furthermore, the SP site at S525 is evolutionarily conserved across different species (Figure 2h). As circRNA-based reporter assays have shown that mitogen-activated protein (MAP) kinase/extracellular signal-regulated kinase (ERK) kinase 1/2 (MEK1/2), c-Jun N-terminal kinase (JNK) 2, and MAP3K8 regulate METTL3 function (Sun et al., 2020), we examined the interaction between PIN1 and METTL3 in MCF7 cells after treatment with specific inhibitors of these kinases. Treatment with PD98059, an inhibitor of MEK1/2, significantly reduced the interaction between METTL3 and PIN1, suggesting that their interaction is modulated by the activity of the MEK/ERK pathway (Figure 2i). In support of the *in vitro* binding results, the FBS stimulation increased the interaction between endogenous PIN1 and METTL3 (Figure 2j). Finally, we examined the METTL3-PIN1 interaction using a bimolecular fluorescence complementation (BiFC) assay. The BiFC analysis revealed that increased complementation occurred in MCF7 cells transfected with pBiFC-METTL3 wild-type (WT), but not its mutant METTL3-S525A, and pBiFC-VC-PIN1 after the FBS stimulation, as evidenced by a significant increase in mVenus-positive cells (Figures 2k and l). The complementation was predominantly localized in the nucleus. (Figure 2k). These results suggest that the phosphorylation of METTL3 at the S525 residue, induced by the MEK/ERK kinases, promotes its interaction with the PPIase domain of PIN1 in the cell nucleus.

Figure 2 (a-b)

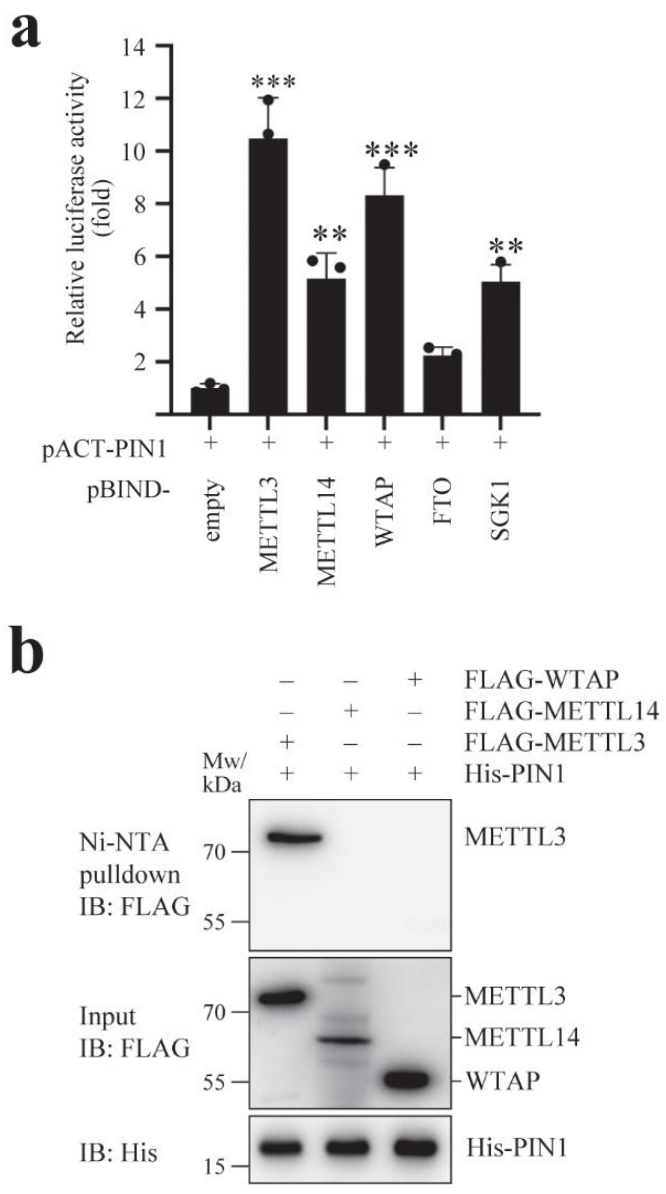

Figure 2 (c-d)

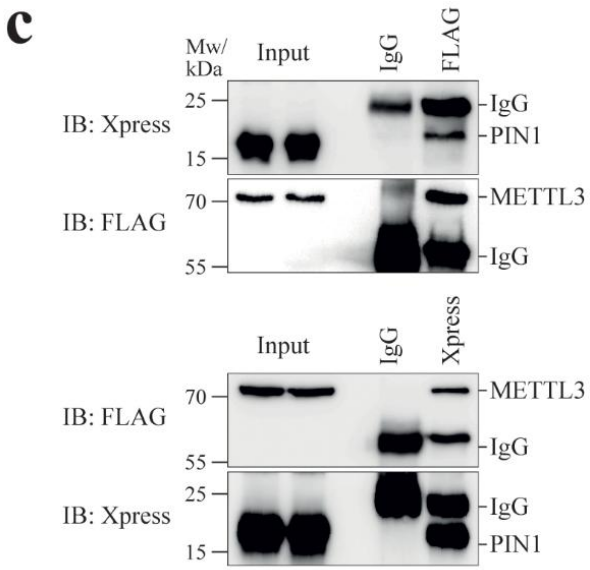

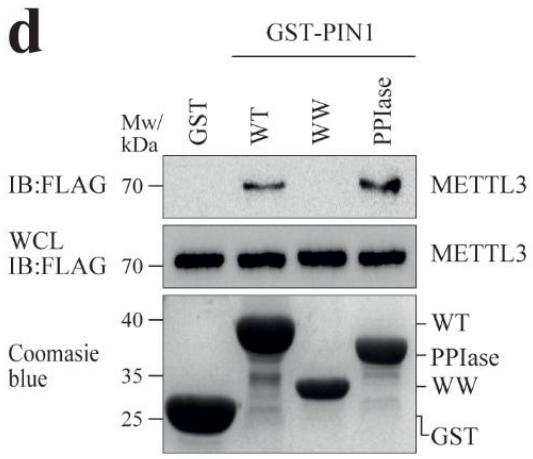

Figure 2 (e-f)

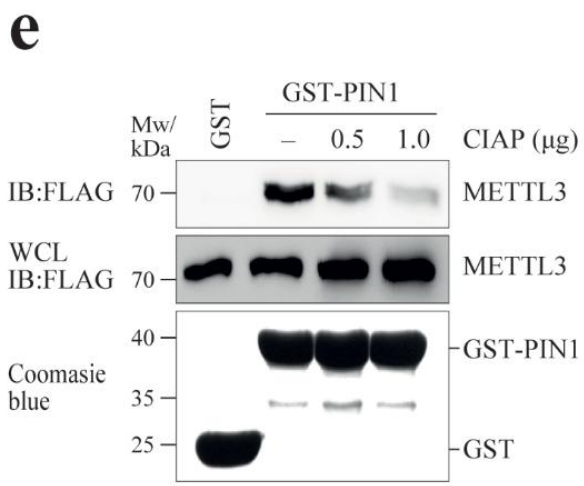

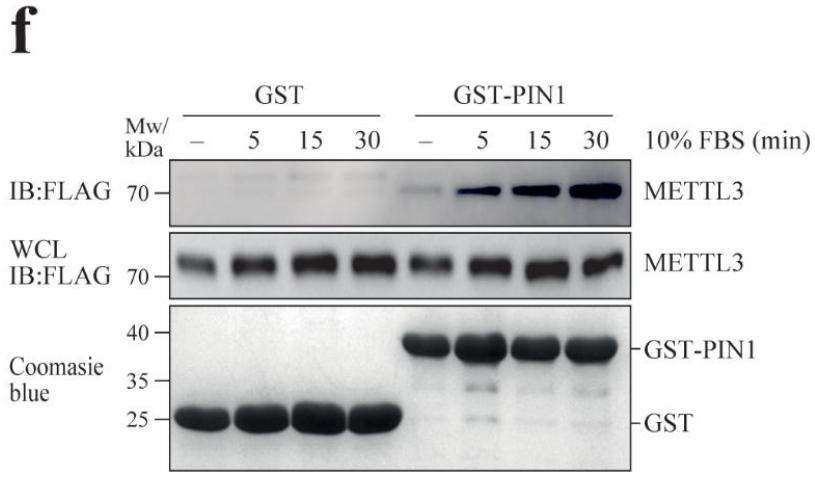

Figure 2 (g-j)

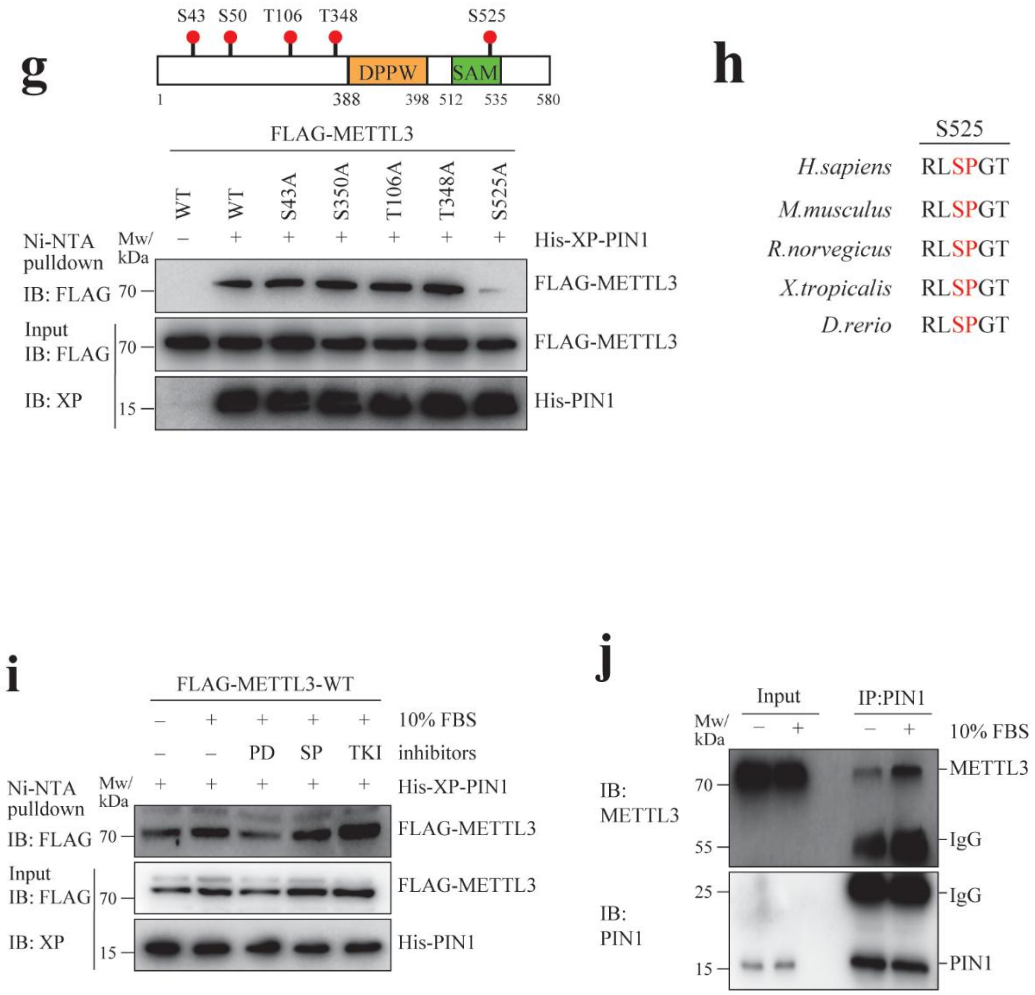

Figure 2 (k-l)

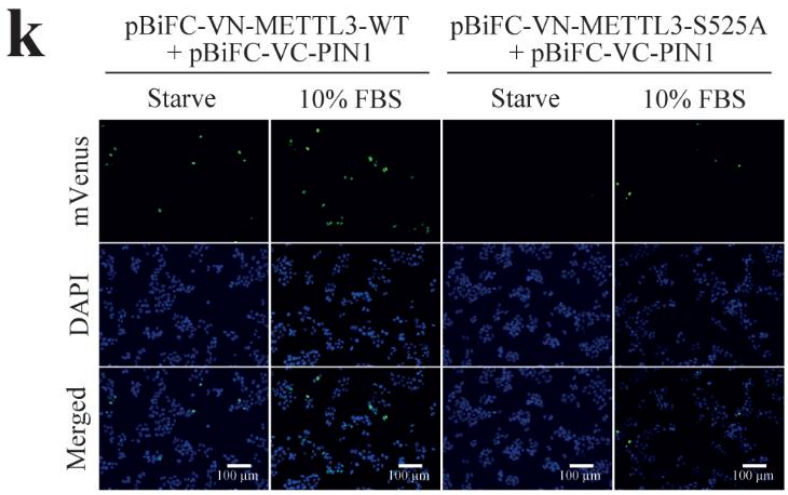

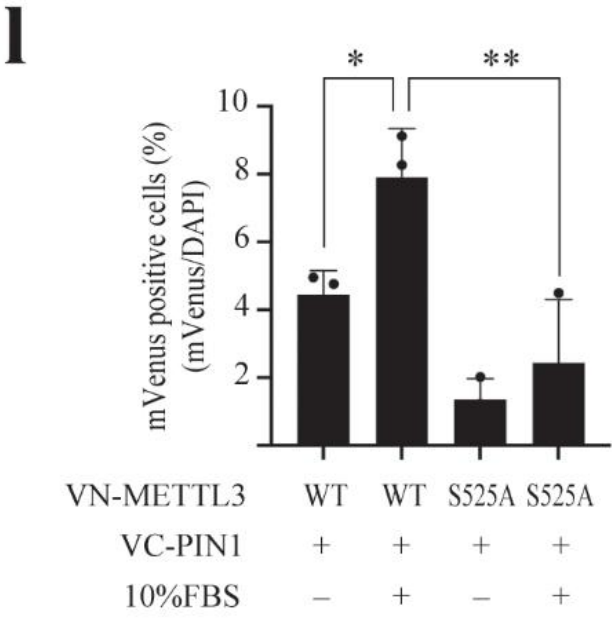

Figure 2. PIN1 interacts with METTL3 *via* its PPIase domain in a phosphorylation-dependent manner

a Screening of protein-protein interactions using the mammalian two-hybrid assay. pACT-PIN1 and pBIND plasmids were co-transfected with the pG5*luc* plasmid into HEK293 cells. Firefly luciferase activity in the lysate was measured and normalized against *Renilla* activity. pBIND-SGK1 was included as a known binding partner for PIN1. Values are presented as mean ± SD, N = 3, one-way ANOVA, $^{**}p < 0.01$, $^{***}p < 0.001$. **b, c** PIN1 interacts with METTL3. His/Xpress-PIN1 expressed in HEK293 cells was pulled down using Ni-NTA resin and incubated with lysates from HEK293 cells expressing FLAG-METTL-3, -14, or WTAP, and the precipitated proteins were detected by immunoblotting (IB) using the indicated antibodies (**b**). Immunoprecipitation (IP) of HEK293 cells overexpressing FLAG-METTL3 and His/Xpress-PIN1 using FLAG (top) or Xpress (bottom) antibodies, followed by IB with the indicated antibodies. Normal mouse IgG was used as an isotype control (**c**). **d** The PPIase domain of PIN1 binds to METTL3. Lysates from HEK293 cells expressing FLAG-METTL3 were incubated with GST, GST-PIN1-WT, -WW, or -PPIase. Bound proteins were detected by IB using an anti-FLAG antibody. GST fusion proteins were stained with Coomassie Blue. **e, f** PIN1 interacts with METTL3 in a phosphorylation-dependent manner. Lysates from HEK293 cells expressing FLAG-METTL3 were treated with 0.5 or 1 unit of CIAP per microgram of protein at 37 °C for 1 h and used for the GST pulldown assay. Proteins bound to GST-PIN1 were detected by IB using an anti-FLAG antibody. GST fusion proteins were stained with the Coomassie stain (**e**). MCF7 cells were treated with 10% FBS for the indicated times, and the lysate was used for the GST pulldown assay using either GST or GST-PIN1. Proteins in the pulldown fraction and cell lysate were detected by IB using the indicated antibodies. GST fusion proteins were stained with Coomassie Blue **(f)**. **g** Schematic representation of the Ser/Thr-Pro motif in METTL3 (upper panel). Lysates from HEK293 cells expressing FLAG-METTL3-WT, -S43A, -S50A, -T106A, -T348A, -S525A, and His/Xpress-PIN1 were incubated with Ni-NTA resin followed by IB with an anti-FLAG antibody.

Cell lysates were analyzed by IB with the indicated antibodies. **h** Sequence alignment of the serine/threonine-proline (S/T-P) motif in METTL3. **i** Inhibition of MEK1/2, but not JNK1/2 and TPL2, suppresses METTL3-PIN1 binding. MCF7 cells were pretreated with PD98059 (MEK1/2 inhibitor, 10 μM), SP600125 (JNK inhibitor, 20 μM), or TKI (TPL2 kinase inhibitor, 20 μM) in serum-free media for 24 h and exposed to 10% FBS for 30 min. Lysates from cells were used for the Ni-NTA pulldown, and the proteins were detected using a FLAG antibody. Proteins in cell lysates were detected using the indicated antibodies. **j** Binding between endogenous METTL3 and PIN1 induced by FBS. IP of cell lysate from MCF7 cells serum-starved for 24 h, then exposed to 10% FBS using PIN1 antibody, followed by IB with the indicated antibodies. **k, l** Visualization of the METTL3-PIN1 interaction with bimolecular fluorescence complementation (BiFC). MCF7 cells transfected with the indicated BiFC plasmids were serum-starved for 24 h, followed by treatment with 10% FBS. Fluorescence examination of mVenus (green) and DAPI to detect nuclear DNA (blue) **(k)**. The population of mVenus-positive cells was counted using Fiji software (http://fiji. ac) (**l**). Values are presented as mean ± SD, N = 3, one-way ANOVA, $*p < 0.05$, $**p < 0.01$.

3. PIN1 promotes the METTL3 protein stability

To check whether the PIN1-METTL3 interaction regulates METTL3 expression, we examined METTL3 protein levels after the overexpression or knockout of PIN1 in breast cancer cells. The overexpression of PIN1 in MCF7 cells increased METTL3 protein expression, whereas its knockout with sgPIN1 reduced its expression (Figure 3a). To determine whether PIN1 regulates METTL3 expression at the transcriptional level, we examined METTL3 mRNA levels after the overexpression or knockout of PIN1. A real-time quantitative polymerase chain reaction (qPCR) analysis showed that PIN1 did not affect METTL3 mRNA levels, indicating that PIN1 may regulate the stability of METTL3 (Figure 3b). Next, we examined the effects of PIN1 on METTL3 expression in response to FBS stimulation. FBS-induced METTL3 expression was significantly increased in PIN1-overexpressing MCF7 cells, suggesting that PIN1 enhanced the FBS-induced expression of METTL3 (Figures 3c and d). Since the interaction between METTL3 and PIN1 is dependent on the phosphorylation of METTL3 at S525, we examined the relative protein expression of METTL3-WT and METTL3-S525A after the transient transfection of the corresponding plasmids into MCF7 cells. METTL3-WT showed a higher expression level than METTL3-S525A (Figure 3e). In addition, FBS starvation significantly reduced the protein expression of both forms, which was rescued upon FBS stimulation for METTL3-WT, but not METTL3-S525A (Figure 3e). These results indicate that METTL3 phosphorylation at S525, the site responsible for binding PIN1, is essential for regulating FBS-induced METTL3 protein expression. To examine the effect of PIN1 on METTL3 stability, protein synthesis was inhibited by cycloheximide treatment. The degradation of METTL3-WT and METTL3-S525A was determined by immunoblotting. The protein half-life of METTL3-S525 was significantly reduced by cycloheximide treatment compared with that of METTL3-WT (Figures 3f and g). Given that protein stability is regulated via the proteasomal and lysosomal degradation pathways,

we examined the precise mechanism underlying the regulation of METTL3 stability by PIN1. Treatment with MG132 elevated the levels of METTL3 in PIN1-overexpressing MCF7 cells (Figure 3h, left panel). In contrast, the reduced METTL3 expression resulting from the PIN1 knockout was rescued by MG132 treatment, indicating that PIN1 prevents the proteasomal degradation of METTL3 to increase its stability (Figure 3h, right panel). As MCF7 cells have increased lysosomal function, we also examined the lysosome-mediated degradation of METTL3. Interestingly, the treatment with chloroquine, an inhibitor of lysosomes, further elevated the expression of METTL3 in PIN1-overexpressing MCF7 cells (Figure 3i, left panel). In contrast, the reduced METTL3 levels in PIN1-knockout cells were augmented by chloroquine treatment (Figure 3i, right panel). The simultaneous inhibition of proteasomal and lysosomal degradation by co-treatment with MG132 and chloroquine synergistically enhanced METTL3 levels in MCF7 cells (Figure 3j), which were augmented in PIN1-overexpressing cells (Figure 3k). These data indicate that PIN1 reduces the proteasomal and lysosomal degradation of METTL3 to increase its stability. Next, we examined the effect of FBS stimulation on METTL3 degradation. METTL3 expression, which was increased by FBS treatment, was enhanced by co-treatment with MG132 and CHQ (Figure 3l). As proteasomal degradation is mediated by protein ubiquitination, we next examined the ubiquitination of METTL3 in PIN1-knockout cells. The knockout of PIN1 in MCF7 cells increased the polyubiquitination of METTL3, suggesting that PIN1 prevents METTL3 ubiquitination (Figure 3m). Furthermore, the decreased expression of METTL3 by GFP-LC3 overexpression was inhibited by the ectopic expression of PIN1, suggesting that PIN1 prevents the lysosomal degradation of METTL3 facilitated by autophagosomes (Figure 3n).

Figure 3 (a-b)

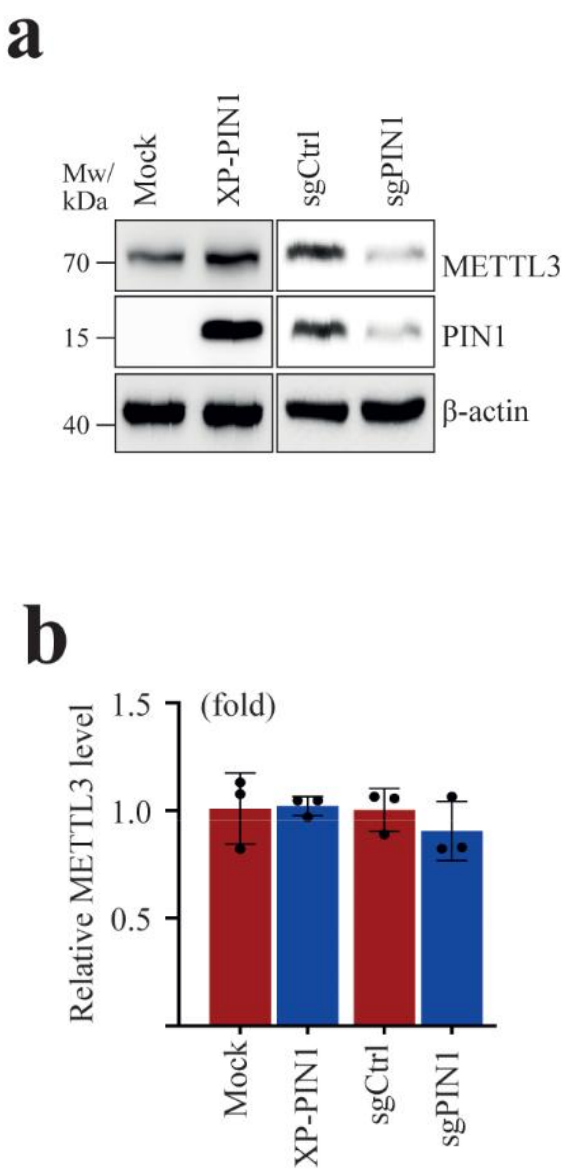

Figure 3 (c-e)

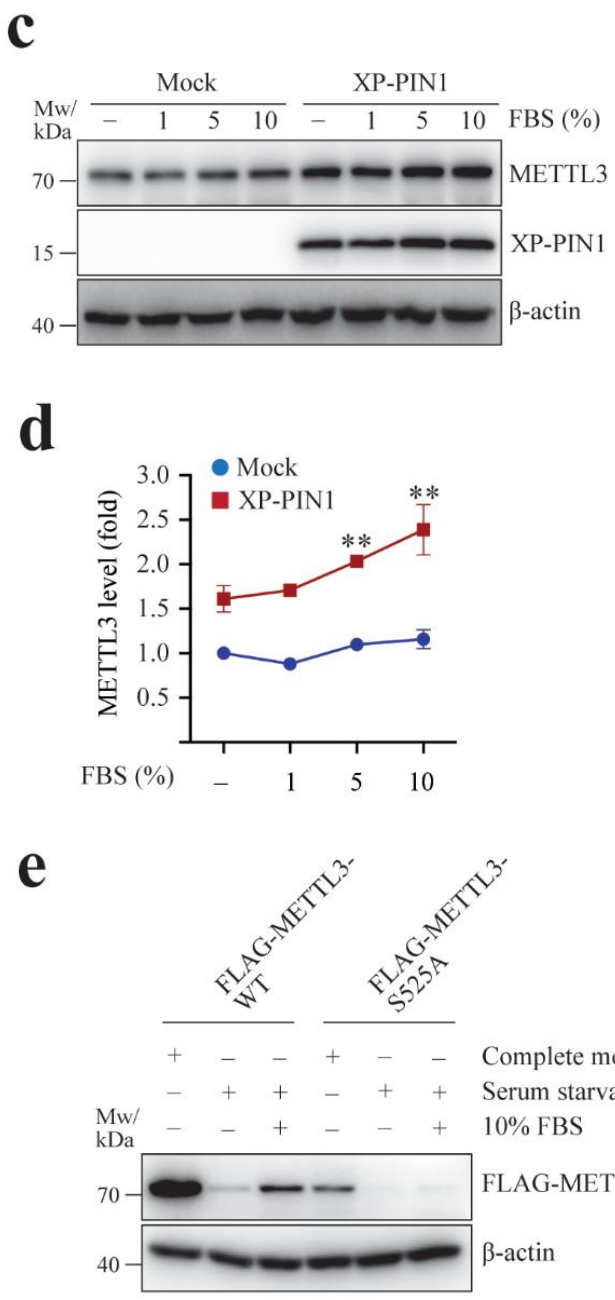

Figure 3 (f-g)

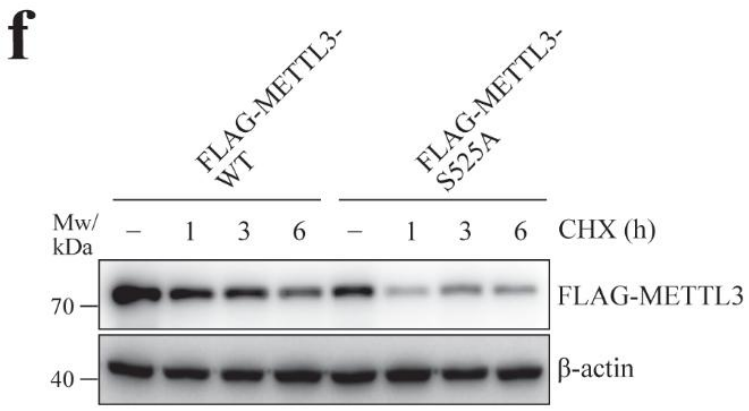

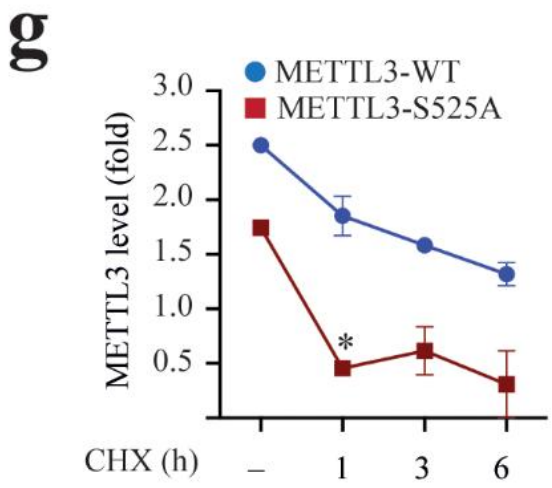

Figure 3 (h-i)

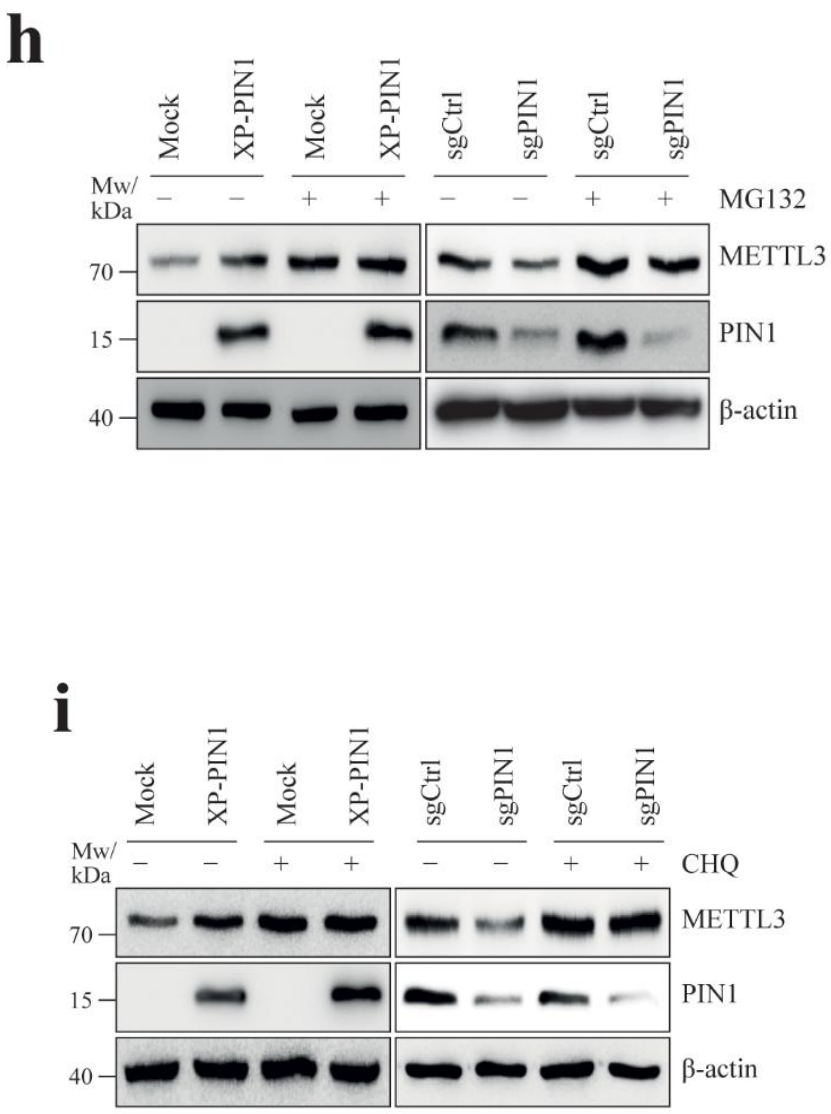

Figure 3 (j-l)

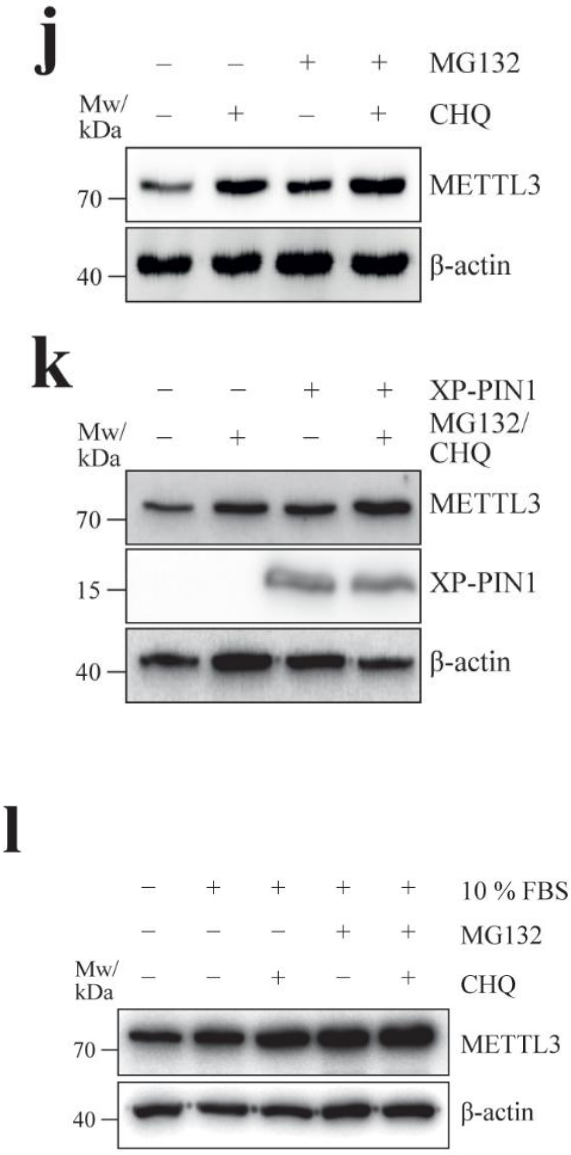

Figure 3 (m-n)

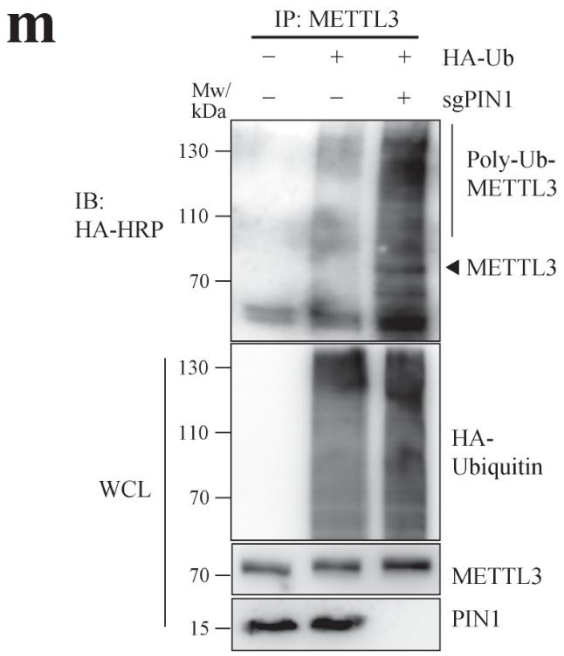

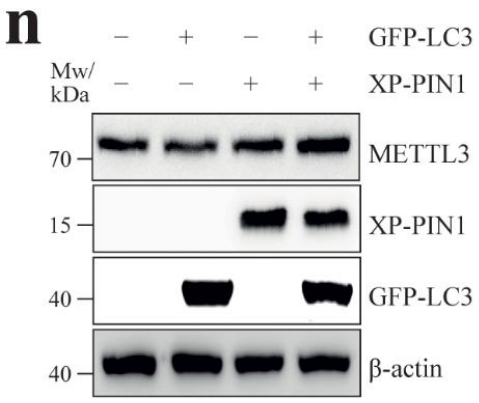

Figure 3. PIN1 enhances METTL3 stability by reducing its ubiquitination and lysosomal degradation

a, b PIN1 increases protein, but not mRNA, levels of METTL3. IB of MCF7 cells transfected with mock or XP-PIN1 (left) and sgCtrl or sgPIN1 (right) as detected using the indicated antibodies (**a**). mRNA expression levels in MCF7 cells transfected with mock or XP-PIN1 and sgCtrl or sgPIN1 were measured using real-time RT-PCR with primers targeting the indicated genes (**b**). Values are presented as mean ± SD, N = 3. **c, d** PIN1 enhances METTL3 expression induced by FBS stimulation. MCF7 cells transfected with mock or XP-PIN1 were serum-starved for 24 h and exposed to different percentages of FBS for 30 min followed by IB with the indicated antibodies (**c**). Band densities were quantified using ImageJ and normalized to those of β-actin (**d**). Values represent mean ± SD, N = 3. Unpaired *t*-test, $^{**}p < 0.01$ (mock versus XP-PIN1, corresponding FBS percentages). **e** FBS stimulation regulated the expression of WT METTL3 but not the S525A mutant. MCF7 cells transfected with FLAG-METTL3-WT or FLAG-METTL3-S525A were grown in either complete media or serum-free media for 24 h. Serum-starved cells were then exposed to 10% FBS for 30 min. Proteins in cell lysates were detected using the indicated antibodies. **f, g** METTL3-S525A had a shorter half-life than METTL3-WT. MCF7 cells expressing FLAG-METTL3-WT or FLAG-METTL3-S525A were treated with cycloheximide (CHX, 100 μg/mL) for the indicated times. The proteins in cell lysates were detected with IB using the indicated antibodies **(f)**. The band densities were measured using ImageJ and normalized to those of β-actin **(g)**. Values are mean ± SD, N = 3, unpaired t-test, $^{*}p < 0.05$ (WT versus S525, corresponding to time). **h, i** The overexpression of PIN1 inhibits the proteasome-mediated and lysosomal degradation of METTL3. IB of MCF7 cells transfected with mock or XP-PIN1 (left) and sgCtrl or sgPIN1 (right) and treated (+) or untreated (–) with MG132 (20 μM) for 3 h as detected using the indicated antibodies (h). IB of MCF7 cells transfected with mock, XP-PIN1, sgCtrl, or sgPIN1 and treated (+) or untreated (-) with chloroquine (CHQ, 100 μg/mL) for 3 h, as detected using the indicated antibodies (i). **j** Synergistic enhancement

of METTL3 stability by the dual inhibition of the proteasomal and lysosomal degradation pathways. IB of MCF7 cells treated (+) or untreated (–) with MG132 or CHQ for 3h as detected using the indicated antibodies. **k** The overexpression of PIN1 rescues METTL3 stability by the simultaneous inhibition of the lysosomal and proteasomal degradation of METTL3. MCF7 cells transfected with XP-PIN1 were treated (+) or untreated (−) with MG132 and CHQ for 3 h. Proteins in the cell lysates were detected by IB using the indicated antibodies. **l** Synergistic enhancement of METTL3 stability induced by FBS stimulation and the dual inhibition of the proteasomal and lysosomal degradation pathways. MCF7 cells were serum-starved for 24 h and pretreated with MG132 and/or CHQ for 3 h followed by stimulation with 10% FBS for 30 min. Proteins in the cell lysates were detected by IB using the indicated antibodies. **m** PIN1 prevented the polyubiquitination of METTL3. MCF7 cells co-transfected with sgPIN1 and HA-Ub were pretreated with MG132 (20 μM) for 3 h, followed by IP with anti-METTL3 and IB with HA-HRP antibodies. Cell lysates were detected by IB using the indicated antibodies. **n** PIN1 inhibits the autophagosome-mediated lysosomal degradation of METTL3. MCF7 cells were co-transfected with GFP-LC3 and/or XP-PIN1, followed by IB with the indicated antibodies

4. PIN1 enhances the m^{6}A modification of TAZ and EGFR mediated by METTL3

As METTL3 is associated with the m^{6}A modification of mRNA, we examined the effect of PIN1 on the m^{6}A levels induced by METTL3. An analysis of poly(A) RNA using an enzyme-linked immunosorbent assay (ELISA) and dot blotting revealed that PIN1 overexpression in MCF7 cells increased m^{6}A levels (Figure 4a), whereas the knockout of METTL3 attenuated the m^{6}A modification induced by PIN1 overexpression (Figure 4b). Additionally, stimulation with FBS synergistically increased the m^{6}A level in PIN1-overexpressing MCF7 cells, which was inhibited by the knockout of METTL3 (Figure 4c). These data indicate that PIN1 increases m^{6}A levels via the enhanced stability of METTL3. As the DepMap data showed that PIN1 expression is positively correlated with TAZ and EGFR protein expression in breast cancer cell, we decided to examine whether PIN1 regulates TAZ and EGFR expression by affecting METTL3-induced m^{6}A modification of their mRNAs. To examine the regulatory role of the PIN1/METTL3 axis in the m^{6}A modification of specific mRNA, we performed methylated RNA immunoprecipitation followed by reverse transcription (RT)-PCR (m^{6}A-RIP-RT-PCR). As expected, the overexpression of PIN1 in MCF7 cells increased the m^{6}A modification of *TAZ* and *EGFR* mRNA (Figure 4d), whereas the knockout of PIN1 in MCF7 cells reduced the m^{6}A modification (Figure 4e). The knockout of METTL3 further abolished the enhanced m^{6}A modification of *TAZ* and *EGFR* induced by the overexpression of PIN1 (Figure 4f). To further ascertain the regulatory role of PIN1 in the m^{6}A modification of *TAZ* and *EGFR*, we knocked out METTL3 in MCF7 cells and ectopically expressed METTL3-WT and METTL3-S525A. The m^{6}A-RIP-RT-PCR analysis revealed that the ectopic expression of METTL3-WT restored the m^{6}A modification of *TAZ* and *EGFR*, whereas the expression of PIN1 binding-deficient METTL3-S525A failed to restore the m^{6}A modification (Figure 4g). The overexpression of PIN1 further increased the m^{6}A modification of *TAZ* and *EGFR* in MCF7 cells treated with FBS, but not in serum-starved cells

(Figures 4h and i), implying that the phosphorylation-dependent stabilization of METTL3 by PIN1 increases the m^6A modification of *TAZ* and *EGFR* mRNA.

Figure 4 (a-c)

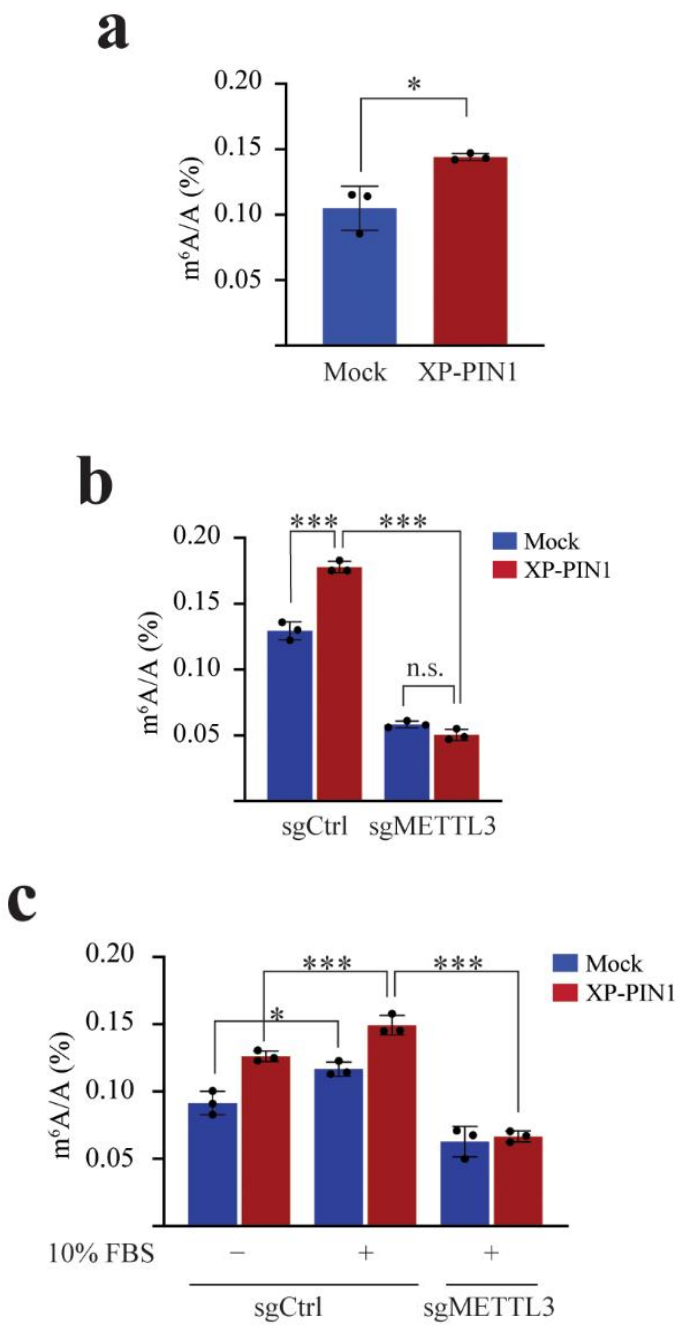

Figure 4 (d-g)

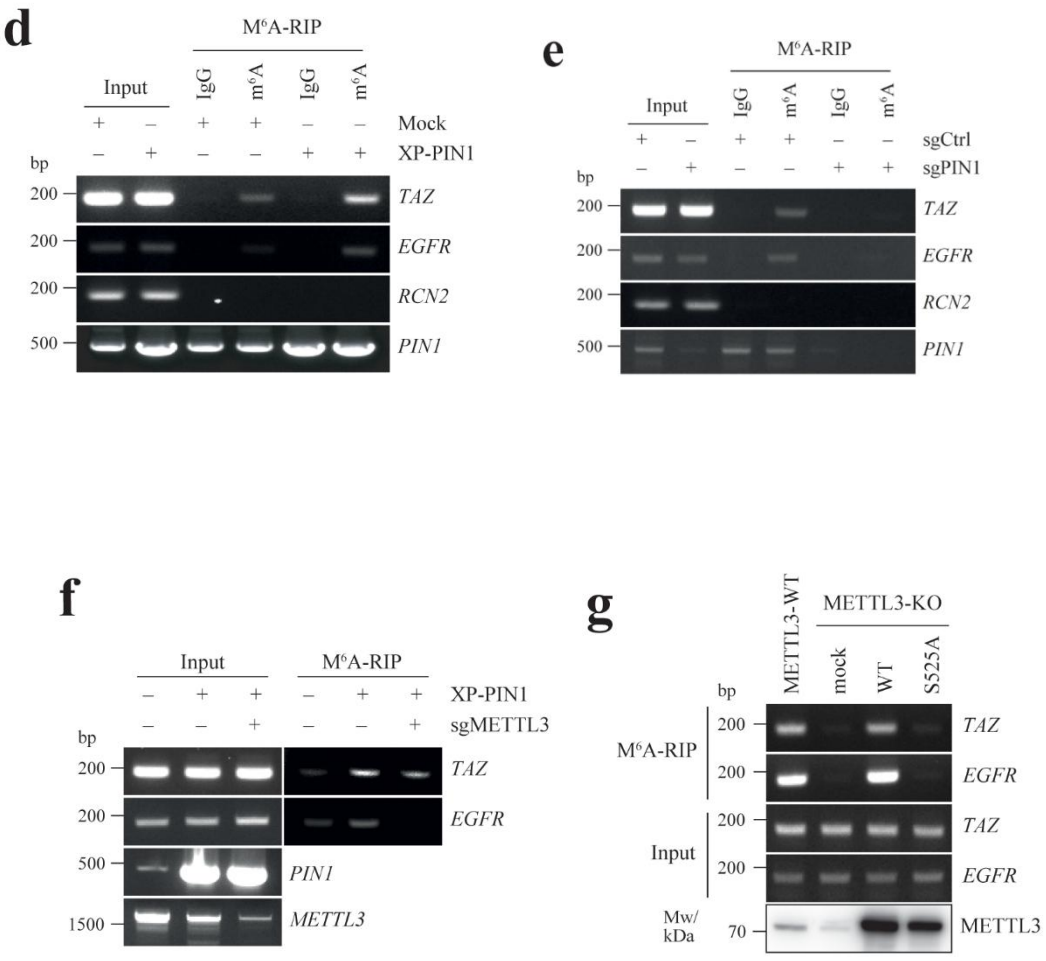

Figure 4 (h-i)

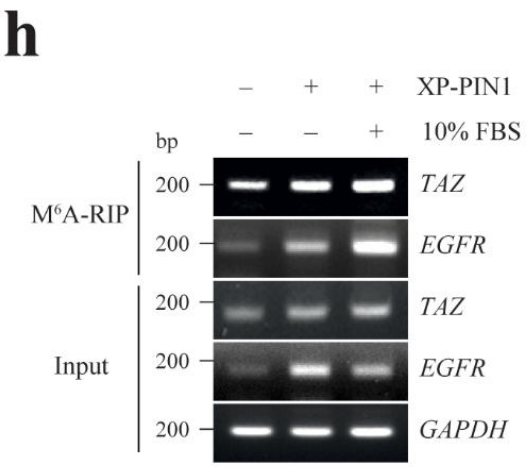

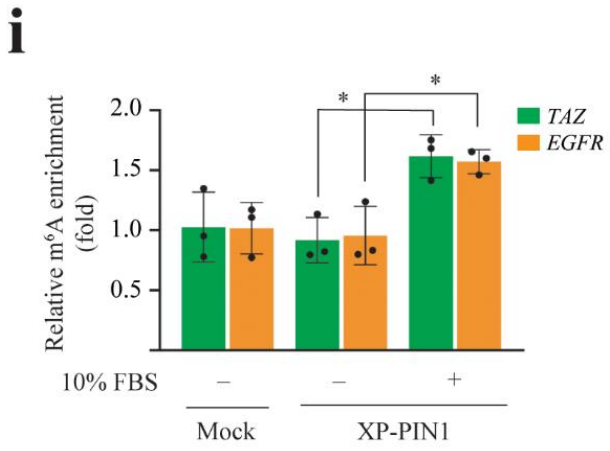

Figure 4. PIN1 promotes the m^{6}A modification of *TAZ* and *EGFR*

a PIN1 overexpression increases global m^{6}A levels. Quantification of m^{6}A levels in MCF7 cells transfected with mock or XP-PIN1 was performed using ELISA. Values are presented as the mean ± SD, N = 3. Unpaired *t*-test, *$p < 0.05$. **b** PIN1 increases the m^{6}A modification mediated by METTL3. PIN1-overexpressing MCF7 cells were transfected with sgCtrl or sgMETTL3. Global m^{6}A levels were measured using ELISA. Values are presented as the mean ± SD, N = 3. One-way ANOVA, ***$p < 0.05$. **c** PIN1 enhances m^{6}A levels induced by FBS stimulation via METTL3. PIN1-overexpressing MCF7 cells were transfected with sgCtrl or sgMETTL3, and serum-starved for 24 h, followed by treatment with 10% FBS for 30 min. The global m^{6}A levels were measured using ELISA. Values are presented as the mean ± SD, N = 3. One-way ANOVA, *$p < 0.05$, ***$p < 0.001$. **d–f** PIN1 increased the m^{6}A modification of *TAZ* and *EGFR* induced by METTL3. Total RNA isolated from MCF7 cells transfected with mock or XP-PIN1 was immunoprecipitated using anti-m^{6}A or normal IgG antibody. Gene expression in the input or IP fractions was analyzed by semi-quantitative RT-PCR with primers targeting the indicated genes (**d**). Total RNA isolated from MCF7 cells transfected with sgCtrl or sgPIN1 was immunoprecipitated using anti-m^{6}A or normal IgG antibody. Gene expression in the input or IP fractions was analyzed by semi-quantitative RT-PCR with primers targeting the indicated genes (**e**). PIN1-overexpressing MCF7 cells were transfected with either sgCtrl or sgMETTL3. Total RNA isolated from cells was immunoprecipitated using an anti-m^{6}A antibody, and gene expression in the input and IP fractions was analyzed by semi-quantitative RT-PCR with primers targeting the indicated genes (**f**). **g** WT METTL3, but not S525A, induced the m^{6}A modification of *TAZ* and *EGFR*. METTL3-knockout MCF7 cells were transfected with mock, FLAG-METTL3-WT, or FLAG-METTL3-S525A constructs. Total RNA isolated from cells was immunoprecipitated using an anti-m^{6}A antibody, and gene expression in the input and IP

fractions was analyzed by semi-quantitative RT-PCR with primers targeting the indicated genes. METTL3 expression was detected by IB using an anti-METTL3 antibody. **h, i** PIN1 enhanced the m^6A modification of *TAZ* and *EGFR* upon FBS stimulation. MCF7 cells overexpressing PIN1 were serum-starved for 24 h and exposed to 10% FBS for 30 min. Total RNA isolated from cells was immunoprecipitated using an anti-m^6A antibody. Gene expression in the input and IP fractions was analyzed by semi-quantitative RT-PCR **(h)**, and real-time RT-PCR **(i)** using primers targeting the indicated genes. Values are presented as the mean ± SD, N = 3, one-way ANOVA, $*p < 0.05$.

5. PIN1 promotes the m^{6}A-dependent translation of *TAZ* and *EGFR* via increased polysome assembly

As the m^{6}A modification of mRNA has the most significant effect on mRNA translation (Choe et al., 2018; Lin et al., 2016), we examined the effects of PIN1-induced m^{6}A modifications of *TAZ* and *EGFR* on translation efficiency. An analysis of previously published m^{6}A-RIP-RNA-seq data(Dominissini et al., 2013) revealed that m^{6}A sites were enriched in the 3' UTR region and around the stop codons of *TAZ* and *EGFR* mRNA [Figure 5a, integrated genomics viewer (IGV) plot].The examination of the nucleotide sequence showed the consensus m^{6}A motif "GGAC" located around the stop codon of the *TAZ* and *EGFR* mRNA (Figure 5a). To further examine the role of m^{6}A modification in translation, we designed translation reporter constructs by inserting the m^{6}A modification sites of *TAZ* and *EGFR* into the 3' UTR of the *Renilla* luciferase gene (RLuc) present in the psiCHECK3 vector (Figure 5a; left side, schematic diagram). The transfection of reporter vectors into MCF7 cells with PIN1 revealed that the overexpression of PIN1 increased the translation of *Renilla* luciferase containing m^{6}A sites derived from *TAZ* and *EGFR* but failed to increase the translation of the reporter gene without the m^{6}A sites (Figure 5b). Furthermore, the stimulation of the MCF7 cells with FBS significantly increased the translation of *Renilla* luciferase, which was attenuated by the knockout of PIN1, suggesting that PIN1 promotes the translation of *TAZ* and *EGFR* mRNA induced by m^{6}A modifications (Figure 5c). To further verify the regulatory role of PIN1 in mRNA translation, nascent protein synthesis in PIN1-knockout MCF7 cells was detected by the immunofluorescent staining of puromycilated proteins. The knockout of PIN1 significantly reduced the incorporation of puromycin into proteins, indicating that PIN1 is essential for the efficient translation of mRNA (Figures 5d and e). To examine whether the knockout of PIN1 reduces the translation efficiency of *TAZ* and *EGFR*, puromycilated EGFR and TAZ were immunoprecipitated with an anti-

puromycin antibody, followed by immunoblotting (IB) with specific antibodies recognizing the N-terminal regions of TAZ and EGFR. As expected, the knockout of PIN1 significantly reduced the levels of puromycilated TAZ and EGFR, indicating that PIN1 promoted the translation efficiency of *TAZ* and *EGFR* (Figures 5f and g). Given that METTL3 directly binds to m^6A-modified mRNA to facilitate mRNA loop formation and polysome assembly(Choe et al., 2018; Lin et al., 2016), we examined the interaction of METTL3 with *TAZ* and *EGFR* mRNA in PIN1-knockout MCF7 cells (Figure 5h). To check the mRNA-protein interactions, *TAZ* and *EGFR* mRNA tagged with the bacteriophage MS2 hairpin loop were precipitated with His-MS2BP using Ni-NTA resin. The METTL3 protein levels associated with corresponding mRNA were detected with IB. The knockout of PIN1 reduced the binding of METTL3 to *TAZ* and *EGFR* mRNA (Figure 5i). Furthermore, the sucrose-gradient fractionation of ribonucleoprotein complexes isolated from MCF7 cells revealed that the knockout of PIN1 significantly reduced translation efficiency, as evidenced by the simultaneous reduction of 40/60/80S and polysome peaks (Figure 5j). In addition, RT-PCR and real-time RT-PCR analyses of the ribosomal fractions showed that the distribution of *TAZ* and *EGFR* mRNA was significantly reduced in polysomal and monosomal fractions (40/60/80S) in PIN1-knockout MCF7 cells (Figures 5k and l). Moreover, the IB of the fractionated samples showed that the m7G cap-binding protein eIF4E, translation initiation factor eIF3 core subunit eIF3b, and METTL3 were shifted from polysomal to monosomal fractions in PIN1-knockout MCF7 cells, suggesting a facilitatory role of PIN1 in METTL3-mediated polysome assembly. Finally, we examined the effect of PIN1 on endogenous TAZ and EGFR expression. Consistent with previous results, the overexpression of PIN1 with FBS treatment significantly increased the expression of TAZ, EGFR, and METTL3 (Figure 5m). These data indicate that PIN1 enhances the translation efficiency induced by METTL3, resulting in increased TAZ and EGFR protein expression in breast cancer cells.

Figure 5 (a-c)

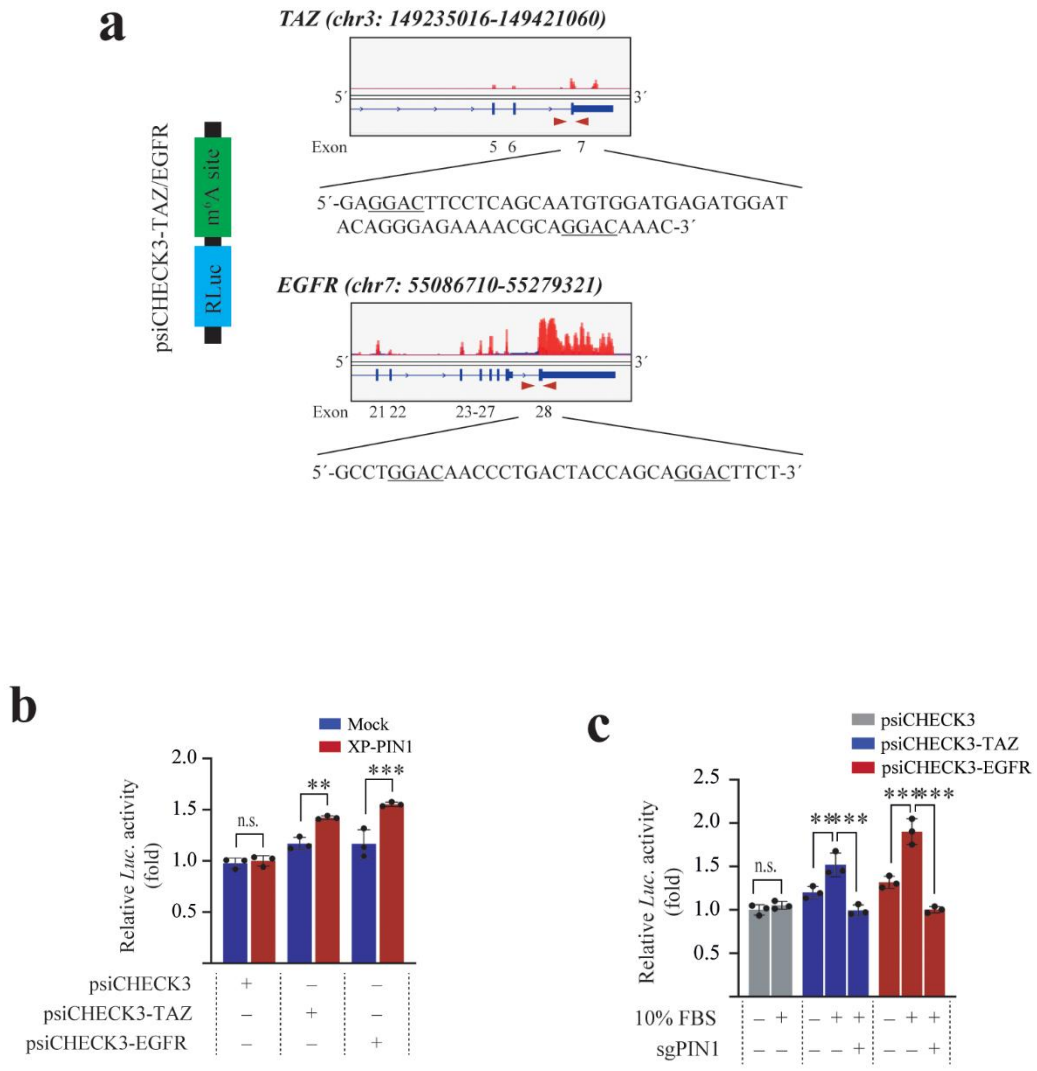

Figure 5 (d-g)

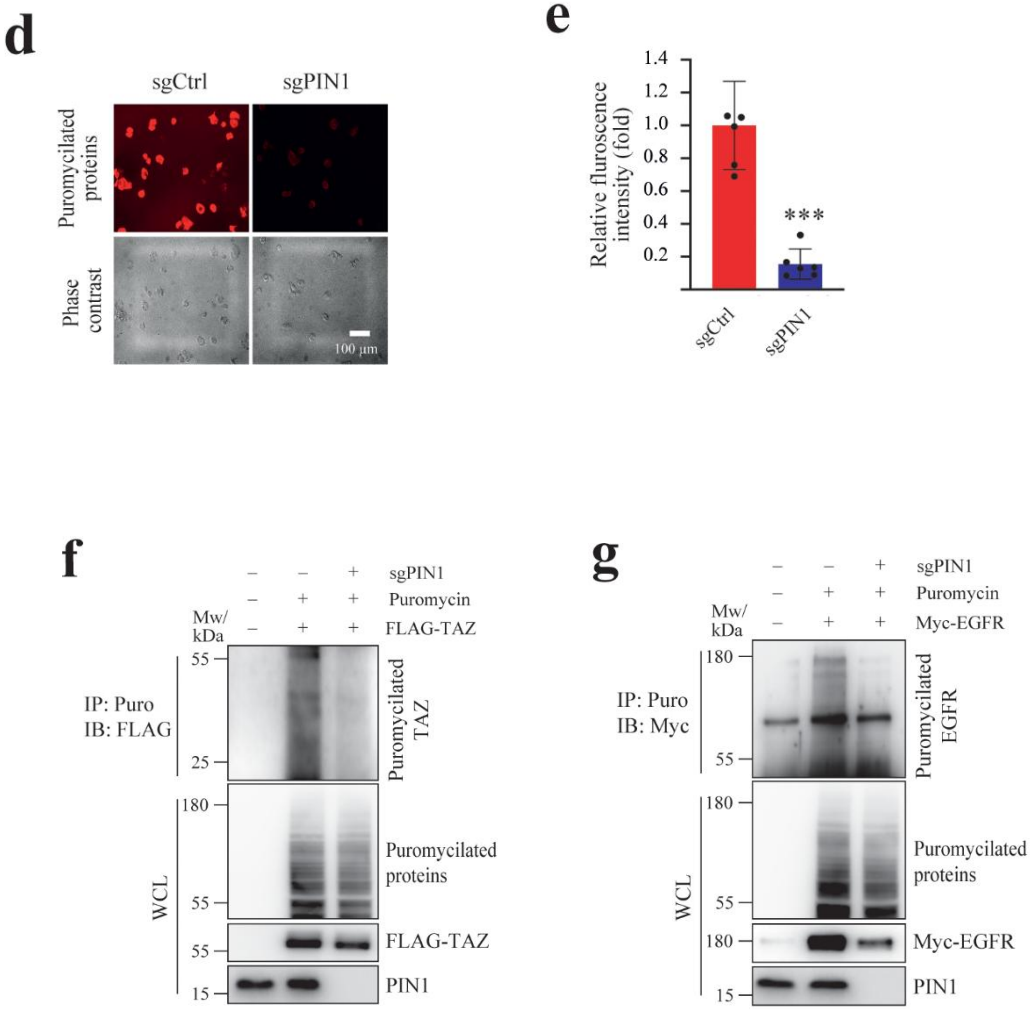

Figure 5 (h-j)

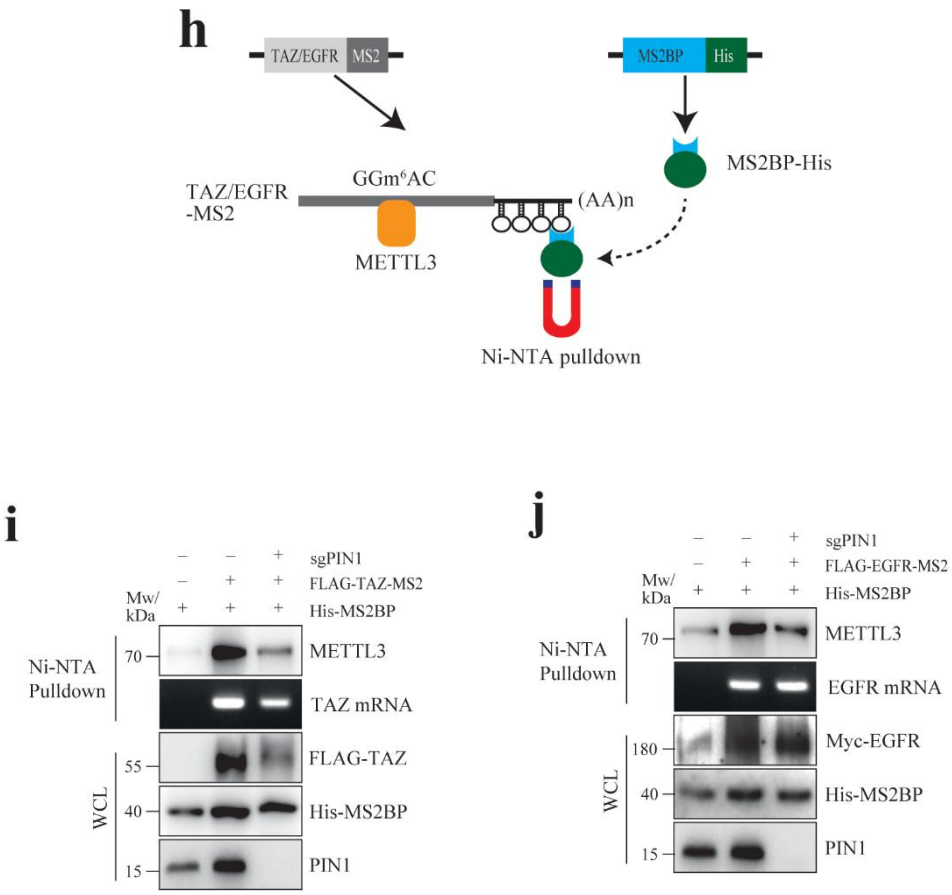

Figure 5 (k-m)

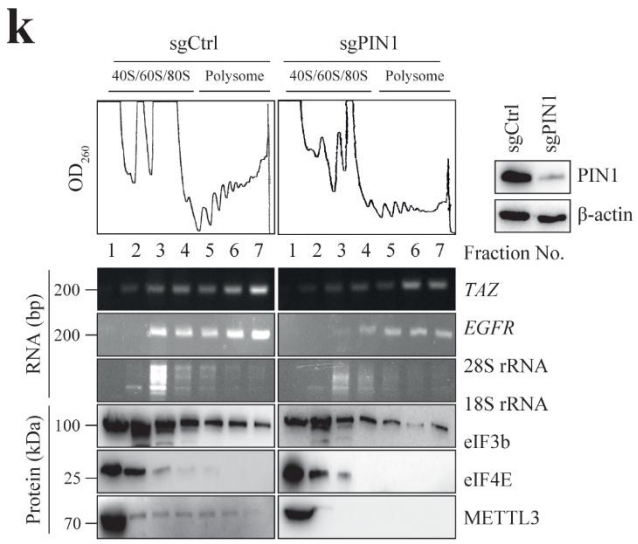

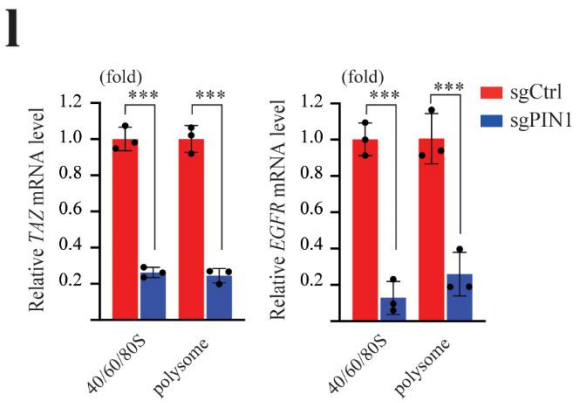

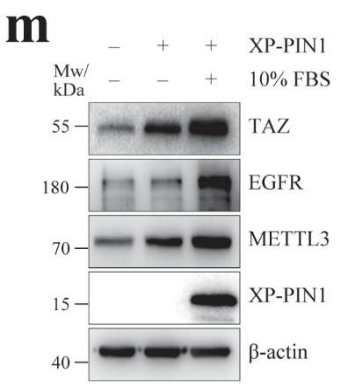

Figure 5. PIN1 promotes the m^{6}A-dependent translation of TAZ and EGFR via increased polysome assembly.

a Schematic representation of the psiCHECK3 translation reporter construct (left). Integrative Genomics Viewer (IGV) plots of m^{6}A peaks at *TAZ* (right, upper) and *EGFR* (right, lower) mRNA, as obtained from the published dataset. The blue boxes represent exons, blue lines represent introns, red histogram indicates the m^{6}A IP sample, and blue histogram indicates the input sample. The nucleotide sequence marked with arrowheads was PCR-amplified and cloned into the psiCHECK3 vector. The consensus m^{6}A modification motifs "GGAC" present in the m^{6}A sites are underlined and shown in each figure. **b** PIN1 promotes the m^{6}A-dependent translation of *TAZ* and *EGFR* mRNA in MCF7 cells. MCF7 cells were transfected with psiCHECK3, psiCHECK3-TAZ, or psiCHECK3-EGFR, with or without XP-PIN1. *Renilla* luciferase activity in lysates from transfected cells was measured and normalized to firefly luciferase activity. Values are presented as the mean ± SD, N = 3. One-way ANOVA, $^{**}p < 0.01$, $^{***}p < 0.001$. **c** FBS stimulation promotes the m^{6}A-mediated translation of TAZ and EGFR in a PIN1-dependent manner. MCF7 cells were transfected with psiCHECK3, psiCHECK3-TAZ, or psiCHECK3-EGFR, with or without sgPIN1, in FBS-free media. After 24 h, cells were exposed to 10% FBS for 1 h, and *Renilla* and firefly luciferase activities in the cell lysates were measured. *Renilla* activity was normalized to the firefly activity. Values are presented as the mean ± SD, N = 3. Unpaired *t*-test, $^{**}p < 0.01$, $^{***}p < 0.001$. **d, e** PIN1 knockout reduces nascent protein synthesis in MCF7 cells. MCF7 cells transfected with sgCtrl or sgPIN1 were treated with puromycin (2 μg/mL) for 2 h. Puromycilated nascent proteins were detected using immunofluorescence with an anti-puromycin antibody (red). The phase-contrast image was taken to visualize the cells (**d**). Fluorescence intensity produced by cells was quantified using Fiji software and is represented as relative fluorescence intensity (**e**). Values are presented as the

mean ± SD, N = 6. Unpaired *t*-test, ***$p < 0.001$. **f, g** PIN1 knockout reduces the puromycilation of TAZ and EGFR proteins. MCF7 cells transfected with FLAG-TAZ, sgCtrl, or sgPIN1 were treated with puromycin (2 μg/mL) for 1 h. Lysates from treated cells were immunoprecipitated with an anti-puromycin antibody, followed by IB with an anti-FLAG antibody (**f**). MCF7 cells transfected with Myc-EGFR, sgCtrl, or sgPIN1 were treated with puromycin (2 μg/μL) for 1 h. Cell lysates were immunoprecipitated with anti-puromycin antibody, followed by IB with anti-EGFR antibody (**g**). The cell lysate was detected by IB using the indicated antibodies. **h** Schematic diagram of the RNA pulldown assay using MS2. **i, j** PIN1 knockout reduced the association of METTL3 with *TAZ* and *EGFR* mRNA. MCF7 cells transfected with FLAG-TAZ-4XMS2 **(i)** or Myc-EGFR **(j)**, and His-MS2BP were irradiated with UV light. The ribonucleoprotein complex was pulled down with Ni-NTA resin, and the protein and mRNAs in pulldown and input fractions were analyzed with IB and RT-PCR using the indicated antibodies and primers, respectively. **k, l** PIN1 knockout reduced the polysome assembly and distribution of TAZ and EGFR mRNA in the polysome fraction. Lysates prepared from MCF7 cells transfected with sgCtrl or sgPIN1 were subjected to sucrose-gradient centrifugation. Fractionated samples were analyzed by IB and RT-PCR using the indicated antibodies and primers, respectively (**k**). Sub-polysome (fractions 1–4), and polysome (fractions 5–7) fractions were separately pooled, and the mRNA levels of TAZ and EGFR were analyzed using real-time RT-PCR (**l**). Values are presented as mean ± SD, N = 3. Unpaired *t*-test, ***$p < 0.001$. **m** PIN1 increased TAZ and EGFR protein expression induced by FBS. PIN1-overexpressing MCF7 cells were serum-starved for 24 h and exposed to 10% FBS for 1 h. Protein levels in the cell lysates were detected by IB using the indicated antibodies.

6. Treatment of MEK1/2 and PIN1 inhibitors in combination synergistically reduces the translation of TAZ and EGFR to inhibit breast tumorigenesis

Because the METTL3-PIN1 interaction was modulated by the MEK/ERK pathway, we aimed to combine the MEK1/2 and PIN1 inhibitors to develop a therapeutic strategy for breast cancer patients (Figure 6a). The simultaneous inhibition of MEK1/2 with PD98059 or trametinib and PIN1 with all-trans retinoic acid (ATRA) synergistically reduced the stability of METTL3, as evidenced by cycloheximide chasing (Figures 6b). Furthermore, the combination of PD98059 and ATRA significantly reduced the global m^6A levels in poly(A) RNA (Figure 6c). The combined treatment also reduced the m^6A modification of TAZ and EGFR mRNA and concomitantly decreased their protein levels (Figure 6d). Consistent with the reduced METTL3 expression, the translation reporter assay showed that co-treatment with PD98059 and ATRA synergistically reduced the translation efficiency of TAZ and EGFR (Figure 6e). Next, we examined the effect of combination therapy on the proliferation of MCF7 cells. An ELISA revealed that co-treatment with PD98059 and ATRA significantly reduced the incorporation of BrdU into the nascent DNA, indicating the inhibitory effects of the drug combination on cell proliferation (Figure 6f). Furthermore, the combination of PD98059 and ATRA induced significant cell cycle arrest in the G0/G1 phase (Figure 6g and h). To demonstrate that the anticancer effects of PD98059 and ATRA resulted from the destabilization of METTL3, we analyzed the effect of the drug combination on the cell cycle and cell proliferation after the ectopic expression of METTL3 in MCF7 cells. The overexpression of METTL3 released MCF7 cells from the PD98059 and ATRA-induced arrest of the G0/G1 phase (Figures 6i and j). Moreover, forced METTL3 expression increased the proliferation of MCF7 cells treated with PD98059 and ATRA, as evidenced by a significant recovery in the population of Ki67-positive cells (Figures 6k and l).

Figure 6 (a-d)

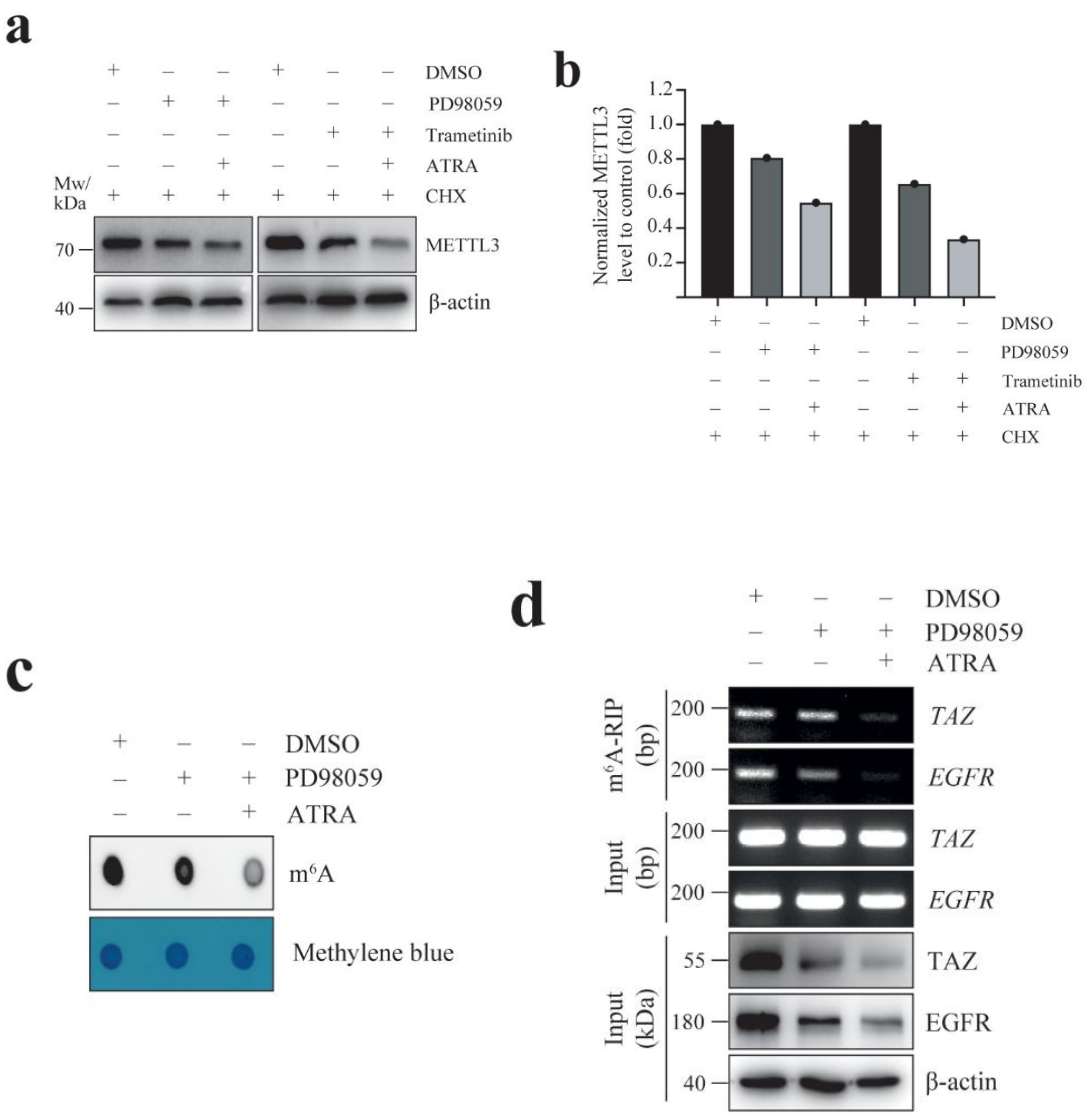

Figure 6 (e-f)

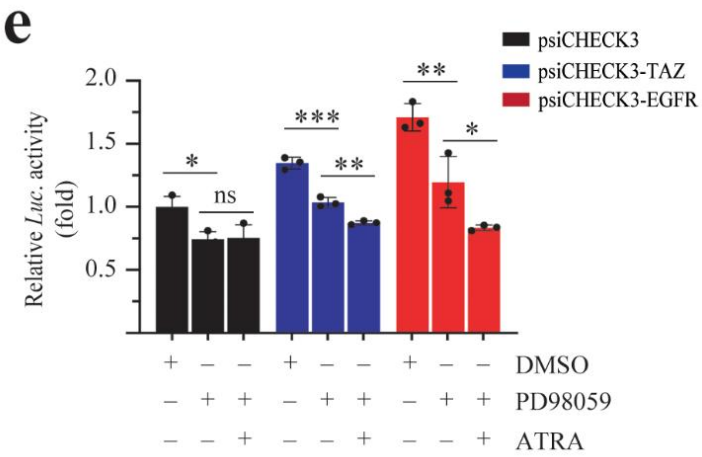

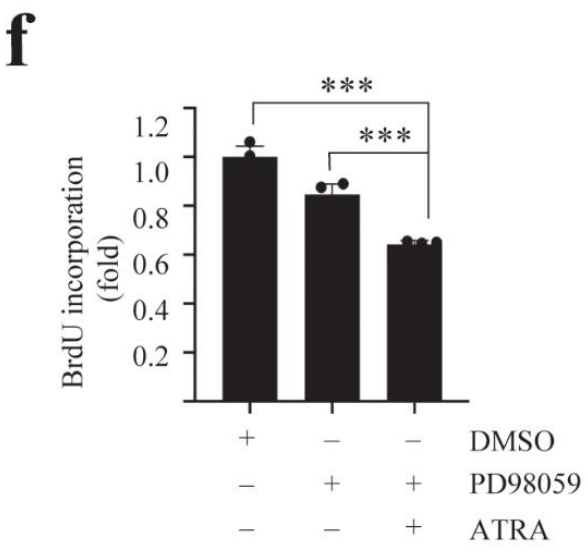

Figure 6 (g-h)

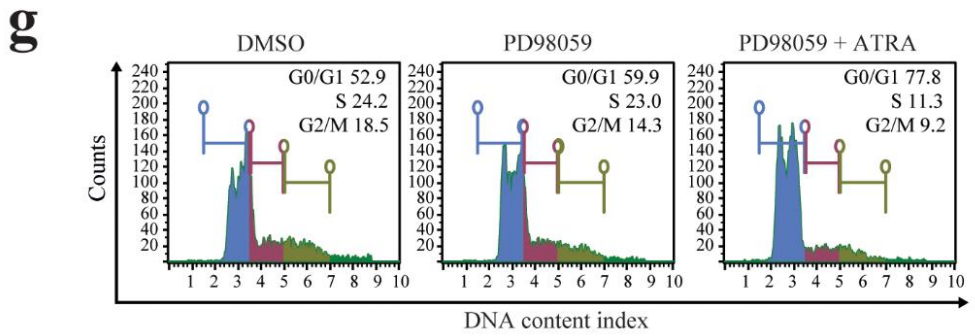

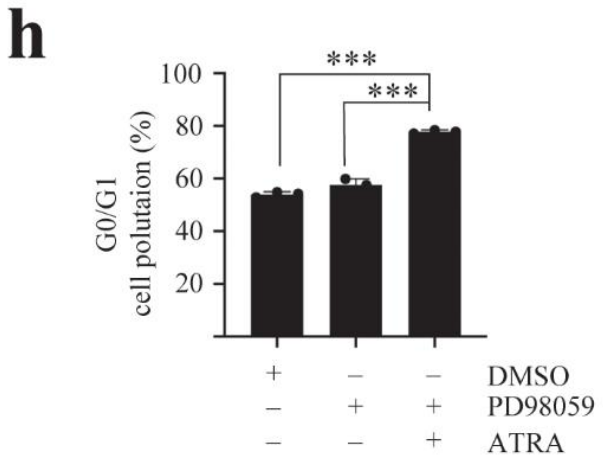

Figure 6 (i-j)

i

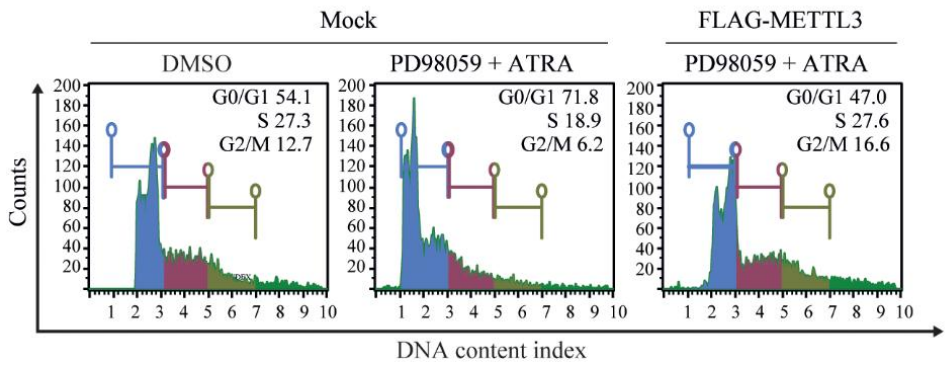

j

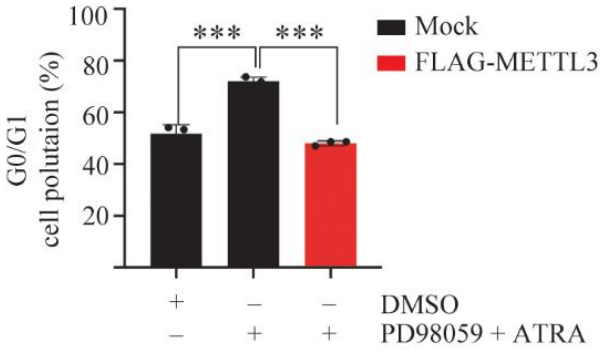

Figure 6 (k-l)

k

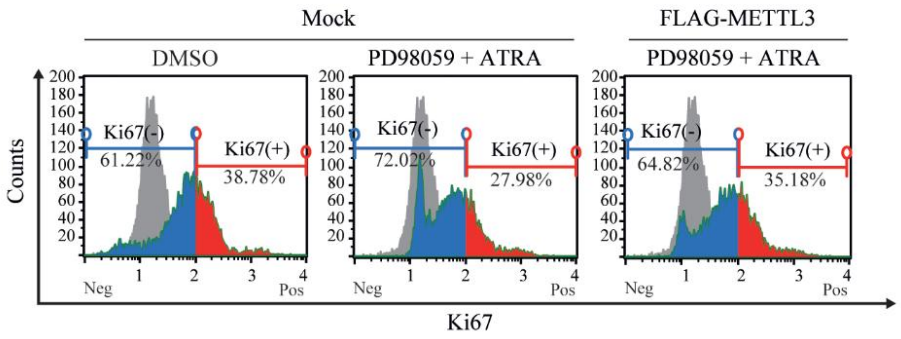

l

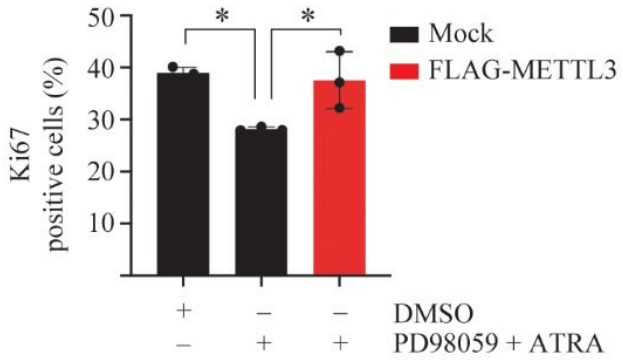

Figure 6. Combined treatment with MEKi and ATRA reduce the m^{6}A-dependent translation of *TAZ* and *EGFR*.

a, b Treatment with MEK inhibitors and ATRA accelerated METTL3 degradation. MCF7 cells were treated with PD98059 (10 μM, left) or trametinib (10 μM, right) either alone or in combination with ATRA (20 μM) for 24 h, followed by treatment with cycloheximide (100 μg/mL) for 6 h. Protein levels in cell lysates were detected with IB using the indicated antibodies (**a**), and the band intensities of METTL3 were measured with ImageJ and normalized to those of β-actin (**b**). **c** Co-treatment with PD98059 and ATRA synergistically reduced m^{6}A levels in MCF7 cells. MCF7 cells were treated with PD98059 (10 μM) and ATRA (20 μM), either alone or in combination for 24 h. m^{6}A levels in poly(A) RNA were detected by dot blotting using an anti-m^{6}A antibody. Methylene blue staining was used as the loading control. **d** Co-treatment with PD98059 and ATRA reduced the m^{6}A modification of *TAZ* and *EGFR* mRNA in MCF7 cells. Total RNA from MCF7 cells treated with PD98059 (10 μM) and ATRA (20 μM) for 24 h was immunoprecipitated using an anti-m^{6}A antibody. The mRNA levels in the input and IP fractions were analyzed by RT-PCR using the indicated primers. The protein expression of TAZ and EGFR in cell lysates was detected by IB using the respective antibodies. **e** Co-treatment with PD98059 and ATRA reduced the m^{6}A-dependent translation of *TAZ* and *EGFR*. MCF7 cells were transfected with psiCHECK3, psiCHECK3-TAZ, or psiCHECK3-EGFR, followed by treatment with PD98059 (10 μM) and/or ATRA (20 μM) for 24 h. *Renilla* luciferase activity in cell lysates was measured and normalized to firefly activity. Values are presented as the mean ± SD, N = 3. One-way ANOVA, $*p < 0.05$, $**p < 0.01$, $***p < 0.001$. **f** MCF7 cells were treated with PD98059 (10 μM) and ATRA (20 μM) for 24 h, and cell proliferation was determined using a BrdU incorporation assay. Values are presented as the mean ± SD, N = 3. $***p < 0.001$. **g, h** Co-treatment with PD98059 and ATRA induced cell cycle arrest in the G0/G1 phase. Histogram

showing the cell cycle distribution of MCF7 cells treated with PD98059 (10 μM) and/or ATRA (20 μM) for 24 h (**g**), and the G0/G1-arrested population (**h**). Values are presented as the mean ± SD, N = 3. One-way ANOVA, ***$p < 0.001$. **i, j** The ectopic expression of METTL3 relieved MCF7 cells from PD98059/ATRA-induced cell cycle arrest. Cell cycle distribution of MCF7 cells overexpressing FLAG-METTL3, followed by treatment with PD98059 (10 μM) and ATRA (20 μM) for 24h (**i**), and the population of cells arrested at the G0/G1 phase (**j**). Values are presented as the mean ± SD, N = 3. One-way ANOVA, ***$p < 0.001$. **k, l** Combination treatment with ATRA and PD98059 reduced the expression of the cell proliferation biomarker Ki67 in a METTL3-dependent manner. METTL3-overexpressing MCF7 cells were treated with PD98059 (10 μM) and ATRA (20 μM) for 24 h and stained with anti-Ki67-PE/7-AAD. Cell distribution was analyzed using a Muse cell analyzer (**k**) and the population of Ki67-positive cells (**l**). Values are presented as the mean ± SD, N = 3. One-way ANOVA, *$p < 0.05$.

7. PIN1 promotes breast tumorigenesis mediated by METTL3 *in vivo*

To study the effects of PIN1-induced METTL3 stability on breast tumorigenesis, we performed a soft agar assay. Increased colony formation in PIN1-overexpressing MCF7 cells was attenuated by the knockout of METTL3, suggesting that PIN1 promotes tumorigenesis via METTL3 stabilization (Figures 7a and b). PIN1-METTL3 axis-induced breast tumorigenesis was studied *in vivo* using an orthotopic mouse model. Mouse breast cancer cells from the cell line 4T1 that stably overexpressed human PIN1 were transfected with either sgCtrl or two separate guide RNAs targeting mouse Mettl3 (sgMettl3-1 and -2). They were then injected into the mammary glands of BALB/c mice (Figure 7c). The overexpression of PIN1 significantly increased the weight and volume of the tumors formed by the 4T1 cells (Figures 7c and d). In contrast, the CRISPR/Cas9-mediated knockout of Mettl3 using separate guide RNAs consistently reduced tumor size and volume in PIN1-overexpressing 4T1 cells (Figures 7c and d). The histopathological staining of tumor sections using hematoxylin and eosin (H&E) staining revealed a significant increase in cellularity in PIN1-overexpressing 4T1 cells, which was suppressed by the knockout of Mettl3 (Figure 7e). Histopathological examination of mice tumors revealed that the increase in tumor size is correlated with the development of necrotic core in tumor. The necrotic area was larger in PIN1-overexpressing 4T1 mice compared with the 4T1 mock mice. Furthermore, Mettl3 knockout reduced the tumor necrosis in PIN1-overexpressing 4T1 mice, suggesting that knockout of Mettl3 reduces the necrotic cell death to suppress the tumor formation in PIN1-overexpressing 4T1 mice (Figure 7e). Finally, we examined whether the increased tumorigenesis induced by PIN1-METTL3 was associated with the enhanced translation of *TAZ* and *EGFR*. Dot blotting using an m^6A antibody showed that PIN1 overexpression significantly increased the global m^6A levels in mouse tumors. The m^6A levels had further been decreased upon the knockout of Mettl3 (Figure 7f). Furthermore, m^6A-RIP using

RNA isolated from tumor samples indicated that the overexpression of PIN1 increased the methylation of *TAZ* and *EGFR* mRNA with a concomitant increase in protein expression in a METTL3-dependent manner (Figures 7g and h). These data indicate that PIN1 increases breast tumorigenesis *in vivo* via increased METTL3 stability. Furthermore, the overexpression of PIN1 was associated with the increased m^6A-dependent translation of TAZ and EGFR in mouse tumors.

Figure 7 (a-b)

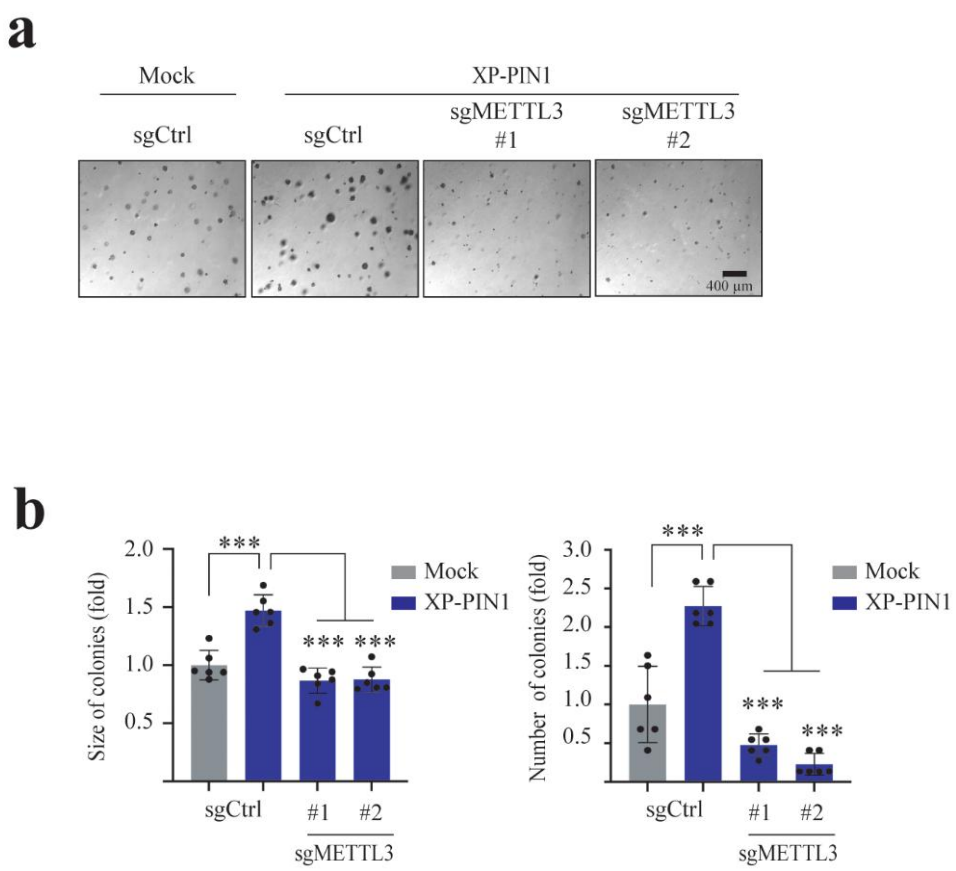

Figure 7 (c-d)

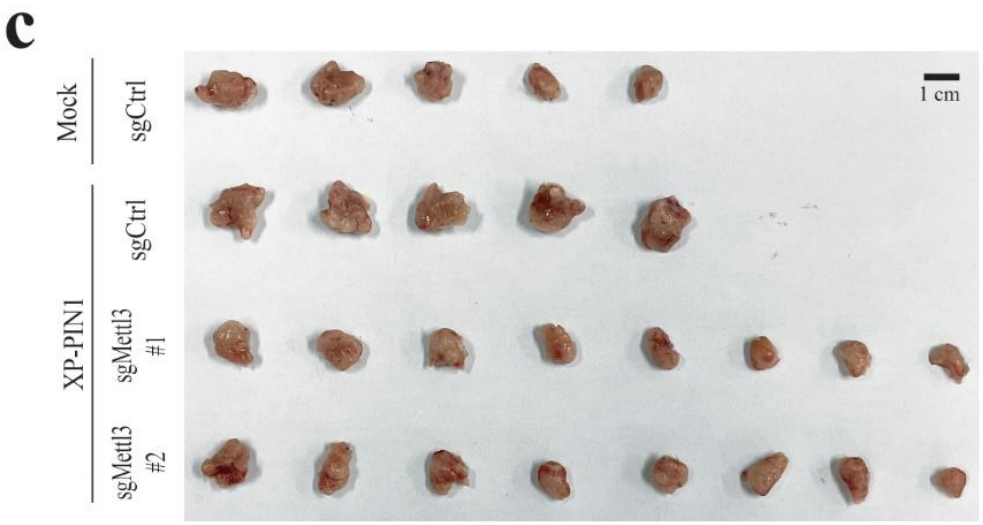

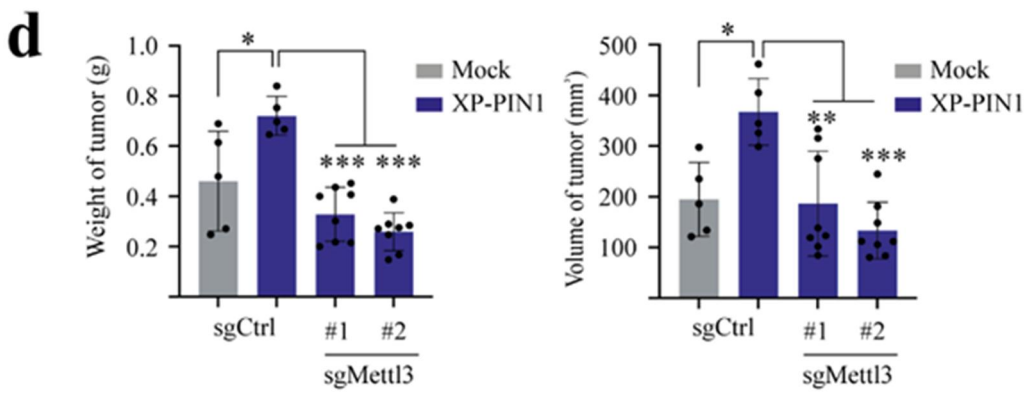

Figure 7 (e-f)

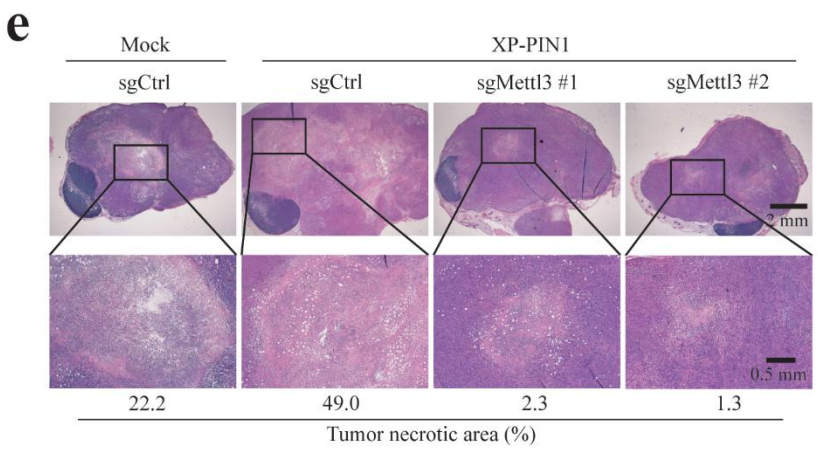

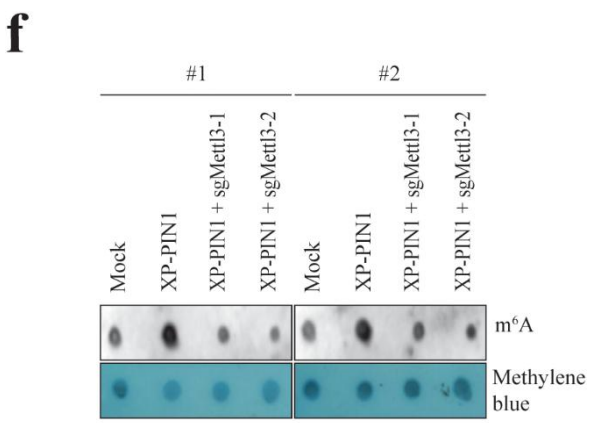

Figure 7 (g-h)

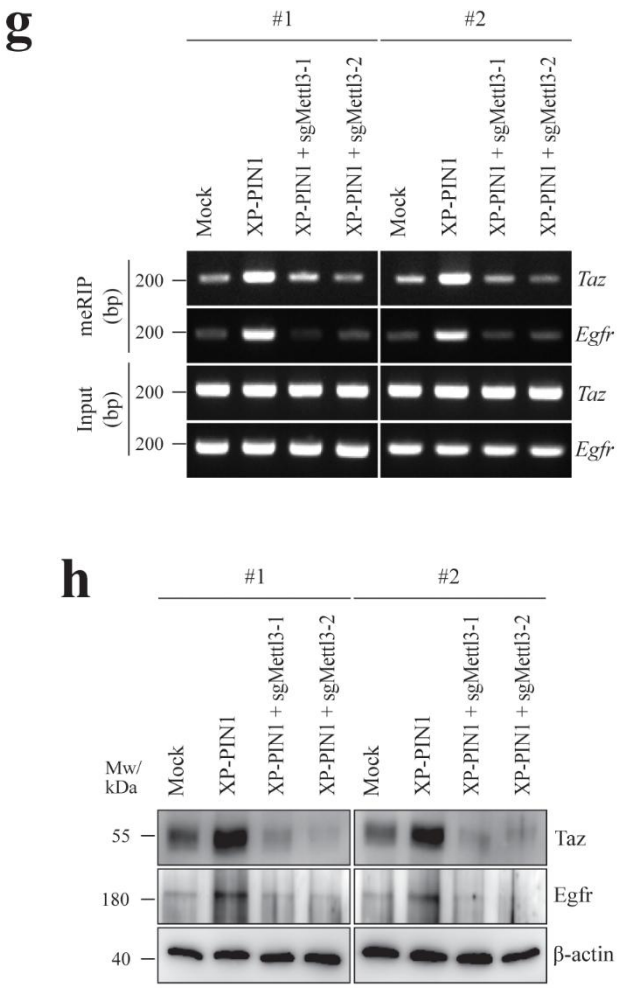

Figure 7. The knockout of METTL3 suppresses PIN1-induced breast tumorigenesis *in vivo*. **a, b** The knockout of METTL3 inhibited colony formation induced by PIN1 overexpression. Representative images of soft agar colonies formed by MCF7 cells stably overexpressing PIN1 followed by the transfection of two separate sgMETTL3 vectors (**a**), and quantification of colony size and numbers (**b**). Values are presented as the mean ± SD, N = 6. One-way ANOVA, ***$p <$ 0.001. **c, d** The knockout of METTL3 reduced PIN1-induced tumorigenesis *in vivo*. Representative images of tumors formed by 4T1 cells stably overexpressing human PIN1 transfected with sgCtrl or sgMettl3 (**c**). Tumor weight and volume at the time of sacrifice (**d**). Values are presented as the mean ± SD; N = 5 (mock or XP-PIN1), 8 (sgMettl3-1 and -2). One-way ANOVA, *$p < 0.05$, **$p < 0.05$, ***$p < 0.001$. **e** Histopathological examination of tumors. Representative images of tumor sections stained with hematoxylin and eosin. The necrotic area is shown below each figure. **f, g** PIN1 increases the m^{6}A modification of *TAZ* and *EGFR* mRNA mediated by METTL3 *in vivo*. Global m^{6}A levels in poly(A) RNA samples isolated from mouse tumors were detected by dot blotting using an anti-m^{6}A antibody (**f**). Total RNA from mouse tumor samples was immunoprecipitated with an anti-m^{6}A antibody. The mRNA levels in the input and IP fractions were analyzed using RT-PCR with primers targeting the indicated genes (**g**). **h** PIN1 increased TAZ and EGFR protein levels via METTL3 stabilization *in vivo*. Immunoblotting of lysates from mouse tumors using the indicated antibodies.

Part II: METTL3 induces PLX4032 resistance in melanoma by promoting m^{6}A-dependent EGFR translation

8. A375R cells exhibit upregulated METTL3 expression associated with enhanced m^{6}A modification

To study the effect of mRNA m^{6}A modification on the development of PLX4032 resistance in melanoma, we established a cellular model of PLX4032-resistant melanoma (A375R) as described in materials and methods. Cell viability analyses confirmed that A375R cells exhibit resistance to PLX4032 (IC 50 > 5 μM) in comparison with parental A375 [BRAF(V600E)] cells (IC 50 = 0.42 μM); conversely, PLX4032 did not affect the viability of BRAF wild-type HMCB melanoma cells (IC 50 > 5 μM) (Figure 8 a). Next, we examined the expression of essential proteins including the core m^{6}A-methyltransferase complex proteins METTL3, METTL14, and WTAP, and the m^{6}A demethylase fat mass and obesity-associated protein (FTO) in A375R cells by immunoblotting. METTL3, METTL14, and WTAP expression was significantly upregulated in A375R compared to A375 cells, whereas FTO expression remained relatively unaltered (Figure 8 b and c). Consistent with this, mining of proteomic data from the Broad Institute DepMap portal revealed that METTL3, METTL14, and WTAP expression positively correlated with PLX4032 resistance area under the curve (AUC) in skin cancer cell lines (Figure 8 d), with METTL3 exhibiting the stronger correlation. The extent of m^{6}A modification was then ascertained through dot blotting of poly(A) RNA using an m^{6}A-specific antibody, which revealed significant upregulation in A375R compared to A375 cells; this was further confirmed via immunofluorescence (Figure 8 e–g). METTL3 knockout in A375R cells abolished the m^{6}A modification of mRNA, as demonstrated by m^{6}A dot blotting and immunofluorescence (Figure8 h–j). Together, these results suggest that METTL3 expression increased in PLX4032-resistant melanoma cells leading to enhanced m^{6}A modification of mRNA.

Figure 8 (a-c)

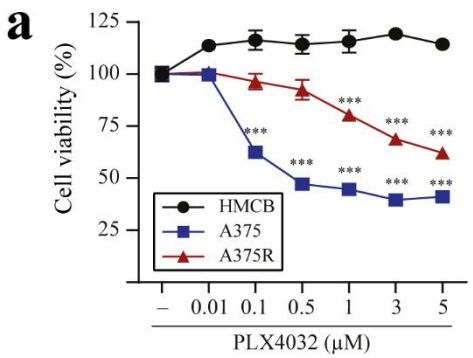

Cell lines	BRAF	PLX4032 IC_{50}
HMCB	WT	> 5 μM
A375	V600E	0.42 μM
A375R	V600E	> 5 μM

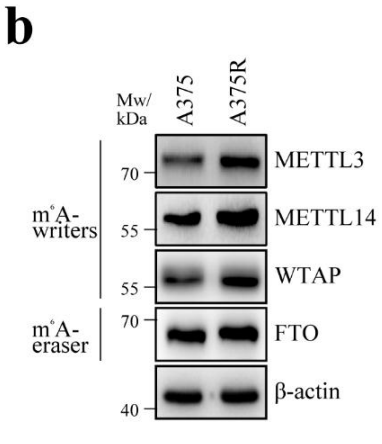

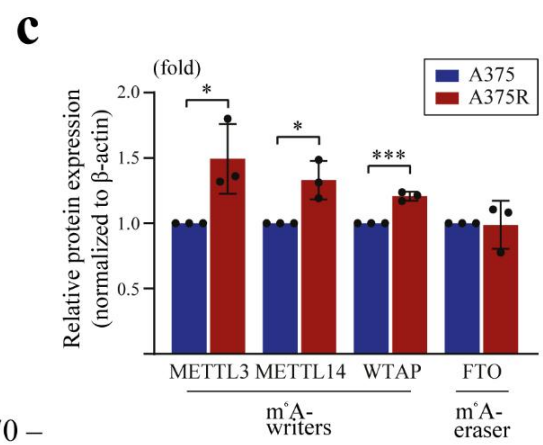

70 –

Figure 8 (d)

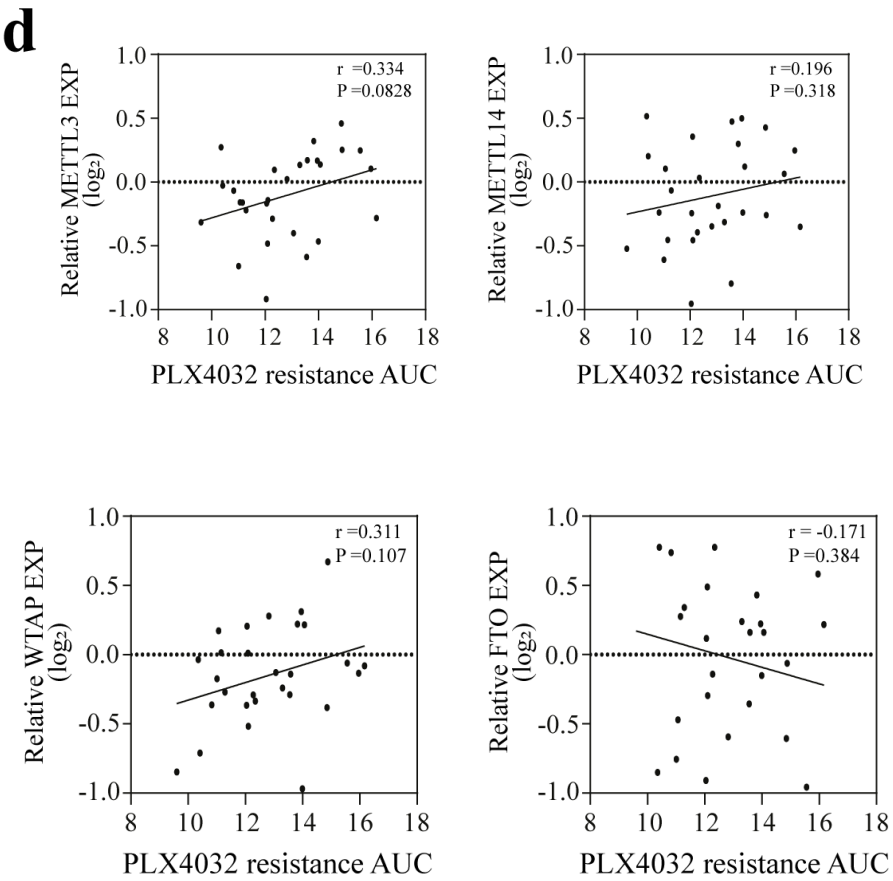

Figure 8 (e-g)

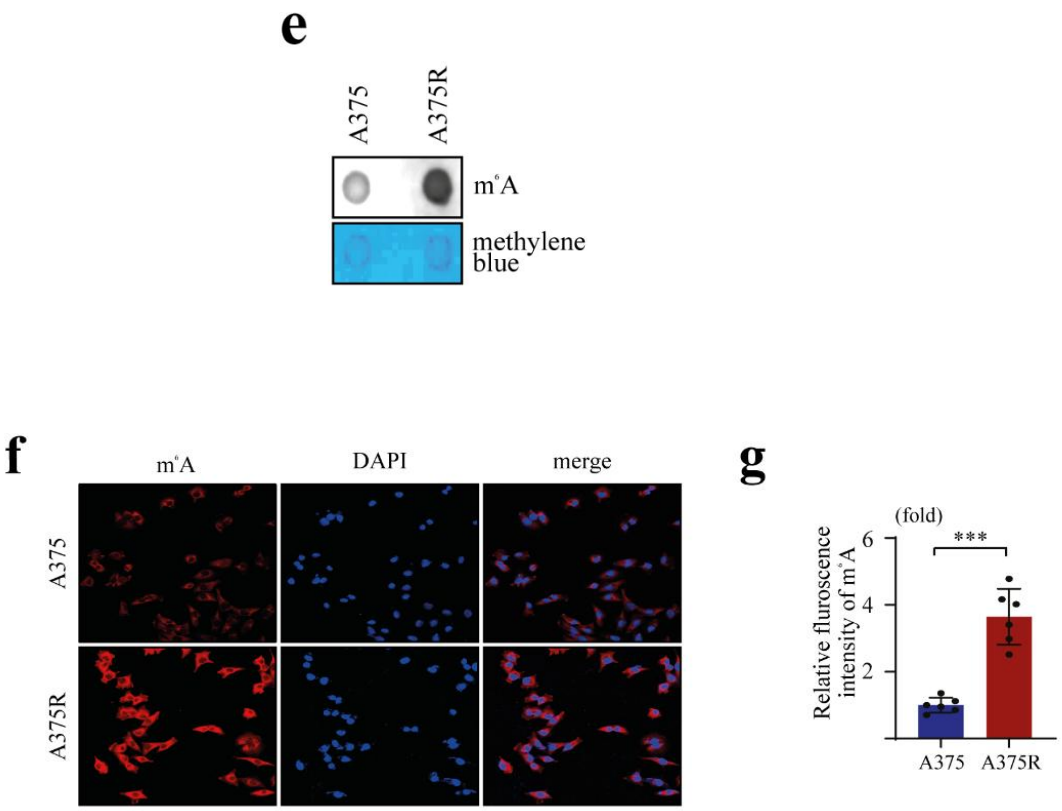

Figure 8 (h-j)

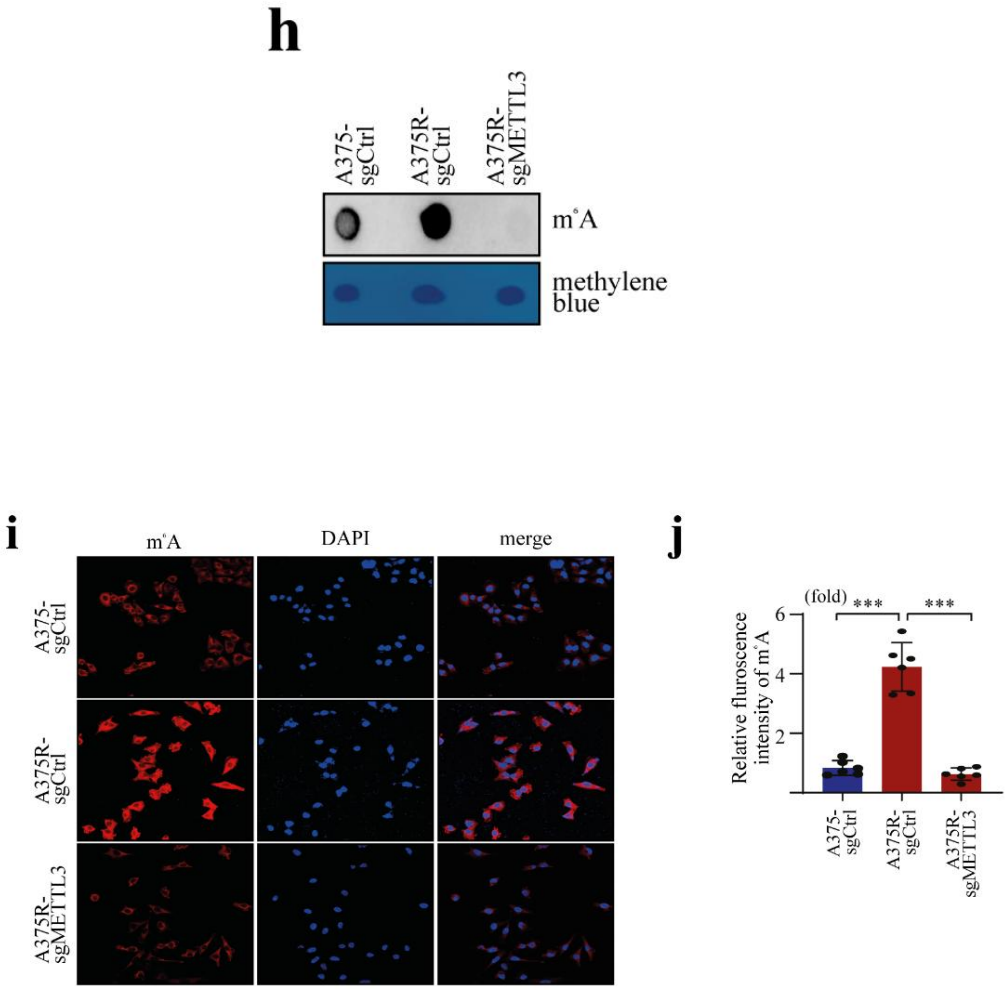

Figure 8. METTL3 abundance is upregulated in A375R cells leading to enhanced m ^{6}A modification of mRNA

a Sensitivity of HMCB, A375, and A375R cells to PLX4032. Cell viability of HMCB, A375, and A375R cells in response to PLX4032 treatment as determined by MTT assay. Values represent the means ± SD, N = 3. One-way ANOVA, *** $P < 0.001$ (A375 versus A375R or HMCB, corresponding concentrations). **b, c** Expression of METTL3, METTL14, and WTAP, but not FTO, is upregulated in A375R cells. Immunoblotting (IB) of whole-cell lysate prepared from A375 and A375R cells using respective antibodies (**b**). Corresponding signal intensities were measured densitometrically and normalized to those of β-actin (**c**). Values represent the means ± SD, N = 3. Unpaired t-test, * $P < 0.05$, *** $P < 0.001$. **d** METTL3 abundance is positively correlated with PLX4032 resistance in a panel of skin cancer cell lines. Protein expression of m^{6}A writers and eraser in a panel of 28 skin cancer cell lines and their correlation with PLX4032 resistance area under the curve (AUC) obtained from the Broad Institute DepMap portal. Higher AUC values correspond to lower sensitivity to the PLX4032. Protein expression was measured using quantitative mass spectrometry. Each dot represents a cell line. Pearson's correlation (r) and significance (P) values are indicated within each graph. e-g m^{6}A modification of mRNA is upregulated in A375R cells. e Dot blotting of poly(A) RNA prepared from A375 and A375R cells, detected using an anti-m^{6}A antibody. f Staining of A375 and A375R cells with an anti-m^{6}A antibody (red) and DAPI to detect nuclear DNA (blue). Scale bars, 50 μm. g Fluorescence intensity produced by cells stained with the anti-m^{6}A antibody was quantified using Fiji software (https://fiji.sc) and represented as relative fluorescence intensity. Values represent the means ± SD, N = 6. Unpaired t -test, *** $P < 0.001$. h-j Knockout of METTL3 abolishes m^{6}A modification of mRNA in A375R cells. h Dot blotting of poly(A) RNA isolated from A375 and A375R cells transfected with sgCtrl or sgMETTL3, detected using an anti-m^{6}A antibody. Methylene blue

staining served as a loading control. i Staining of A375 and A375R cells transfected with sgCtrl or sgMETTL3 as detected using an anti-m^6A antibody (red) or DAPI to detect nuclear DNA (blue). Scale bars, 50 μm. j Fluorescence intensity of cells stained with an anti-m^6A antibody was quantified using Fiji software and expressed as relative fluorescence intensity. Values represent the means ± SD, N = 6. One-way ANOVA, *** $P < 0.001$.

9. m^{6}A-modified mRNAs in A375R cells are associated with rebound activation of the RAF/MEK/ERK pathway

Rebound activation of the RAF/MEK/ERK signaling pathway is frequently associated with PLX4032 resistance in melanoma (Moriceau et al., 2015). To identify specific genes that promote activation of this pathway in a METTL3-dependent manner, we explored the data available through the cancer DepMap portal. First, we examined the correlation between the expression of several oncogenic proteins and METTL3 in melanoma cell lines (Figure 9a), which revealed that RAF/MEK/ERK pathway-related proteins such as EGFR and RAF1 positively correlated with METTL3 expression. Next, we examined the correlation between oncogenic protein expression and PLX4032 sensitivity in the same group of cell lines. As expected, EGFR and RAF1 expression was associated with resistance to PLX4032 (Figure 9b). A comparison of proteins that positively correlated with METTL3 expression or PLX4032 sensitivity confirmed that EGFR and RAF1 were commonly associated with both groups (Figure 9c). As the positive correlation between protein levels and METTL3 expression suggested a potential role of m^{6}A modification, we next investigated the m^{6}A modification of EGFR and RAF1 along with that of other vital transcripts involved in rebound activation of the RAF/MEK/ERK pathway using methylated RNA immunoprecipitation-quantitative polymerase chain reaction (meRIP-qPCR). Notably, m^{6}A modification of *EGFR*, *NRAS*, *RAF1*, *NF1*, and *NF2* was significantly upregulated in A375R compared to parental A375 cells (Figure 9d and e). Given that METTL3 function is essential for m^{6}A deposition, we knocked out METTL3 in A375R cells and examined the m^{6}A modification of the transcripts involved in rebound activation of the RAF/MEK/ERK pathway. METTL3 knockout reduced the m^{6}A modification of mRNAs upregulated in A375R cells (Figure 9f). As an alternative approach to study m^{6}A modification, we treated A375R cells with cycloleucine, a competitive inhibitor of methionine adenosyltransferase 2 (MATII) that reduces mRNA

methylation by depleting the source of the methyl group. The results showed that treatment with cycloleucine reduces the m^6A modification of *EGFR*, *NRAS*, *RAF1*, *NF1*, and *NF2* in A375R cells (Figure 9g). Taken together, these results suggest that enhanced m^6A modification of specific genes related to rebound activation of the RAF/MEK/ERK pathway is associated with PLX4032 resistance in melanoma

Figure 9 (a-b)

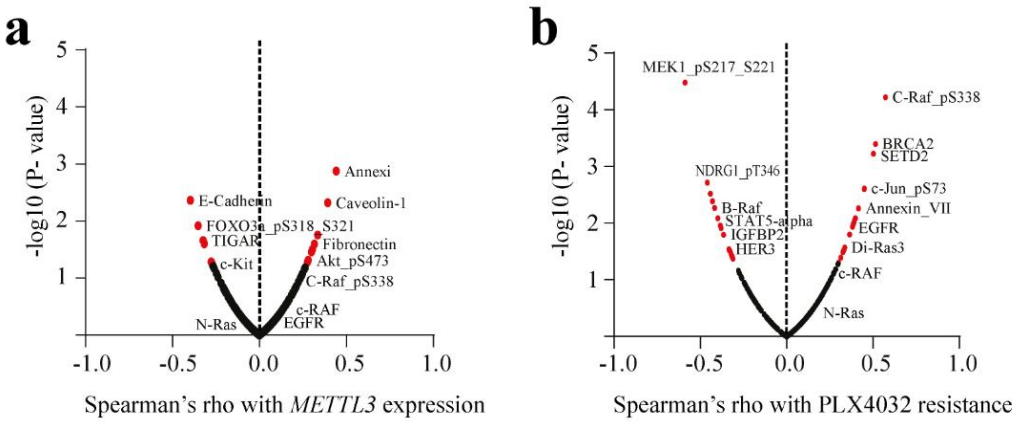

Figure 9 (c)

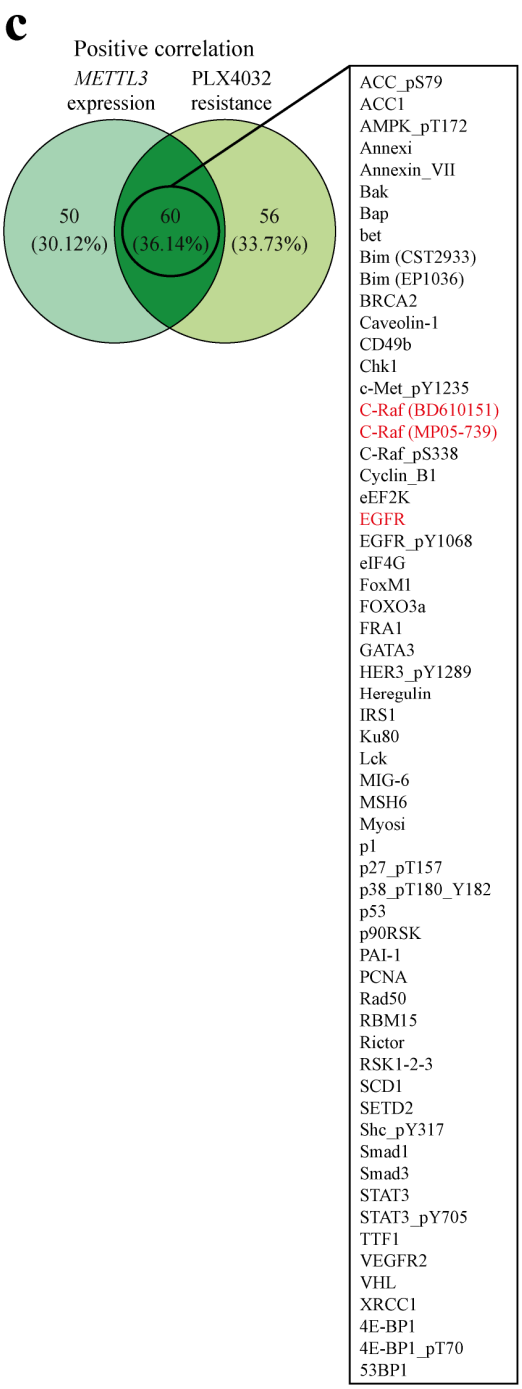

Figure 9 (d-g)

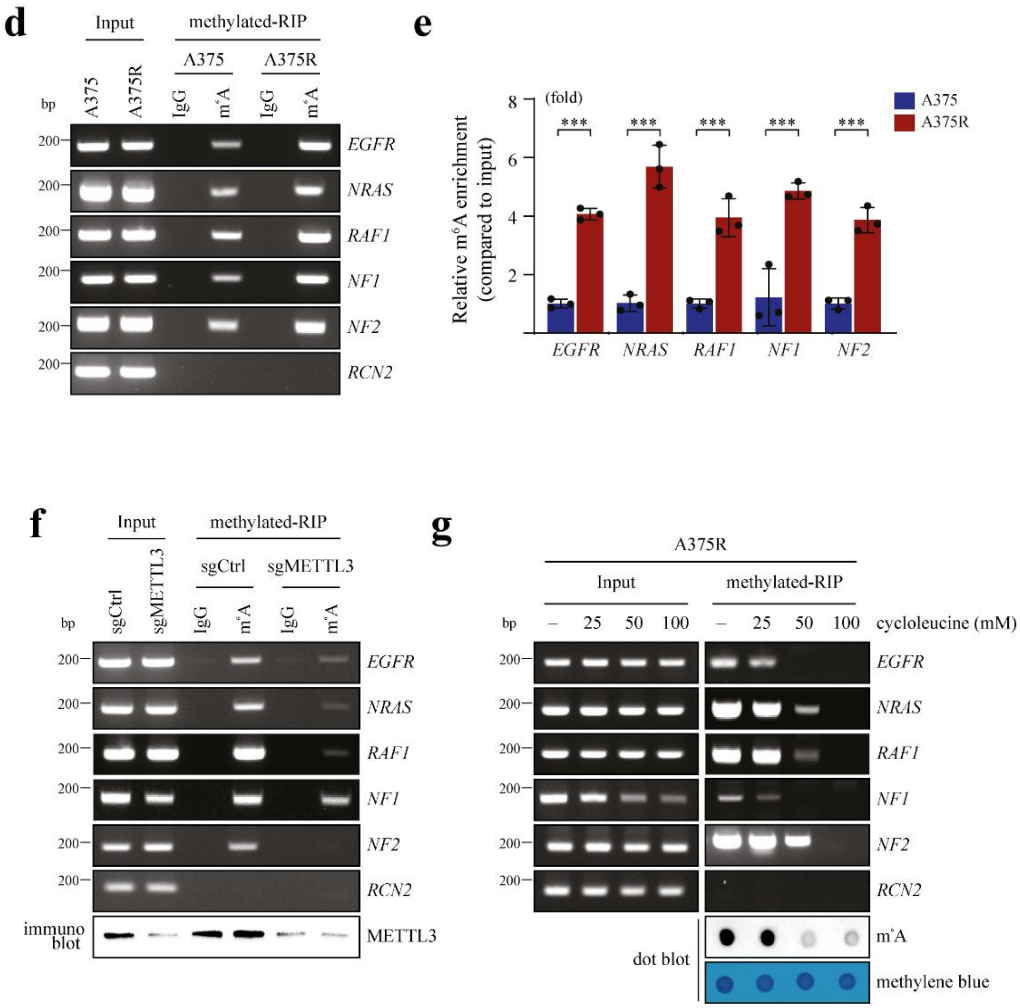

Figure 9. METTL3 promotes the m^{6}A modification of genes associated with PLX4032 resistance in A375R cells

a-c Proteomic analysis of cancer cell lines. Volcano plot depicting the expression of several oncogenic proteins as determined using reverse-phase protein array in a panel of 43 melanoma cell lines and their correlation with METTL3 expression (a), PLX4032 sensitivity (**b**) and Venn diagram showing the proteins that are positively correlated with METTL3 expression and PLX4032 resistance (**c**). The data was obtained from the Broad Institute DepMap portal. Significant correlations ($P < 0.05$) are highlighted in red. **d, e** m^{6}A modification of specific genes related to PLX4032 resistance is upregulated in A375R cells. Total RNA isolated from A375 and A375R cells was immunoprecipitated (IP) using anti-m^{6}A or normal IgG antibodies. Gene expression in input or IP fractions was analyzed by semi-quantitative reverse transcriptase-polymerase chain reaction (RT-PCR) (**d**) or by real-time RT-PCR (**e**) with primers targeting the indicated genes. The non-methylated mRNA RCN2 served as a negative control for IP. Values represent the means ± SD, N = 3. Unpaired t -test, *** $P < 0.001$. **f** Knockout of METTL3 reduces the m^{6}A modification of mRNAs associated with PLX4032 resistance. Total RNA prepared from A375R cells transfected with sgCtrl or sgMETTL3 were immunoprecipitated using anti-m^{6}A or normal IgG antibodies. Gene expression in the input sample or IP fraction was analyzed by semi-quantitative RT-PCR with primers targeting the indicated genes. The non-methylated mRNA RCN2 served as a negative control for IP. **g** Cycloleucine treatment inhibits the m^{6}A modification of mRNAs associated with PLX4032 resistance. Total RNAs prepared from A375R cells treated with cycloleucine were immunoprecipitated using an anti-m^{6}A antibody. Gene expression in the input sample and IP fraction were analyzed by semi-quantitative RT-PCR with primers targeting the indicated genes. The non-methylated mRNA RCN2 served as a negative control for IP.

10. METTL3 enhances the translation efficiency of *EGFR* in A375R cells

Previous studies have shown that m^6A modification can promote the translation efficiency of specific genes (Lin et al., 2016). As EGFR expression is frequently upregulated in PLX4032-resistant melanoma, we next evaluated whether the increased m^6A EGFR level observed in A375R cells was associated with enhanced *EGFR* translation. First, we investigated the association of EGFR expression with PLX4032 resistance in melanoma cell lines using data from the cancer DepMap portal, which revealed that EGFR expression positively correlated ($r = 0.387$, $P < 0.05$) with PLX4032 drug resistance AUC (Figure 10a). Next, immunoblotting of EGFR expression in A375R cells showed significant upregulation compared with that in parental A375 cells (Figures 10b and c). To examine whether m^6A modification mediated by METTL3 is responsible for the enhanced translation of EGFR mRNA in A375R cells, we designed translation reporter constructs by inserting the putative m^6A modification site derived from EGFR into the 3′-UTR region of the luciferase gene (Figure 10d). Analysis of luciferase activity in cell lysates revealed that translation of the luciferase reporter carrying a wild-type EGFR m^6A motif in its 3′-UTR was increased in A375R compared to A375 cells (Figure 10e). In contrast, mutations in the EGFR m^6A motif diminished translation of the luciferase reporter, suggesting that increased m^6A modification of EGFR enhances its translation in A375R cells (Figure 10e). The mechanism that regulates the translation of EGFR was further examined via METTL3 knockout in A375R cells, which led to the reduced translation of the luciferase reporter harboring the EGFR m^6A motif (Figure 10f). In agreement with previous results, treatment with cycloleucine reduced translation of the luciferase reporter containing the EGFR m^6A motif in a dose-dependent manner (Figure 10g). Together, these results suggest that m^6A modification is essential for the enhanced translation of EGFR in A375R cells. To compare the protein synthesis rate (translation efficiency) of EGFR between A375 and A375R cells, we terminated the protein translation via puromycin

treatment and examined the level of newly synthesized EGFR using immunoprecipitation/immunoblotting (Figure 10h). The amount of puromycilated EGFR was higher in A375R than in A375 cells, whereas cycloleucine treatment reduced the incorporation of puromycin into EGFR (Figures 10i and j). The results indicated that the translation efficiency of EGFR is higher in A375R than in A375 cells and that inhibition of m^6A modification by cycloleucine diminished the efficiency of EGFR translation in A375R cells. Next, we examined whether the METTL3-regulated translation efficiency of EGFR affected its protein level in A375 and A375R cells. Ectopic expression of METTL3 in A375 cells significantly increased EGFR protein expression, whereas METTL3 knockout in A375R cells reduced EGFR expression (Figure 10k and l). Additionally, treatment of A375R cells with cycloleucine significantly reduced EGFR protein but not EGFR mRNA levels (Figure 10m). To examine whether cycloleucine decreases EGFR expression by reducing m^6A modification, we treated A375 cells overexpressing METTL3 with cycloleucine. As expected, the enhanced expression of EGFR induced by METTL3 was reduced following cycloleucine treatment, further suggesting that METTL3 increases EGFR expression through m^6A modification of mRNA (Figure 10n). Taken together, these results indicate that increased m^6A modification mediated by METTL3 promotes the translation efficiency of EGFR in A375R cells.

Figure 10 (a-c)

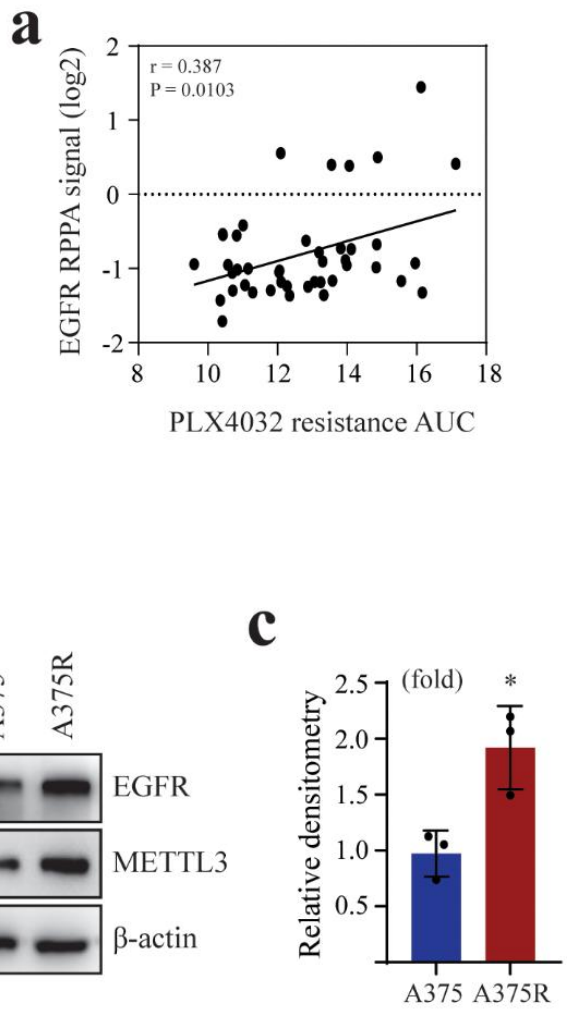

Figure 10 (d-g)

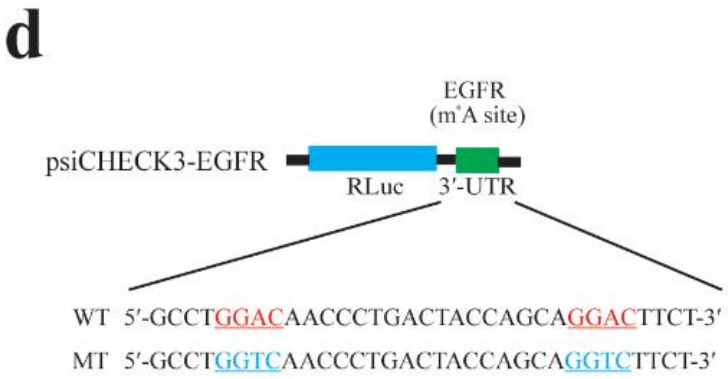

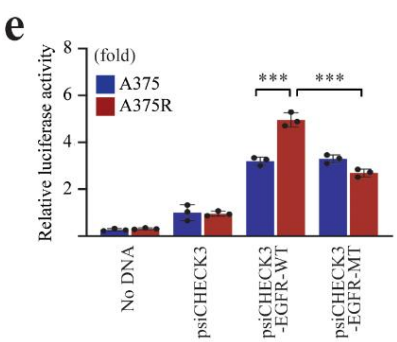

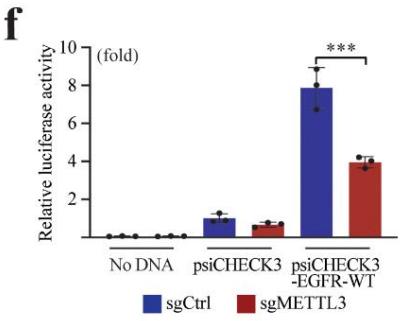

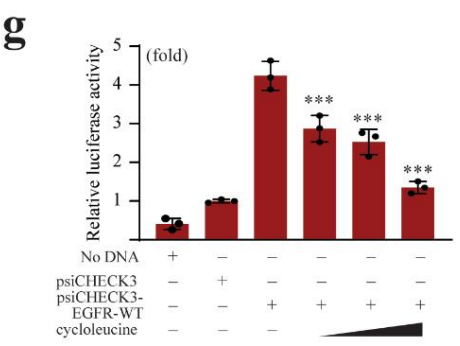

Figure 10 (h-j)

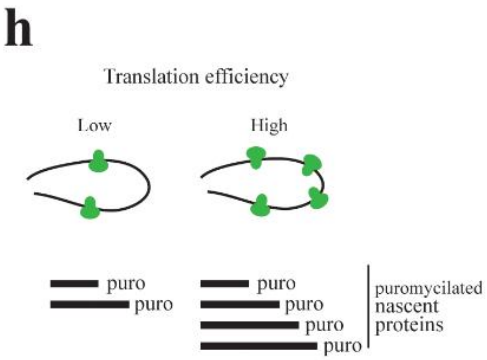

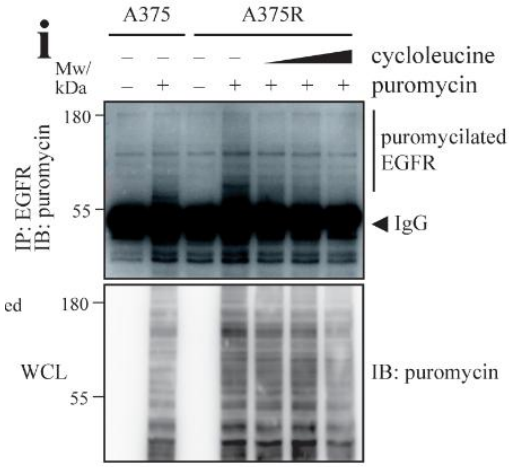

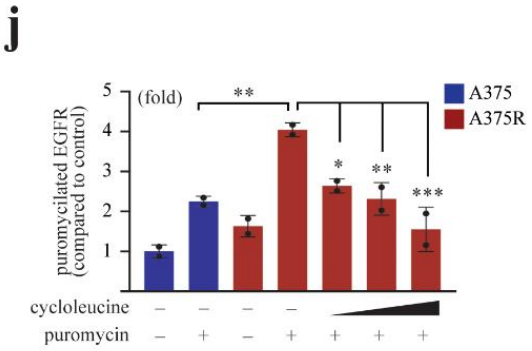

Figure 10 (k-n)

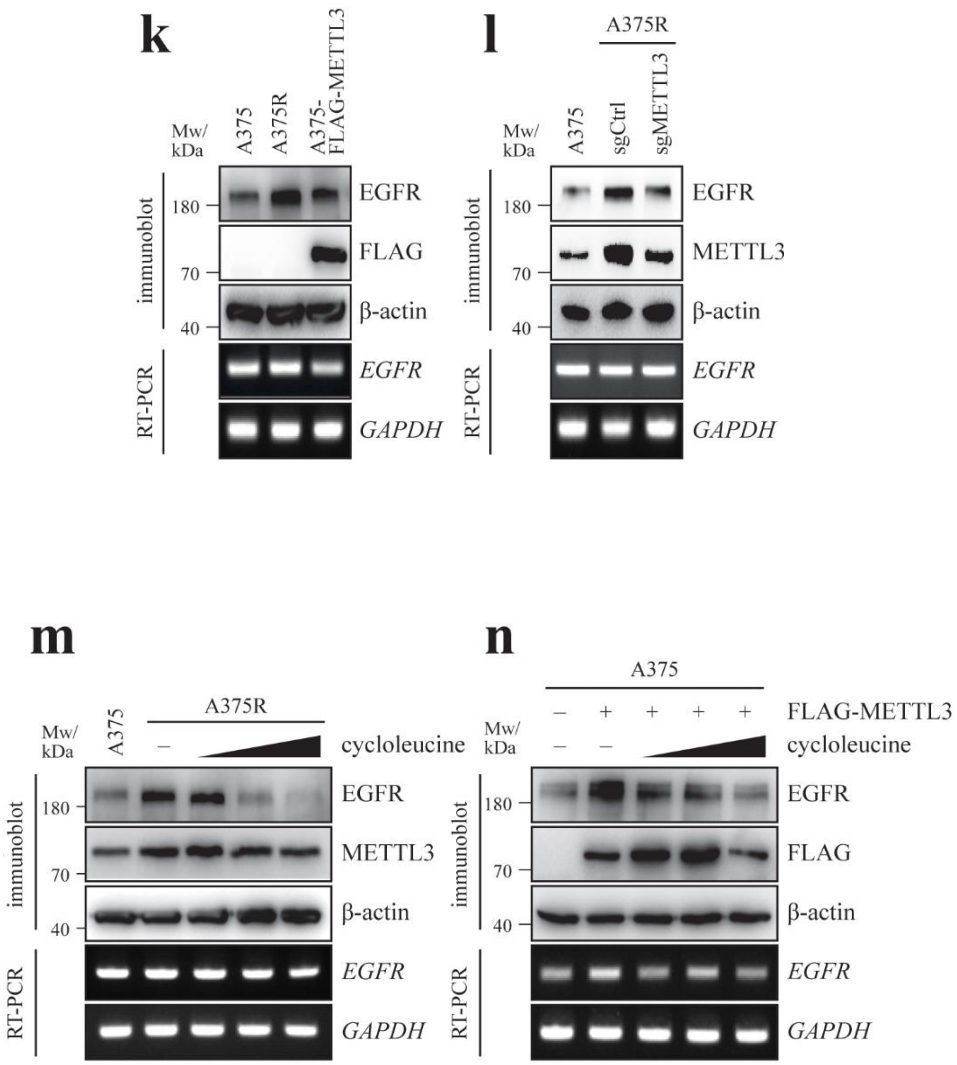

Figure 10. METTL3 promotes the translation efficiency of EGFR in A375R cells

a EGFR expression positively correlates with PLX4032 resistance in a panel of skin cancer cell lines. Protein expression of EGFR and its correlation with PLX4032 resistance area under the curve (AUC) in skin cancer cell lines (N = 43 cell lines) obtained from the Broad Institute DepMap portal. Protein expression was measured using a reverse-phase protein array (RPPA). The dots represent the cell lines. Pearson's correlation (r) and significance (P) values are indicated within the graph. **b, c** EGFR protein level is upregulated in A375R cells. Immunoblotting (IB) of cell lysates prepared from A375 and A375R cells detected using the indicated antibodies (**b**); optical densities of the bands were quantified using Image J (**c**). Values represent the means ± SD, N = 3. Unpaired t -test, * $P < 0.05$. **d** Schematic diagram of the translation reporter construct (upper), and the cDNA sequence of the putative mRNA methylation site in EGFR mRNA (lower). RLuc indicates Renilla luciferase gene. Consensus m^6A modification motif (GGAC) is underlined and was mutated into GGTC to create a methylation-deficient construct. **e** Enhanced translation of EGFR in A375R cells is mediated via m^6A modification of mRNA. Renilla luciferase activity in cell lysates prepared from A375 and A375R cells transfected with psiCHECK3 or psiCHECK3-EGFR (WT or Mut) was measured and normalized against firefly luciferase activity. Values represent the means ± SD, N = 3. One-way ANOVA, *** $P < 0.001$. **f** METTL3 promotes translation of EGFR in A375R cells via m^6A modification of mRNA. Renilla luciferase activity in cell lysates prepared from A375R cells transfected with sgCtrl or sgMETTL3 was measured and normalized against firefly luciferase activity. Values represent the means ± SD, N = 3. One-way ANOVA, *** $P < 0.001$. **g** Cycloleucine treatment reduces the translation of EGFR mediated by m^6A modification of mRNA. Renilla luciferase activity in cell lysates prepared from A375R cells treated with cycloleucine. Values represent the means ± SD, N = 3. One-way ANOVA, *** $P < 0.001$ (psiCHECK3-EGFR-WT versus cycloleucine

treatment). **h-j** Cycloleucine treatment reduces the translation efficiency of EGFR in A375R cells. Schematic representation of the experimental plan to measure the translation efficiency of EGFR using puromycin labeling (**h**). Whole-cell lysates (WCL) prepared from A375 and A375R cells treated with cycloleucine and/or puromycin were immunoprecipitated using an anti-EGFR antibody followed by IB with an anti-puromycin antibody (**i**). The protein signal density above IgG heavy chain was quantified using Image J (**j**). Values represent the means ± SD, N = 2. One-way ANOVA, * $P < 0.05$, ** $P < 0.01$, *** $P < 0.001$. **k** Overexpression of METTL3 increases EGFR protein level in A375 cells. IB of A375 and A375R cells transfected with mock or Flag-METTL3 detected using the respective antibodies (upper), and measurement of mRNA expression using semi-quantitative RT-PCR with the indicated primers (lower). **l** Knockout of METTL3 reduces EGFR protein level in A375R cells. IB of A375 and A375R cells transfected with sgCtrl or sgMETTL3 detected using the indicated antibodies (upper), and measurement of mRNA expression using semi-quantitative RT-PCR with the indicated primers (lower). **m** Cycloleucine treatment reduces the EGFR protein level in A375R cells. IB of cell lysates prepared from A375 cells and A375R cells treated with cycloleucine as detected using the indicated antibodies (upper), and measurement of mRNA expression using semi-quantitative RT-PCR with primers targeting the indicated genes (lower). **n** Cycloleucine treatment reduces the EGFR protein level increased by METTL3. IB of cell lysates prepared from A375 cells transfected with METTL3 followed by cycloleucine treatment (10–50 mM) as detected using the indicated antibodies (upper), and measurement of mRNA expression using semi-quantitative RT-PCR with primers targeting the indicated genes (lower).

11. METTL3 confers PLX4032 resistance in melanoma via rebound activation of the RAF/MEK/ERK pathway

We next examined whether upregulation of EGFR expression could activate the downstream RAF/MEK/ERK pathway and induce PLX4032 resistance. First, we compared RAF/MEK/ERK pathway activity between A375 and A375R cells. In agreement with our previous findings (KIM et al., 2019), the activation of the RAF/MEK/ERK pathway was notably upregulated in A375R cells (Figure 11a). To examine whether METTL3 could activate the RAF/MEK/ERK pathway through upregulation of EGFR expression, we overexpressed METTL3 in A375 cells; this led to increased phosphorylation of the RAF/MEK/ERK pathway as well as increased EGRF levels (Figure 11b). In contrast, METTL3 knockout in A375R cells reduced pathway activity (Figure 11c), suggesting that METTL3 led to rebound activation of the RAF/MEK/ERK pathway through upregulation of EGFR expression. Moreover, cycloleucine treatment significantly reduced RAF/MEK/ERK pathway activation in A375R cells (Figure 11d). Next, we examined whether METTL3-enhanced EGFR expression affected the inhibitory effect of PLX4032 on the RAF/MEK/ERK pathway. Ectopic METTL3 expression in A375 cells reduced the inhibitory effect of PLX4032 on the RAF/MEK/ERK pathway (Figure 11e). Additionally, METTL3 knockout reduced RAF/MEK/ERK pathway activation in A375R cells, with the inhibition further augmented by PLX4032 treatment (Figure 11f), and decreased A375R cell viability upon PLX4032 treatment (Figure 11g). Next, we examined whether increased EGFR expression was sufficient to induce PLX4032 resistance in A375R cells. Ectopic EGFR expression reduced the inhibitory effect of PLX4032 on RAF/MEK/ERK pathway activation and A375R cell viability (Figures 11h and i). In contrast, EGFR knockout decreased RAF/MEK/ERK pathway activity and reduced A375R cell viability upon PLX4032 treatment (Figures 11j and k). Finally, we examined whether METTL3-induced rebound activation of the RAF/MEK/ERK pathway in

A375R cells was due to upregulation of EGFR expression. To determine the effect of METTL3 on RAF/MEK/ERK pathway activation, we overexpressed METTL3 in either EGFR wild-type or EGFR knockout A375 cells. METTL3 overexpression activated the RAF/MEK/ERK pathway and induced resistance to PLX4032 in EGFR wild-type but not in EGFR knockout A375 cells (Figures 11l and m). These results show that the increased expression of EGFR mediated by METTL3 activates the RAF/MEK/ERK pathway and induces resistance to PLX4032 in A375R cells.

Figure 11 (a-d)

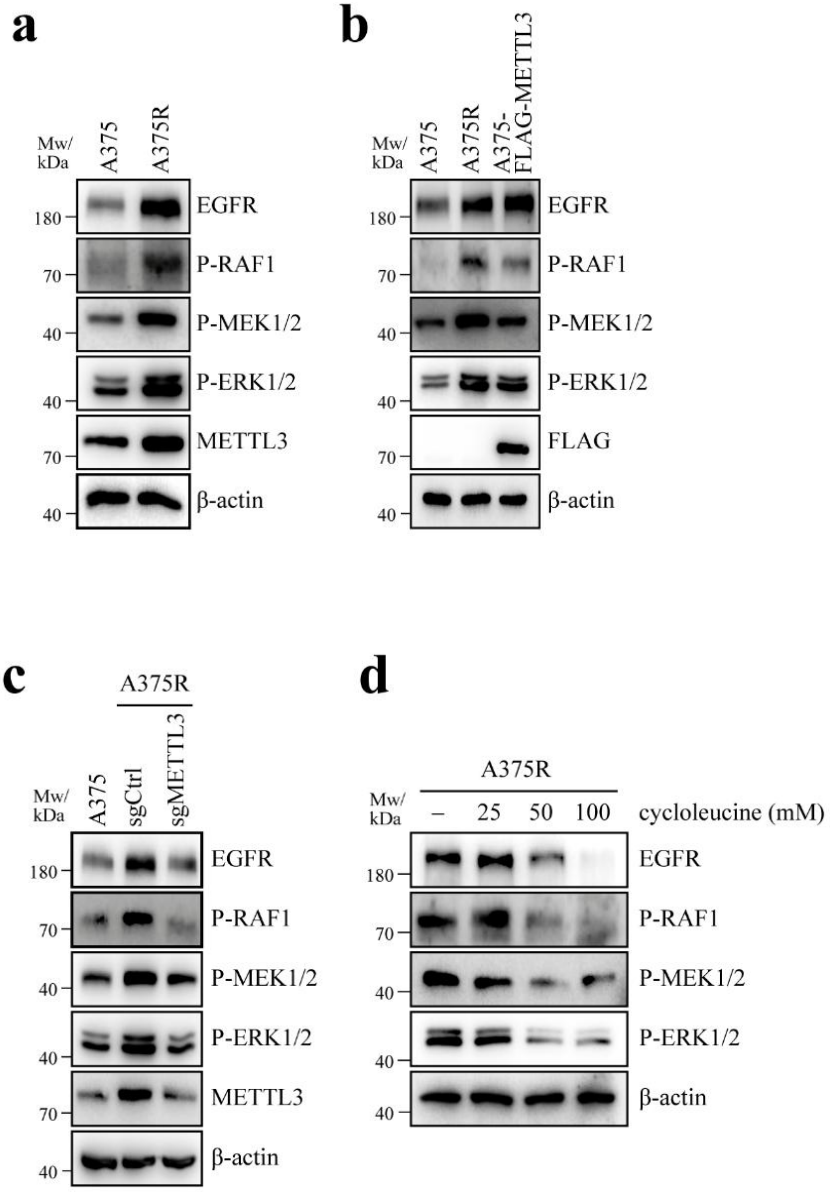

Figure 11 (e-g)

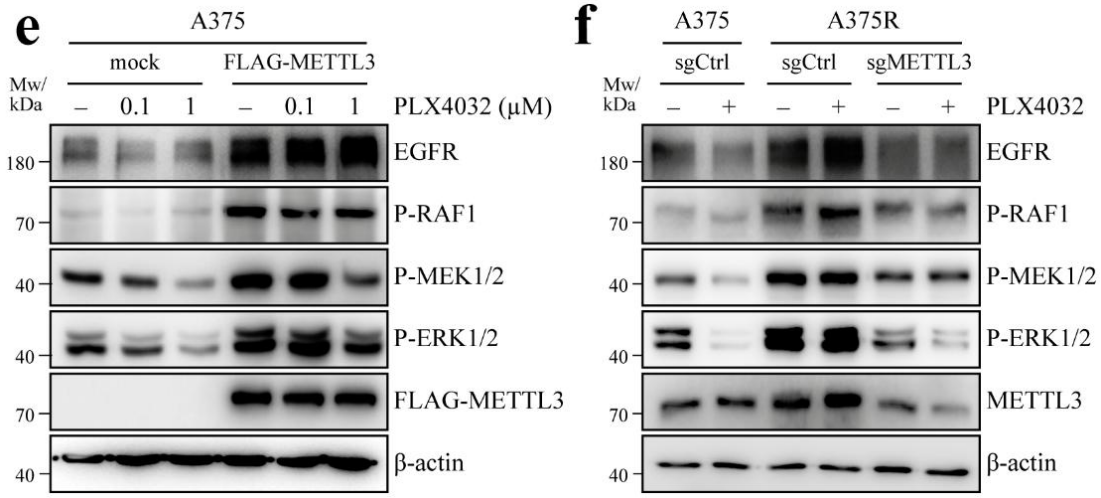

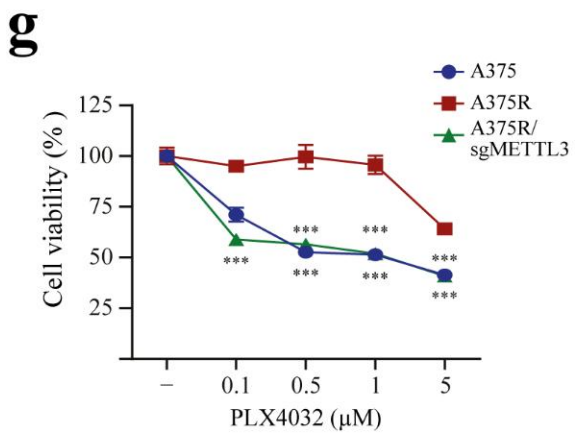

Figure 11 (h-k)

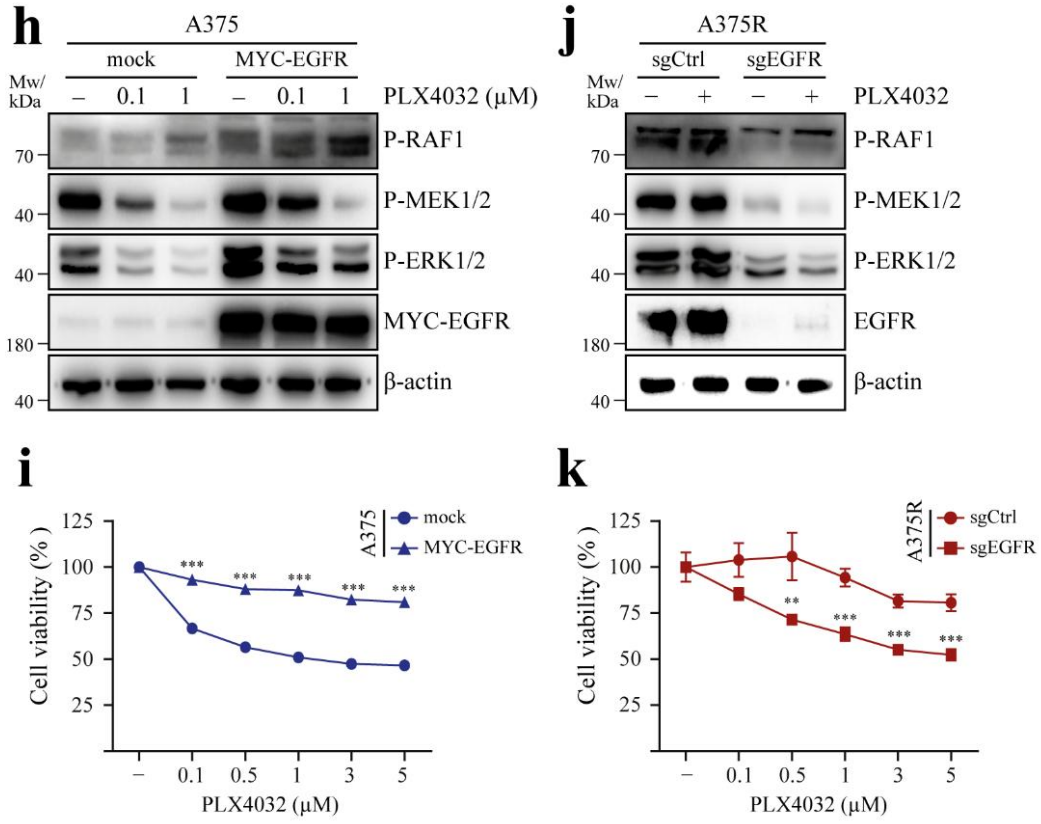

Figure 11 (l-m)

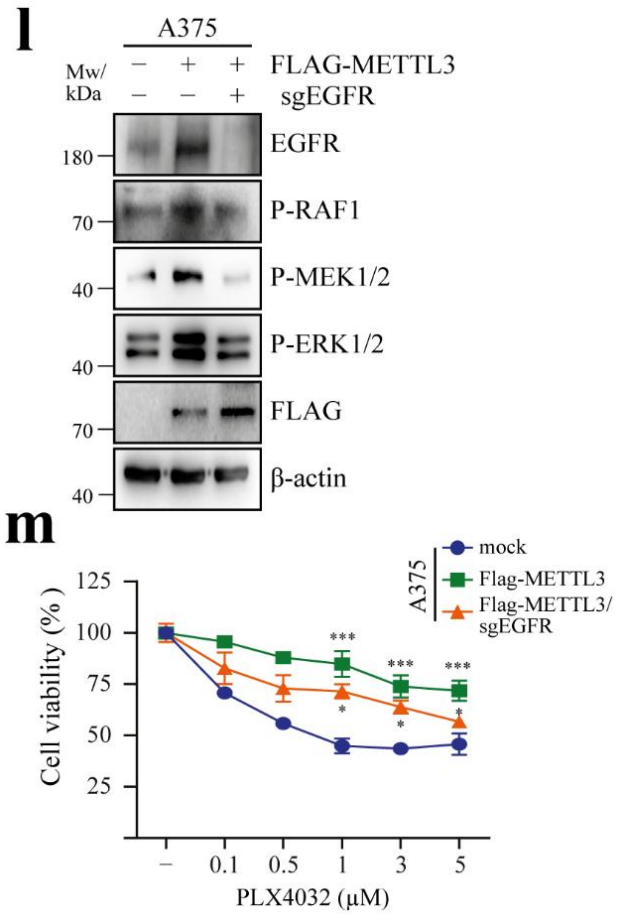

Figure 11. METTL3 induces rebound activation of the RAF/MEK/ERK pathway through enhanced expression of EGFR.

a The RAF/MEK/ERK pathway is upregulated in A375R cells. Immunoblotting (IB) of cell lysates prepared from A375 and A375R cells detected using the indicated antibodies. **b** Overexpression of METTL3 in A375 cells upregulates the RAF/MEK/ERK pathway. IB of A375 and A375R cells transfected with mock or Flag-METTL3 as detected using the indicated antibodies. **c** Knockout of METTL3 in A375R cells downregulates the RAF/MEK/ERK pathway. IB of A375 and A375R cells transfected with sgCtrl or sgMETTL3 as detected using the indicated antibodies. **d** Cycloleucine treatment reduces the activation of the RAF/MEK/ERK pathway in A375R cells. IB of cell lysates prepared from A375R cells treated with cycloleucine as detected using the indicated antibodies. **e** Overexpression of METTL3 reduces the sensitivity of A375 cells to PLX4032. IB of A375 cells expressing Flag-METTL3 and treated with PLX4032 as detected using the indicated antibodies. **f** Knockout of METTL3 restores the sensitivity of A375R cells to PLX4032. IB of A375 and A375R cells transfected with sgCtrl or sgMETTL3 and treated with PLX4032 as detected using the indicated antibodies. **g** Cell viability of A375 and A375R cells transfected with sgCtrl or sgMETTL3 in response to PLX4032 treatment as determined by MTT assay. Values represent the means ± SD, N = 3. One-way ANOVA, *** $P < 0.001$ (A375 versus A375R, A375R versus A375R/sgMETTL3, corresponding concentrations). **h, i** Overexpression of EGFR reduces the sensitivity of A375 cells to PLX4032. IB of cell lysates prepared from A375 cells overexpressing MYC-EGFR and treated with PLX4032 as detected using the indicated antibodies (**h**), and cell viability of A375 cells transfected with mock or myc-EGFR in response to PLX4032 treatment as determined by MTT assay (**i**). Values represent the means ± SD, N = 3. Unpaired t -test, *** $P < 0.001$ (mock versus MYC-EGFR, corresponding concentrations). **j, k** Knockout of EGFR reduces the sensitivity of A375R cells to PLX4032. IB

of A375R cells transfected with sgCtrl or sgEGFR and treated with PLX4032 as detected using the indicated antibodies (**j**), and cell viability of A375R cells transfected with sgCtrl or sgEGFR in response to PLX4032 treatment as determined by MTT assay (**k**). Values represent the means ± SD, N = 3. Unpaired t -test, ** $P < 0.01$, *** $P < 0.001$ (sgCtrl versus sgEGFR, corresponding concentrations). **l, m** Rebound activation of the RAF/MEK/ERK pathway induced by METTL3 is mediated via EGFR. IB of cell lysates prepared from A375-EGFR wild-type or knockout cells transfected with Flag-METTL3 as detected using the indicated antibodies (**l**), and cell viability of A375-EGFR wild-type or knockout cells transfected with FLAG-METTL3 with or without sgEGFR in response to PLX4032 treatment as determined by MTT assay (**m**). Values represent the means ± SD, N = 3. One-way ANOVA, * $P < 0.05$, *** $P < 0.001$ (mock versus FLAG-METTL3, FLAG-METTL3 versus FLAG-METTL3/sgEGFR, corresponding concentrations).

12. METTL3-promoted EGFR expression inhibits PLX4032-induced apoptosis in A375R cells

To demonstrate whether METTL3-promoted rebound activation of the RAF/MEK/ERK pathway underlies the inhibition of apoptosis induced by PLX4032, we overexpressed METTL3 in A375 cells followed by PLX4032 treatment. The results showed that METTL3 inhibited the cleavage of caspase 3 and PARP induced by PLX4032, whereas METTL3 knockout in A375R cells increased PLX4032-mediated caspase 3 and PARP cleavage (Figures 12a and b). To demonstrate whether the anti-apoptotic function of METTL3 in A375R cells was due to increased EGFR expression, we knocked out EGFR in A375R cells, which led to increased caspase 3 and PARP cleavage; these effects were augmented by PLX4032 treatment (Figure 12c). Cell cycle analysis revealed sub-G1 peaks following METTL3 or EGFR knockout in A375R cells followed by PLX4032 treatment, with a concomitant increase in the population of sub-G1 cells (Figure 12d and e). Finally, terminal deoxynucleotidyl transferase (TdT)-mediated dUTP nick end labeling (TUNEL) staining to examine the apoptotic fragmentation of DNA revealed extensive DNA fragmentation after METTL3 or EGFR knockout in A375R cells followed by PLX4032 treatment (Figure 12f). Together, these results indicated that inhibition of METTL3 reduces EGFR protein expression to restore PLX4032-induced apoptosis in A375R cells.

Figure 12 (a-c)

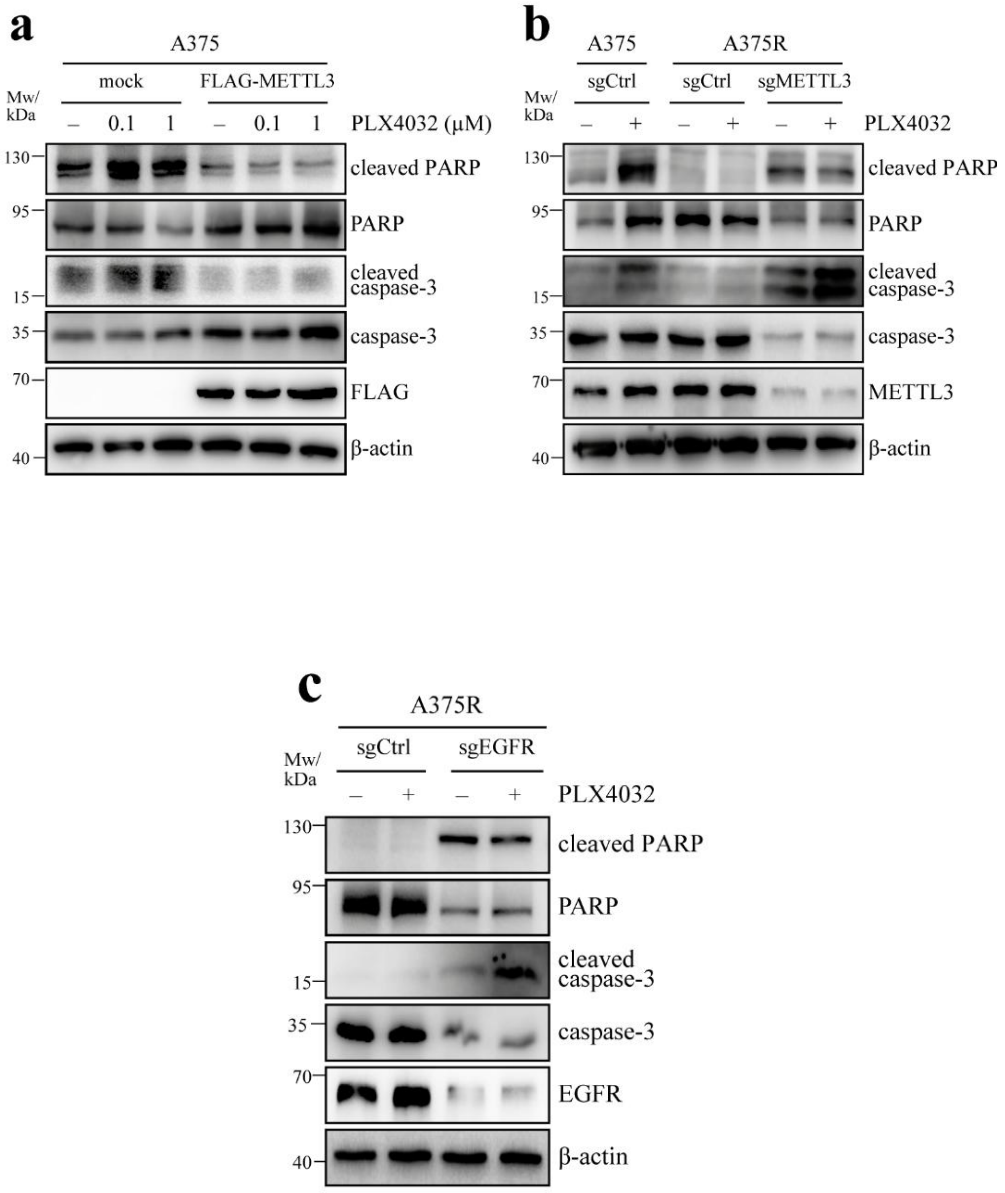

Figure 12 (d-e)

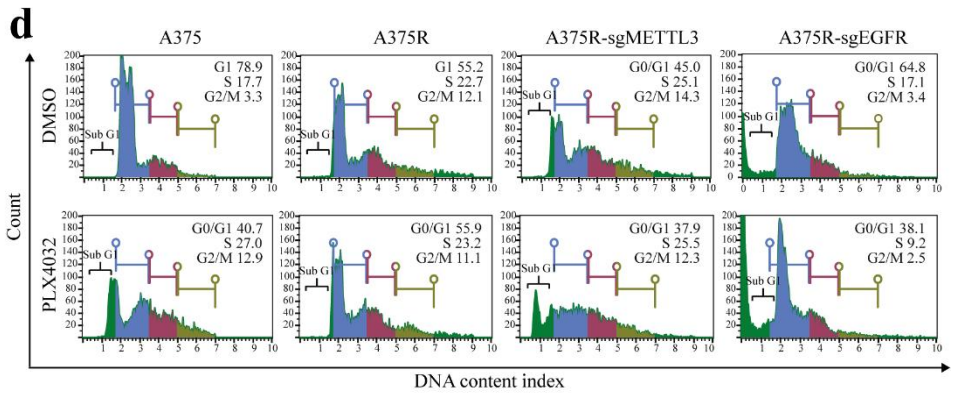

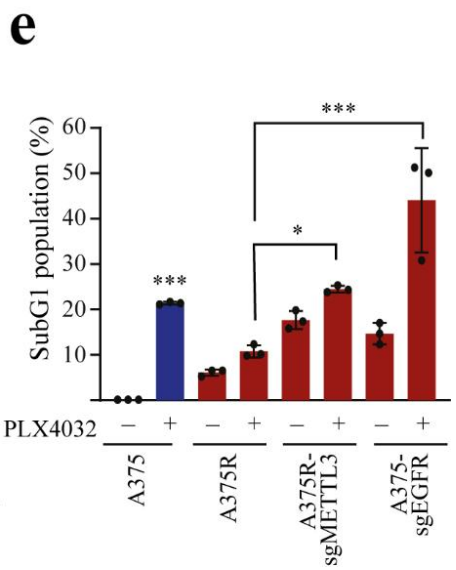

Figure 12 (f)

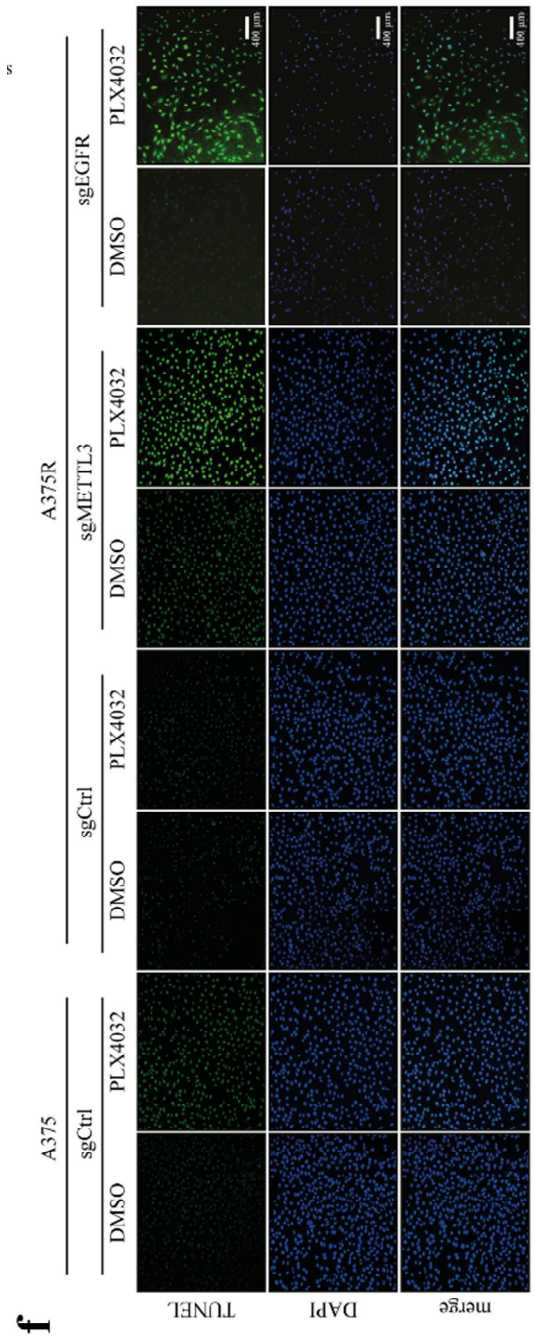

Figure 12. Knockout of METTL3 restores PLX4032-mediated apoptosis in A375R cells

a Overexpression of METTL3 prevents the apoptosis induced by PLX4032 in A375 cells. Immunoblotting (IB) of cell lysates prepared from A375 cells transfected with mock or Flag-METTL3 followed by treatment with PLX4032 as detected using the indicated antibodies. **b** Knockout of METTL3 restores the apoptosis induced by PLX4032 in A375R cells. IB of cell lysates prepared from A375 and A375R cells transfected with sgCtrl or sgMETTL3 followed by treatment with PLX4032 as detected using the indicated antibodies. **c** Knockout of EGFR restores the apoptosis induced by PLX4032 in A375R cells. IB of cell lysates prepared from A375R cells transfected with sgCtrl or sgMETTL3 followed by treatment with PLX4032 as detected using the indicated antibodies. **d-e** Knockout of METTL3 or EGFR in A375R cells increases the population of sub-G1 cells. Cell cycle distribution of A375 and A375R cells transfected with sgCtrl, sgMETTL3 or sgEGFR was analyzed using the muse cell cycle analyzer (**d**), and population of subG1 cells (**e**). Values represent the means ± SD, N = 3. One-way ANOVA, * $P < 0.05$, *** $P < 0.001$. **f** Knockout of METTL3 or EGFR increases the fragmentation of DNA. A375 or A375R cells transfected with sgMETTL3 or sgEGFR were stained with TUNEL reagent (green) or DAPI (blue) and DNA fragmentation was examined. Scale bars, 400 μm.

13. Inhibition of METTL3 restores PLX4032 sensitivity *in vivo* by decreasing EGFR expression

To study the effect of METTL3 on the tumorigenesis of PLX4032-resistant cells, we performed a soft agar assay using A375 and A375R cells. METTL3 knockout followed by PLX4032 treatment significantly reduced the number and size of colonies formed by A375R cells (Figures 13a and b). The effect of METTL3 on PLX4032 resistance in vivo was then studied using a xenograft model. A375 and A375R cells transfected with sgCtrl or sgMETTL3 were injected subcutaneously into the flanks of BALB/c nude mice. PLX4032 significantly reduced tumor volume and weight in A375-sgCtrl but not in A375R-sgCtrl mice (Figures 13c and d). In contrast, PLX4032 significantly reduced tumor weight and volume in A375R-sgMETTL3 mice compared to that in A375R-sgCtrl mice (Figures 13c and d). Additionally, we found that METTL3 knockout alone significantly reduced A375R cell tumorigenesis in BALB/c mice. The results indicated that inhibition of METTL3 sensitizes the A375R cells to PLX4032 treatment in vivo. Histopathological examination of mice tumors revealed that the increase in tumor size is correlated with the development of necrotic core in the tumor. The necrotic area was larger in A375R-sgCtrl mice than in A375-sgCtrl mice. Furthermore, METTL3 knockout followed by PLX4032 treatment reduced the tumor necrosis in A375R-sgMETTL3 mice compared to A375R-sgCtrl mice, suggesting that knockout of METTL3 potentiates the anti-necrotic effect of PLX4032 in A375R cells to suppress tumor formation (Figure 13e). Finally, we investigated whether the increased sensitivity to PLX4032 observed in A375R-sgMETTL3 mice was due to decreased EGFR expression. METTL3 knockout significantly reduced global and EGFR m^6A levels in mouse tumors without reducing EGFR mRNA levels (Figures 13f and g). In contrast, EGFR protein expression was significantly decreased in A375R sgMETTL3 mice (Figure 13h). Together, these results indicate that knockout of METTL3 sensitizes A375R cells to PLX4032

via reduced EGFR protein expression, resulting in the suppression of colony formation and tumorigenicity in melanoma.

Figure 13 (a-b)

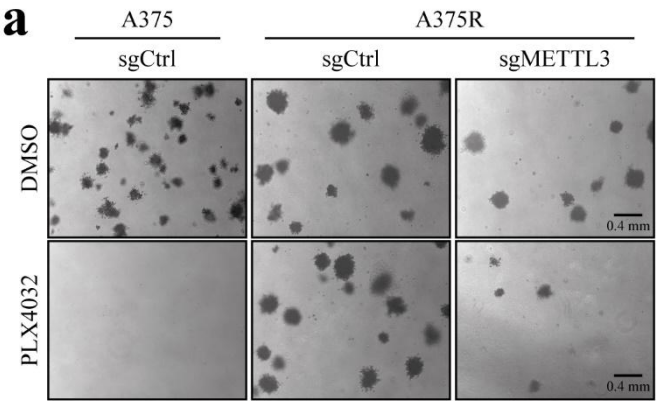

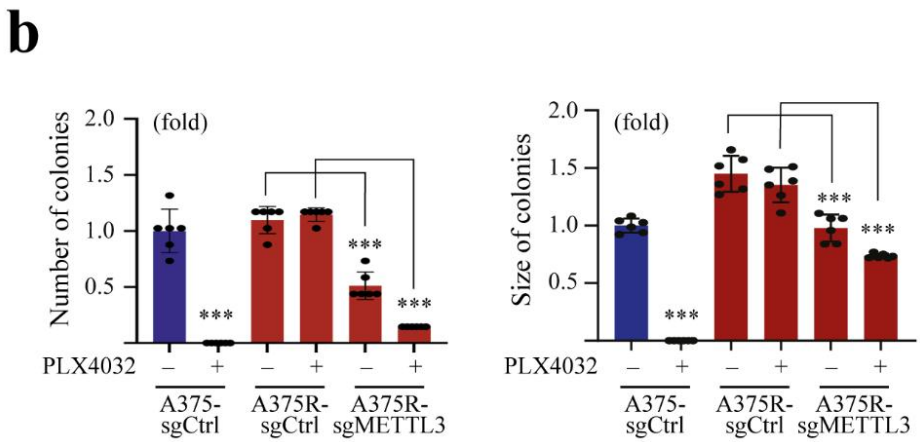

Figure 13 (c-d)

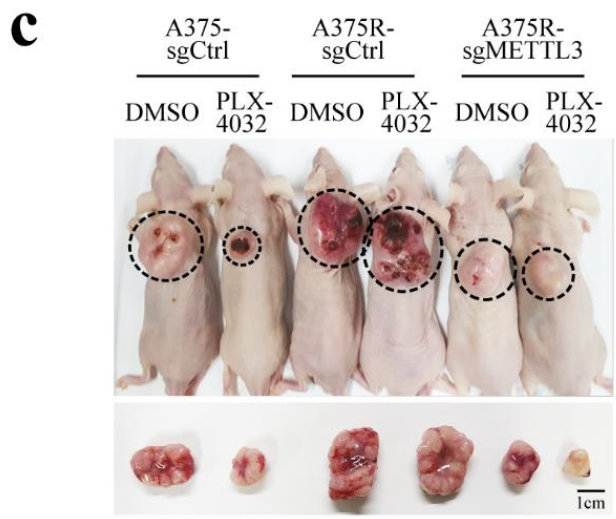

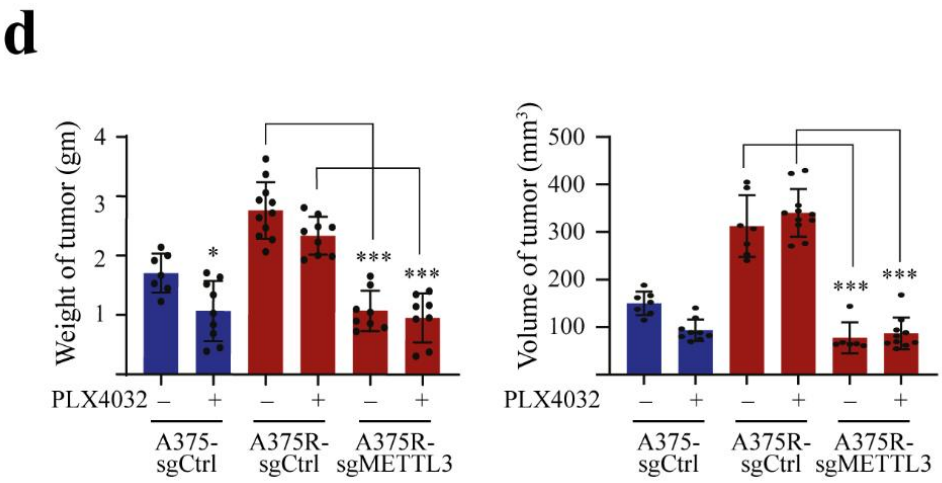

Figure 13 (e)

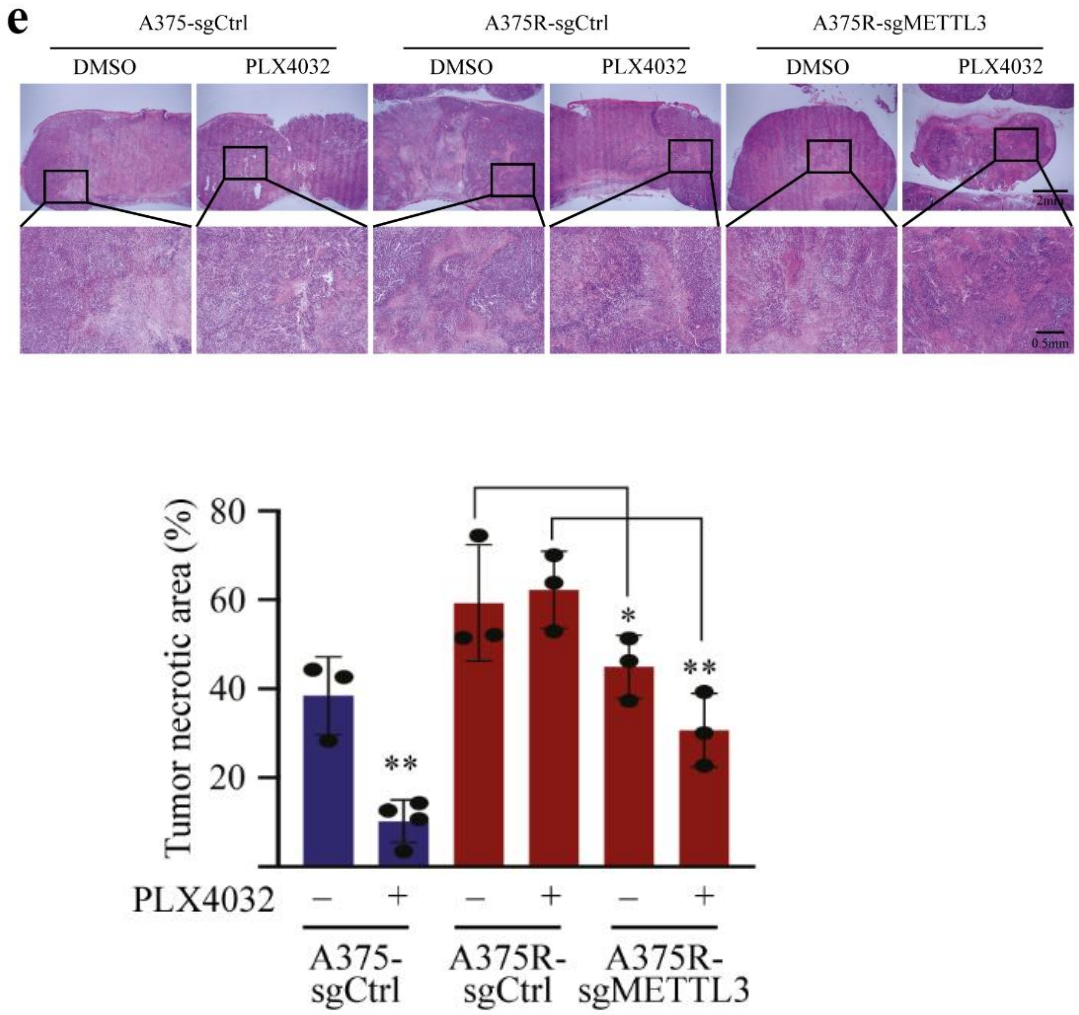

Figure 13 (f-h)

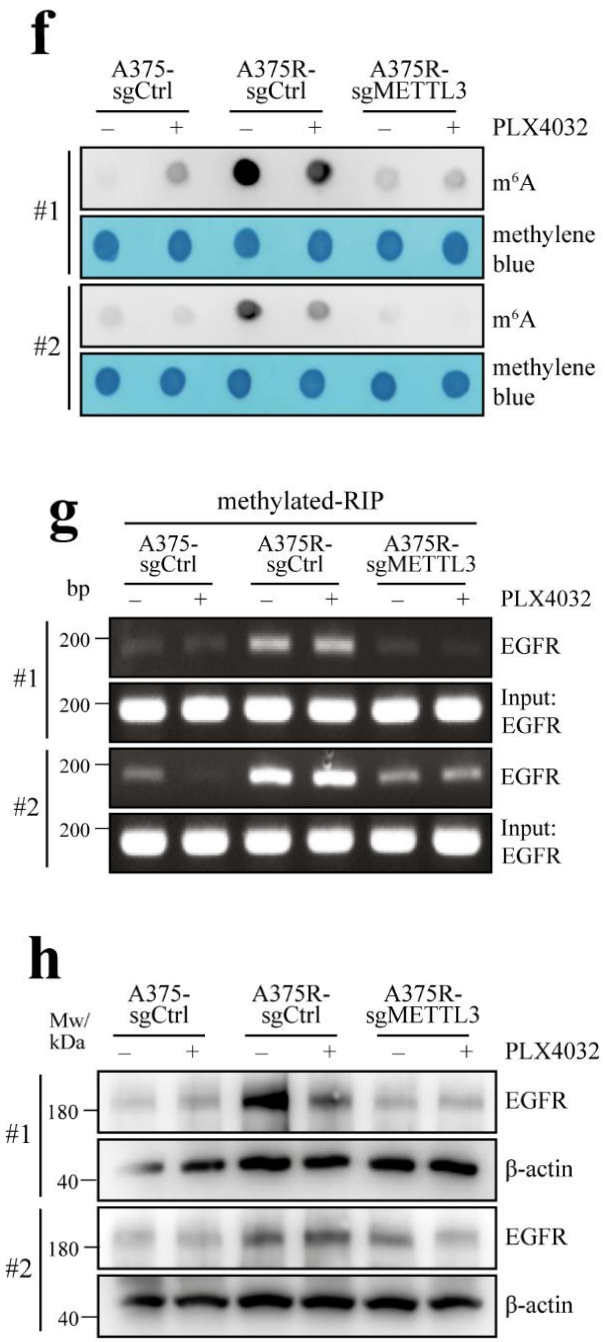

Figure 13. Knockout of METTL3 increases the PLX4032 sensitivity of A375R cells during colony formation and tumorigenesis.

a, b Knockout of METTL3 reduces the formation of PLX4032-resistant colonies in A375R cells. Representative images of colonies formed by A375 and A375R cells transfected with sgCtrl or sgMETTL3 plasmids in the presence or absence of PLX4032 in soft agar matrix **(a)** and quantification of colony size and number **(b)**. Values represent the means ± SD, N = 6. One-way ANOVA, *** $P < 0.001$. Scale bars, 0.4 mm **c-e** Knockout of METTL3 restores the PLX4032 sensitivity of A375R cells in vivo. A375 and A375R cells transfected with sgCtrl or sgMETTL3 were subcutaneously injected into BALB/c nude mice, followed by injection with 20 mg/kg PLX4032 for 25 days. Representative images of tumors **(c)**, tumor weight and volume at the time of sacrifice **(d)**, and tumor sections of each group stained with hematoxylin and eosin (**e**, left). Quantification of necrotic area (**e**, right). Values represent the means ± SD, N = 8 or 12. One-way ANOVA, * $P < 0.05$, *** $P < 0.001$. **f-h** Biochemical analysis of mice tumors. Dot blotting of poly(A) RNA purified from tumor samples as detected using an anti-m^6A antibody **(f)**. Total RNA prepared from tumor samples was immunoprecipitated using an anti-m^6A antibody. Gene expression in the input sample or IP fraction was analyzed by using semi-quantitative RT-PCR with primers that target EGFR **(g)**. WB of lysates prepared from tumor samples as detected using the indicated antibodies **(h)**. Scale bars in **(c)** or **(e)**, 1 cm or 0.5 mm, respectively.

IV. Discussion

Part I: : Stabilization of METTL3 by PIN1 promotes breast tumorigenesis via enhanced m6A-dependent translation

The epitranscriptomic modification of RNA serves as an important mechanism for regulating gene expression (Kumar & Mohapatra, 2021). The term "epitranscriptomic modification" refers to the chemical modification of ribonucleotides present in RNA molecules, including mRNA, rRNA, tRNA, and lncRNA (Wiener & Schwartz, 2021). To date, over 130 chemical modifications have been reported in RNA molecules with m^6A being the most common modification present in mRNA (Kumar & Mohapatra, 2021). M^6A regulates various aspects of mRNA biology, such as stability, splicing, and translation efficiency, to mediate important physiological processes, including neurodevelopment, immune response, and gametogenesis.(Jiang et al., 2021; Wang et al., 2022) The upregulation of the key m^6A methyltransferase, METTL3, promotes the progression of various human cancers, including breast cancer (Hu et al., 2022; Wang et al., 2020). However, the mechanisms underlying the regulation of METTL3 expression and function remain unclear. In this study, we identified PIN1 as a positive regulator of METTL3 stability in breast cancer cells. In addition, we found that PIN1 promoted the translation efficiency of *TAZ* and *EGFR* via an m^6A-dependent mechanism to promote breast tumorigenesis. Furthermore, MEK1/2 were identified as modulators of PIN-regulated METTL3 stability. The dual inhibition of MEK1/2 and PIN1 synergistically reduced the half-life of METTL3, resulting in the inhibition of breast tumorigenesis.

Previous studies have shown that METTL3 expression is higher in breast cancer cells than in normal cells (Hu et al., 2022; Wang et al., 2020). Moreover, the overexpression of METTL3 in breast cancer promotes tumor cell invasion, metastasis, and resistance to chemotherapy, which

are phenotypes that are often associated with high-grade breast cancer (Cheng et al., 2021; Pan et al., 2021; Wan et al., 2022). However, the examination of gene expression at the mRNA level did not reveal a significant increase in METTL3 expression in breast tumors, suggesting that enhanced protein stability may be responsible for increased METTL3 expression (Wu et al., 2019). The regulation of protein stability depends on protein phosphorylation and subsequent changes in protein ubiquitination levels (Nishi et al., 2014). A previous study showed that the phosphorylation of METTL3 induced by proline-directed ERK1/2 promotes its stability by reducing polyubiquitination (Sun et al., 2020). However, the molecular mechanism by which METTL3 ubiquitination is regulated remains poorly understood. Furthermore, the role of lysosomal degradation on METTL3 stability has not yet been elucidated. Here, we found that PIN1 binds to METTL3 through its PPIase domain. Although the WW domain of PIN1 has a 10-fold-higher binding affinity for peptides with the pSer/Thr motif, the PPIase domain alone has been reported to bind with and induce *cis/trans* isomerization around the motif (Innes et al., 2013). Moreover, the phosphorylation of METTL3 at S525 was crucial for its interaction with PIN1. Interestingly, METTL3 phosphorylation at S525 has previously been implicated in increased METTL3 stability, suggesting that the PIN1-METTL3 interaction may play an important role in the regulation of METTL3 stability. Here, we showed that PIN1 reduces the polyubiquitination levels and lysosomal degradation of METTL3 to increase its stability and half-life in breast cancer cells. Furthermore, the stabilization of METTL3 by PIN1 was associated with increased global m^6A mRNA modification.

To understand the precise mechanism by which m^6A modifications promote breast tumorigenesis, it is essential to identify specific mRNA substrates. Several studies have shown that TAZ and EGFR play critical roles in breast tumorigenesis (Guo et al., 2016; Hashmi et al., 2019; Masuda

et al., 2012; Shen et al., 2019). Therefore, the combined inhibition of these proteins may be a potential therapeutic strategy for the treatment of breast cancer (Guo et al., 2016). However, the feasibility of this combination chemotherapy is limited by the lack of specific pharmacological inhibitors. This has triggered interest in the search for alternative mechanisms that may interfere with the function of both TAZ and EGFR. Interestingly, both *TAZ* and *EGFR* have been reported to undergo METTL3-mediated m^6A modification in lung cancer (Lin et al., 2016). In light of these findings, we aimed to study the regulatory role of PIN1 in the m^6A modification of *TAZ* and *EGFR* mRNA in breast cancer. PIN1 increased the METTL3-mediated m^6A modification of *TAZ* and *EGFR*. The increased m^6A modification of mRNA has the potential to regulate gene expression through several mechanisms, including the recruitment of m^6A reader proteins, such as YTH domain-containing proteins (YTHDF1/2/3), or by recruiting other indirect m^6A readers, such as eIF3b (Zaccara et al., 2019). The outcome of m^6A deposition depends largely on the location of m^6A residues in the mRNA. For instance, the presence of m^6A in the 5' UTR promotes cap-independent translation via the recruitment of eIF3b, whereas m^6A located within the coding sequence promotes translation by recruiting elongation factors such as eEF2 in a YTHDF1-dependent manner (Lin et al., 2019; K. D. Meyer et al., 2015). In contrast, m^6A is present around stop codons, as is the case with *TAZ* and *EGFR*, and promotes translation efficiency via the facilitation of polysome formation in a METTL3-dependent manner (Lin et al., 2016). Using translation reporter constructs containing m^6A sites derived from *TAZ* and *EGFR* mRNA, we showed that PIN1 enhanced the translation efficiency of these mRNAs in response to stimulation with FBS. Previous studies have shown that METTL3 can directly bind to m^6A-modified mRNA in the cytosol, thereby promoting mRNA looping and translation efficiency via METTL3-eIF3h bridge formation (Choe et al., 2018). Furthermore, METTL3 bound to the 3' UTR of an mRNA recruits the initiation factor eIF3b to eIF4E to initiate mRNA translation (Lin et al., 2016).

Consistent with previous reports, we detected a strong interaction between METTL3 and *TAZ* or *EGFR* mRNA, which was strongly reduced by the knockout of PIN1. Consequently, polysome formation and ribosome loading into *TAZ* and *EGFR* mRNAs were significantly reduced in PIN1-knockout breast cancer cells.

Given the direct involvement of METTL3 in mRNA translation, it is arguable that the inhibition of METTL3 is of key interest for therapeutic purposes (Zeng et al., 2020). However, few METTL3 inhibitors are currently available or have not been approved for clinical trials (Yankova et al., 2021). As PIN1 interacts with METTL3 in a phosphorylation-dependent manner, we hypothesized that the dual inhibition of PIN1 and the upstream kinase pathway responsible for METTL3 phosphorylation may be an alternative therapeutic strategy. A previous study showed that the MEK/ERK pathway phosphorylates METTL3 at S525, which also facilitates its interaction with PIN1 (Lugowska et al., 2015; Wei et al., 2015). Here, we showed that the dual inhibition of MEK1/2 and PIN1 using PD98059 and ATRA synergistically reduced METTL3 protein stability to suppress the m^6A-dependent translation of *TAZ* and *EGFR*. The combination of these compounds induced cell cycle arrest at the G0/G1 phase, reduced cell proliferation, and decreased the expression of the cell proliferation biomarker Ki67. Interestingly, the overexpression of METTL3 attenuated the anticancer effects of ATRA and PD98059. Previous studies have shown that PD98059 alone is not effective against breast cancer; however, the sensitivity of cancer cells to ATRA is variable (Centritto et al., 2015; Wei et al., 2015; Zhao et al., 2017). Here, we showed that a combination of PD98059 and ATRA offers a unique possibility to tackle breast tumorigenesis by inhibiting METTL3-induced translation. A previous report showed that the combination of ATRA and PLX4032, which is a BRAF V600E kinase inhibitor, synergistically reduced EGFR expression in melanoma cells (KIM et al., 2019). Consistent with

the *in vitro* results, the knockout of METTL3 reduced the growth of tumors formed by PIN1-overexpressing 4T1 cells in an orthotopic mouse model, implying that PIN1-induced breast tumorigenesis depends on METTL3 stabilization. Altogether, our study shows that PIN1 increases the stability of METTL3 to enhance the m^6A modification of specific mRNAs, such as TAZ and EGFR. Increased m^6A modification promotes the translation efficiency of TAZ and EGFR and is associated with the progression of breast cancer. Furthermore, the inhibition of PIN1 and MEK1/2 with small-molecule inhibitors provides a potential strategy to inhibit the m^6A-dependent translation of TAZ and EGFR to suppress breast tumorigenesis.

The adaptability of cancer cells to their microenvironment and cell plasticity remains a challenging problem in anticancer chemotherapy. Emerging evidence has suggested that the dysregulation of protein synthesis is a central feature of cancer cell plasticity (Lee et al., 2021). Specifically, the regulation of protein synthesis via the epitranscriptomic modification of mRNA has attracted significant interest from a therapeutic perspective. However, the molecular mechanisms underlying the regulation of epitranscriptome-related proteins remain poorly understood. In this study, we revealed the regulatory role of PIN1 in mRNA translation through the regulation of METTL3 stability in breast cancer cells (Figure B). *In vivo* studies and clinical trials using a combination of MEK and PIN1 inhibitors in breast cancer may further reveal useful information about the clinical application of our findings. Furthermore, a structural analysis of METTL3 and PIN1 binding interfaces may lead to the development of a small-molecule inhibitor of the METTL3-PIN1 interaction for therapeutic purposes. In conclusion, we showed that PIN1 mediated METTL3 stabilization is a critical regulator of breast tumorigenesis.

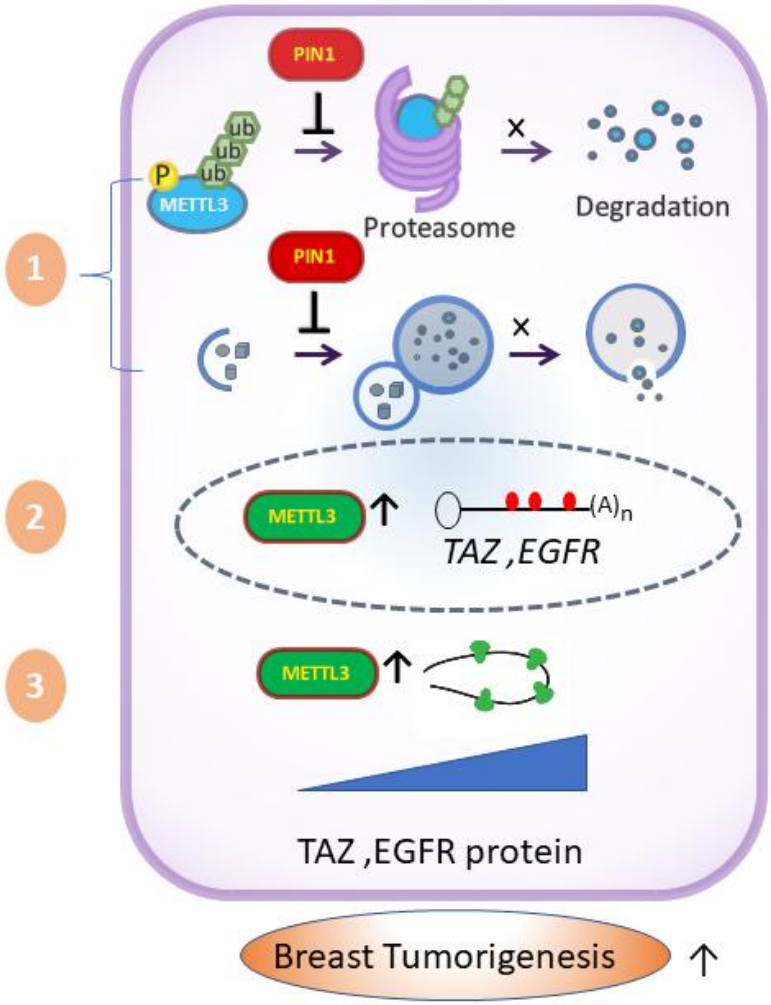

Figure B. A proposed model for the regulation of METTL3-mediated translation by PIN1 in breast cancer cells

Part II: METTL3 induces PLX4032 resistance in melanoma by promoting m^{6}A-dependent EGFR translation

BRAF-V600E constitutes an attractive target for chemotherapy, being the most frequent oncogenic mutation in patients with melanoma (Ascierto et al., 2012; Cantwell-Dorris et al., 2011). Developed as a specific inhibitor of BRAF kinase (V600E),(Flaherty, 2011; Flaherty & McArthur, 2010) PLX4032 exhibits a high response rate of 80% at the beginning of chemotherapy; however, tumor relapse occurs within six months in most patients (Sun et al., 2014). Previous studies have shown that rebound activation of the RAF/MEK/ERK pathway is associated with the acquired resistance to PLX4032 and subsequent tumor relapse (Chan et al., 2017; Girotti et al., 2013; Lito et al., 2013; McCubrey et al., 2006). Several reports have also shown that EGFR protein levels are upregulated in PLX4032-resistant melanoma cells, which play an essential role in rebound activation of the MAPK and PI3K/AKT pathways (Dratkiewicz et al., 2020; KIM et al., 2019; Prahallad et al., 2012). However, mechanisms underlying the EGFR upregulation in PLX4032-resistant tumors remain poorly understood. In the present study, we identified METTL3 as a positive regulator of EGFR expression in PLX4032-resistant melanoma cells.

The RNA methyltransferase METTL3 catalyzes the formation of m^{6}A within the consensus “GGAC” motif in mRNAs (Roundtree et al., 2017). Although m^{6}A modification in mRNA has been recognized for almost 50 years, the distribution of these modifications and their role in physiology and disease have only recently been elucidated (Jiang et al., 2021). Recent advancements in the sequencing of the global m^{6}A methylome have revealed that m^{6}A is the most abundant internal chemical modification in mRNAs (Roundtree et al., 2017; Zaccara et al., 2019). Notably, the expression of METTL3 is upregulated in several tumors (Xiang et al., 2020).

Herein we found that METTL3 expression is also increased in a PLX4032-resistant melanoma cell line, whereas expression of the m^6A demethylase FTO was not changed. Our data agree with the data included in the Broad Institute DepMap portal, which reveals a positive correlation between m^6A methyltransferase complex proteins including METTL3, METTL14, and WTAP, and PLX4032 resistance AUC. We further demonstrated that the global m^6A modification of mRNA mediated by METTL3 is also increased in PLX4032-resistant melanoma cells.

Rebound activation of the RAF/MEK/ERK pathway in PLX4032-resistant melanoma cells is mediated through several mechanisms including amplification and enhanced transcription of genes encoding e.g. B-RAF and C-RAF, activating mutation in RAFs, MEKs, and NF1, and enhanced protein stability of related signaling proteins (Ascierto et al., 2012; Cantwell-Dorris et al., 2011; Lito et al., 2013; McCubrey et al., 2006; Sun et al., 2014). However, the role of chemical modifications of mRNA such as m^6A on activation of the RAF/MEK/ERK pathway has not been described. In the present study, we examined the m^6A level of several genes related to this pathway. Analysis of the data available in the DepMap portal revealed that mRNAs including *EGFR* and *RAF1* may constitute potential targets for METTL3-induced m^6A modification in PLX4032-resistant melanoma cells. Using meRIP–qPCR, we confirmed that the mRNA m^6A levels of *EGFR*, *NRAS*, *RAF1*, *NF1*, and *NF2* were increased in PLX4032-resistant melanoma cells. Amongst these, only *EGFR* mRNA has previously been reported to contain m^6A modification (Lin et al., 2016). We hypothesized that the elevation of both METTL3 expression and *EGFR* mRNA m^6A modification in PLX4032-resistant melanoma cells might promote the translation of EGFR. However, independent of its catalytic activity, METTL3 might also be involved in the enhanced translation of specific mRNAs such as *EGFR* via polysome formation (Lin et al., 2016). To clarify the underlying mechanism, we utilized a luciferase-based translation reporter and puromycin labeling, which revealed that increased m^6A modification mediated by

METTL3 promotes the translation efficiency of EGFR in PLX4032-resistant cells. Moreover, overexpression or knockout of METTL3 did not alter the *EGFR* mRNA level, further corroborating that the increased EGFR protein derives from enhanced mRNA translation.

Recent studies have demonstrated that m^6A promotes the translation of specific mRNAs to induce drug resistance in cancer (Jin et al., 2019). In the present study, the protein levels of EGFR exhibited the strongest correlation with PLX4032 resistance AUC among several m^6A-modified mRNAs in melanoma cells. Consistent with this, previous reports have indicated that increased expression of EGFR facilitates the acquired resistance to PLX4032 in melanoma, as well as intrinsic resistance to PLX4032 in colon cancer and thyroid cancer (Jia et al., 2018; KIM et al., 2019; Prahallad et al., 2012). Here, we further demonstrated that METTL3 knockout in PLX4032-resistant melanoma cells reduces EGFR expression and suppresses the activity of the RAF/MEK/ERK pathway to restore PLX4032 sensitivity in melanoma cells. In addition, we confirmed that the METTL3-induced RAF/MEK/ERK pathway activation was dependent on EGFR expression as the knockout of EGFR suppressed this activation. Moreover, previous studies have indicated that increased expression of METTL3 promotes the survival of cancer cells through inhibition of apoptosis (Jin et al., 2019). Herein we showed that knockout of METTL3 restored PLX4032-induced apoptosis in PLX4032-resistant melanoma cells by reducing EGFR expression. In addition, METTL3 knockout in resistant cells increased the population of sub-G1 cells, indicating the critical role of METTL3 in the inhibition of apoptosis. Our results are consistent with a recent report showing that METTL3 inhibition via a pharmacological inhibitor markedly increased the population of sub-G1 cells in acute myeloid leukemia (Yankova et al., 2021). Additionally, ablation of METTL3 increased the sensitivity of PLX4032-resistant melanoma cells to PLX4032 during colony formation. The inhibition of PLX4032 resistance upon METTL3 knockout was further supported by our findings from a

mouse xenograft model, in which ablation of METTL3 in PLX4032-resistant melanoma cells reduced the volume of tumors in BALB/c nude mice following PLX4032 treatment. Together, our data indicated that enhanced translation of EGFR mediated by increased expression of METTL3 promotes PLX4032 resistance in melanoma. As METTL3 regulates the m^6A modification of several mRNAs, it is possible that METTL3 promotes PLX4032 resistance through RAF/MEK/ERK-independent mechanisms. Future studies should analyze m^6A-modified transcriptome from PLX4032-sensitive and resistant tumor samples to identify the most critical target of METTL3 in PLX4032 resistance.

Current strategies to overcome PLX4032 resistance in melanoma have primarily focused on developing novel RAF/MEK inhibitors or combining therapies with MEK inhibitors (Aplin et al., 2011; Larkin et al., 2014; Lim et al., 2017; Sun et al., 2014; Villanueva et al., 2011) but have afforded limited success owing to various factors such as high toxicity and inevitable tumor relapse (Villanueva et al., 2011). Here, we reveal the METTL3-induced upregulation of EGFR expression and subsequent rebound activation of RAF/MEK/ERK as a novel mechanism of PLX4032 resistance in melanoma and suggest METTL3 as a novel target for chemotherapy (Figure C). Notably, a potent inhibitor of METTL3 has recently been described (Yankova et al., 2021). Although further studies utilizing a pharmacological inhibitor of METTL3 are needed to provide information regarding the clinical efficacy of METTL3 inhibition in PLX4032-resistant melanoma, our findings highlight the possibility of inhibiting METTL3 function to restore PLX4032 sensitivity in patients with melanoma.

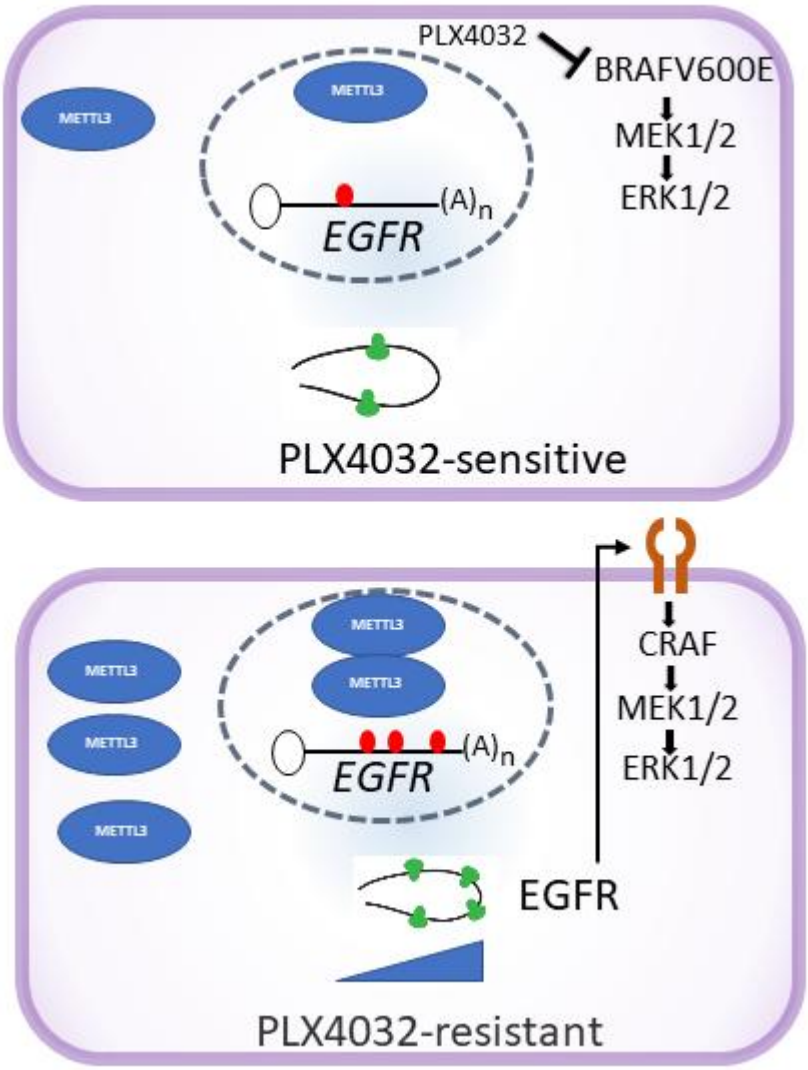

Figure C. A proposed model for the role of METTL3 in PLX4032-resistant melanoma

V. References

Aplin, A. E., Kaplan, F. M., & Shao, Y. (2011). Mechanisms of Resistance to RAF Inhibitors in Melanoma. *Journal of Investigative Dermatology*, *131*(9), 1817-1820. https://doi.org/10.1038/jid.2011.147

Ascierto, P. A., Kirkwood, J. M., Grob, J. J., Simeone, E., Grimaldi, A. M., Maio, M., Palmieri, G., Testori, A., Marincola, F. M., & Mozzillo, N. (2012). The role of BRAF V600 mutation in melanoma. *J Transl Med*, *10*, 85. https://doi.org/10.1186/1479-5876-10-85

Barbieri, I., Tzelepis, K., Pandolfini, L., Shi, J., Millán-Zambrano, G., Robson, S. C., Aspris, D., Migliori, V., Bannister, A. J., Han, N., De Braekeleer, E., Ponstingl, H., Hendrick, A., Vakoc, C. R., Vassiliou, G. S., & Kouzarides, T. (2017). Promoter-bound METTL3 maintains myeloid leukaemia by m(6)A-dependent translation control. *Nature*, *552*(7683), 126-131. https://doi.org/10.1038/nature24678

Beretta, G. L., De Cesare, M., Albano, L., Magnifico, A., Carenini, N., Corna, E., Perego, P., & Gatti, L. (2016). Targeting Peptidyl-Prolyl Isomerase Pin1 to Inhibit Tumor Cell Aggressiveness. *Tumori Journal*, *102*(2), 144-149. https://doi.org/10.5301/tj.5000471

Bokar, J. A., Shambaugh, M. E., Polayes, D., Matera, A. G., & Rottman, F. M. (1997). Purification and cDNA cloning of the AdoMet-binding subunit of the human mRNA (N6-adenosine)-methyltransferase. *RNA (New York, N.Y.)*, *3*(11), 1233-1247. https://pubmed.ncbi.nlm.nih.gov/9409616

https://www.ncbi.nlm.nih.gov/pmc/articles/PMC1369564/

Cai, Y., Feng, R., Lu, T., Chen, X., Zhou, X., & Wang, X. (2021). Novel insights into the m6A-RNA methyltransferase METTL3 in cancer. *Biomarker Research*, *9*(1), 27. https://doi.org/10.1186/s40364-021-00278-9

Cantwell-Dorris, E. R., O'Leary, J. J., & Sheils, O. M. (2011). BRAFV600E: implications for carcinogenesis and molecular therapy. *Mol Cancer Ther*, *10*(3), 385-394. https://doi.org/10.1158/1535-7163.MCT-10-0799

Carroll, M. J., Parent, C. R., Page, D., & Kreeger, P. K. (2019). Tumor cell sensitivity to vemurafenib can be predicted from protein expression in a BRAF-V600E basket trial setting. *BMC Cancer*, *19*(1), 1025. https://doi.org/10.1186/s12885-019-6175-2

Centritto, F., Paroni, G., Bolis, M., Garattini, S. K., Kurosaki, M., Barzago, M. M., Zanetti, A., Fisher, J. N., Scott, M. F., Pattini, L., Lupi, M., Ubezio, P., Piccotti, F., Zambelli, A., Rizzo, P., Gianni', M., Fratelli, M., Terao, M., & Garattini, E. (2015). Cellular and molecular determinants of

all-trans retinoic acid sensitivity in breast cancer: Luminal phenotype and RARα expression. *EMBO Molecular Medicine*, *7*(7), 950-972. https://doi.org/https://doi.org/10.15252/emmm.201404670

Chan, X. Y., Singh, A., Osman, N., & Piva, T. J. (2017). Role Played by Signalling Pathways in Overcoming BRAF Inhibitor Resistance in Melanoma. *International Journal of Molecular Sciences*, *18*(7). https://doi.org/10.3390/ijms18071527

Chen, Y., Wu, Y.-r., Yang, H.-y., Li, X.-z., Jie, M.-m., Hu, C.-j., Wu, Y.-y., Yang, S.-m., & Yang, Y.-b. (2018). Prolyl isomerase Pin1: a promoter of cancer and a target for therapy. *Cell Death & Disease*, *9*(9), 883. https://doi.org/10.1038/s41419-018-0844-y

Cheng, L., Zhang, X., Huang, Y.-Z., Zhu, Y.-L., Xu, L.-Y., Li, Z., Dai, X.-Y., Shi, L., Zhou, X.-J., Wei, J.-F., & Ding, Q. (2021). Metformin exhibits antiproliferation activity in breast cancer via miR-483-3p/METTL3/m6A/p21 pathway. *Oncogenesis*, *10*(1), 7. https://doi.org/10.1038/s41389-020-00290-y

Choe, J., Lin, S., Zhang, W., Liu, Q., Wang, L., Ramirez-Moya, J., Du, P., Kim, W., Tang, S., Sliz, P., Santisteban, P., George, R. E., Richards, W. G., Wong, K.-K., Locker, N., Slack, F. J., & Gregory, R. I. (2018). mRNA circularization by METTL3–eIF3h enhances translation and promotes oncogenesis. *Nature*, *561*(7724), 556-560. https://doi.org/10.1038/s41586-018-0538-8

Choi, J., Chen, J., Schreiber, S. L., & Clardy, J. (1996). Structure of the FKBP12-rapamycin complex interacting with the binding domain of human FRAP. *Science*, *273*(5272), 239-242. https://doi.org/10.1126/science.273.5272.239

Cordenonsi, M., Zanconato, F., Azzolin, L., Forcato, M., Rosato, A., Frasson, C., Inui, M., Montagner, M., Parenti, Anna R., Poletti, A., Daidone, Maria G., Dupont, S., Basso, G., Bicciato, S., & Piccolo, S. (2011). The Hippo Transducer TAZ Confers Cancer Stem Cell-Related Traits on Breast Cancer Cells. *Cell*, *147*(4), 759-772. https://doi.org/10.1016/j.cell.2011.09.048

Dahal, U., Le, K., & Gupta, M. (2019). RNA m6A methyltransferase METTL3 regulates invasiveness of melanoma cells by matrix metallopeptidase 2. *Melanoma Res*, *29*(4), 382-389. https://doi.org/10.1097/cmr.0000000000000580

Dominissini, D., Moshitch-Moshkovitz, S., Salmon-Divon, M., Amariglio, N., & Rechavi, G. (2013). Transcriptome-wide mapping of N6-methyladenosine by m6A-seq based on immunocapturing and massively parallel sequencing. *Nature Protocols*, *8*(1), 176-189. https://doi.org/10.1038/nprot.2012.148

Dominissini, D., Moshitch-Moshkovitz, S., Schwartz, S., Salmon-Divon, M., Ungar, L., Osenberg, S., Cesarkas, K., Jacob-Hirsch, J., Amariglio, N., Kupiec, M., Sorek, R., & Rechavi, G. (2012).

Topology of the human and mouse m6A RNA methylomes revealed by m6A-seq. *Nature*, *485*(7397), 201-206. https://doi.org/10.1038/nature11112

Dratkiewicz, E., Simiczyjew, A., Pietraszek-Gremplewicz, K., Mazurkiewicz, J., & Nowak, D. (2020). Characterization of Melanoma Cell Lines Resistant to Vemurafenib and Evaluation of Their Responsiveness to EGFR- and MET-Inhibitor Treatment. *International Journal of Molecular Sciences*, *21*(1). https://doi.org/10.3390/ijms21010113

Du, H., Zhao, Y., He, J., Zhang, Y., Xi, H., Liu, M., Ma, J., & Wu, L. (2016). YTHDF2 destabilizes m(6)A-containing RNA through direct recruitment of the CCR4-NOT deadenylase complex. *Nat Commun*, *7*, 12626. https://doi.org/10.1038/ncomms12626

Farrell, A. S., Pelz, C., Wang, X., Daniel, C. J., Wang, Z., Su, Y., Janghorban, M., Zhang, X., Morgan, C., Impey, S., & Sears, R. C. (2013). Pin1 regulates the dynamics of c-Myc DNA binding to facilitate target gene regulation and oncogenesis. *Molecular and Cellular Biology*, *33*(15), 2930-2949. https://doi.org/10.1128/MCB.01455-12

Flaherty, K. T. (2011). BRAF inhibitors and melanoma. *Cancer J*, *17*(6), 505-511. https://doi.org/10.1097/PPO.0b013e31823e5357

Flaherty, K. T., & McArthur, G. (2010). BRAF, a target in melanoma: implications for solid tumor drug development. *Cancer*, *116*(21), 4902-4913. https://doi.org/10.1002/cncr.25261

Fujiyama-Nakamura, S., Yoshikawa, H., Homma, K., Hayano, T., Tsujimura-Takahashi, T., Izumikawa, K., Ishikawa, H., Miyazawa, N., Yanagida, M., Miura, Y., Shinkawa, T., Yamauchi, Y., Isobe, T., & Takahashi, N. (2009). Parvulin (Par14), a peptidyl-prolyl cis-trans isomerase, is a novel rRNA processing factor that evolved in the metazoan lineage. *Mol Cell Proteomics*, *8*(7), 1552-1565. https://doi.org/10.1074/mcp.M900147-MCP200

Gerken, T., Girard, C. A., Tung, Y.-C. L., Webby, C. J., Saudek, V., Hewitson, K. S., Yeo, G. S. H., McDonough, M. A., Cunliffe, S., McNeill, L. A., Galvanovskis, J., Rorsman, P., Robins, P., Prieur, X., Coll, A. P., Ma, M., Jovanovic, Z., Farooqi, I. S., Sedgwick, B., . . . Schofield, C. J. (2007). The obesity-associated FTO gene encodes a 2-oxoglutarate-dependent nucleic acid demethylase. *Science (New York, N.Y.)*, *318*(5855), 1469-1472. https://doi.org/10.1126/science.1151710

Girotti, M. R., Pedersen, M., Sanchez-Laorden, B., Viros, A., Turajlic, S., Niculescu-Duvaz, D., Zambon, A., Sinclair, J., Hayes, A., Gore, M., Lorigan, P., Springer, C., Larkin, J., Jorgensen, C., & Marais, R. (2013). Inhibiting EGF receptor or SRC family kinase signaling overcomes BRAF inhibitor resistance in melanoma. *Cancer Discov*, *3*(2), 158-167. https://doi.org/10.1158/2159-8290.CD-12-0386

Guo, L., Zheng, J., Zhang, J., Wang, H., Shao, G., & Teng, L. (2016). Knockdown of TAZ modifies triple-negative breast cancer cell sensitivity to EGFR inhibitors by regulating YAP expression. *Oncol Rep*, *36*(2), 729-736. https://doi.org/10.3892/or.2016.4875

Hashmi, A. A., Naz, S., Hashmi, S. K., Irfan, M., Hussain, Z. F., Khan, E. Y., Asif, H., & Faridi, N. (2019). Epidermal growth factor receptor (EGFR) overexpression in triple-negative breast cancer: association with clinicopathologic features and prognostic parameters. *Surgical and Experimental Pathology*, *2*(1), 6. https://doi.org/10.1186/s42047-018-0029-0

Hu, S., Song, Y., Zhou, Y., Jiao, Y., & Li, G. (2022). METTL3 Accelerates Breast Cancer Progression via Regulating EZH2 m⁶A Modification. *Journal of Healthcare Engineering*, *2022*, 5794422. https://doi.org/10.1155/2022/5794422

Hua, W., Zhao, Y., Jin, X., Yu, D., He, J., Xie, D., & Duan, P. (2018). METTL3 promotes ovarian carcinoma growth and invasion through the regulation of AXL translation and epithelial to mesenchymal transition. *Gynecol Oncol*, *151*(2), 356-365. https://doi.org/10.1016/j.ygyno.2018.09.015

Huang, H., Weng, H., & Chen, J. (2020). The Biogenesis and Precise Control of RNA m^6A Methylation. *Trends in Genetics*, *36*(1), 44-52. https://doi.org/10.1016/j.tig.2019.10.011

Innes, B., Bailey, M., Brandl, C., Shilton, B., & Litchfield, D. (2013). Non-catalytic participation of the Pin1 peptidyl-prolyl isomerase domain in target binding [Original Research]. *Frontiers in Physiology*, *4*. https://doi.org/10.3389/fphys.2013.00018

Jia, Y., Zhang, C., Hu, C., Yu, Y., Zheng, X., Li, Y., & Gao, M. (2018). EGFR inhibition enhances the antitumor efficacy of a selective BRAF V600E inhibitor in thyroid cancer cell lines. *Oncology letters*, *15*(5), 6763-6769. https://doi.org/10.3892/ol.2018.8093

Jiang, X., Liu, B., Nie, Z., Duan, L., Xiong, Q., Jin, Z., Yang, C., & Chen, Y. (2021). The role of m6A modification in the biological functions and diseases. *Signal Transduction and Targeted Therapy*, *6*(1), 74. https://doi.org/10.1038/s41392-020-00450-x

Jin, D., Guo, J., Wu, Y., Du, J., Yang, L., Wang, X., Di, W., Hu, B., An, J., Kong, L., Pan, L., & Su, G. (2019). m^6A mRNA methylation initiated by METTL3 directly promotes YAP translation and increases YAP activity by regulating the MALAT1-miR-1914-3p-YAP axis to induce NSCLC drug resistance and metastasis. *Journal of Hematology & Oncology*, *12*(1), 135-135. https://doi.org/10.1186/s13045-019-0830-6

Kan, L., Grozhik, A. V., Vedanayagam, J., Patil, D. P., Pang, N., Lim, K.-S., Huang, Y.-C., Joseph, B., Lin, C.-J., Despic, V., Guo, J., Yan, D., Kondo, S., Deng, W.-M., Dedon, P. C., Jaffrey, S. R., &

Lai, E. C. (2017). The m6A pathway facilitates sex determination in Drosophila. *Nature Communications*, *8*(1), 15737. https://doi.org/10.1038/ncomms15737

Keene, J. D. (2001). Ribonucleoprotein infrastructure regulating the flow of genetic information between the genome and the proteome. *Proceedings of the National Academy of Sciences*, *98*(13), 7018-7024. https://doi.org/doi:10.1073/pnas.111145598

Khanal, P., Kim, G., Lim, S. C., Yun, H. J., Lee, K. Y., Choi, H. K., & Choi, H. S. (2013). Prolyl isomerase Pin1 negatively regulates the stability of SUV39H1 to promote tumorigenesis in breast cancer. *Faseb j*, *27*(11), 4606-4618. https://doi.org/10.1096/fj.13-236851

Khanal, P., Yeung, B., Zhao, Y., & Yang, X. (2019). Identification of Prolyl isomerase Pin1 as a novel positive regulator of YAP/TAZ in breast cancer cells. *Scientific Reports*, *9*(1), 6394. https://doi.org/10.1038/s41598-019-42767-w

Khanal, P., Yun, H. J., Lim, S. C., Ahn, S. G., Yoon, H. E., Kang, K. W., Hong, R., & Choi, H. S. (2012). Proyl isomerase Pin1 facilitates ubiquitin-mediated degradation of cyclin-dependent kinase 10 to induce tamoxifen resistance in breast cancer cells. *Oncogene*, *31*(34), 3845-3856. https://doi.org/10.1038/onc.2011.548

KIM, G., BHATTARAI, P. Y., OH, C.-H., & CHOI, H. S. (2019). All- *trans* Retinoic Acid Overcomes Acquired Resistance to PLX4032 *via* Inhibition of PIN1 in Melanoma Cells. *Anticancer Research*, *39*(12), 6537-6546. https://doi.org/10.21873/anticanres.13869

Kumar, S., & Mohapatra, T. (2021). Deciphering Epitranscriptome: Modification of mRNA Bases Provides a New Perspective for Post-transcriptional Regulation of Gene Expression [Review]. *Frontiers in Cell and Developmental Biology*, *9*. https://doi.org/10.3389/fcell.2021.628415

Larkin, J., Ascierto, P. A., Dreno, B., Atkinson, V., Liszkay, G., Maio, M., Mandala, M., Demidov, L., Stroyakovskiy, D., Thomas, L., de la Cruz-Merino, L., Dutriaux, C., Garbe, C., Sovak, M. A., Chang, I., Choong, N., Hack, S. P., McArthur, G. A., & Ribas, A. (2014). Combined vemurafenib and cobimetinib in BRAF-mutated melanoma. *N Engl J Med*, *371*(20), 1867-1876. https://doi.org/10.1056/NEJMoa1408868

Lee, L. J., Papadopoli, D., Jewer, M., del Rincon, S., Topisirovic, I., Lawrence, M. G., & Postovit, L.-M. (2021). Cancer Plasticity: The Role of mRNA Translation. *Trends in Cancer*, *7*(2), 134-145. https://doi.org/10.1016/j.trecan.2020.09.005

Lee, N. Y., Choi, H.-K., Shim, J.-H., Kang, K.-W., Dong, Z., & Choi, H. S. (2009). The prolyl isomerase Pin1 interacts with a ribosomal protein S6 kinase to enhance insulin-induced AP-1 activity and cellular transformation. *Carcinogenesis*, *30*(4), 671-681. https://doi.org/10.1093/carcin/bgp027

Li, T., Hu, P.-S., Zuo, Z., Lin, J.-F., Li, X., Wu, Q.-N., Chen, Z.-H., Zeng, Z.-L., Wang, F., Zheng, J., Chen, D., Li, B., Kang, T.-B., Xie, D., Lin, D., Ju, H.-Q., & Xu, R.-H. (2019). METTL3 facilitates tumor progression via an m6A-IGF2BP2-dependent mechanism in colorectal carcinoma. *Molecular Cancer*, *18*(1), 112. https://doi.org/10.1186/s12943-019-1038-7

Lim, S. Y., Menzies, A. M., & Rizos, H. (2017). Mechanisms and strategies to overcome resistance to molecularly targeted therapy for melanoma. *Cancer*, *123*(S11), 2118-2129. https://doi.org/10.1002/cncr.30435

Lin, S., Choe, J., Du, P., Triboulet, R., & Gregory, R. I. (2016). The m(6)A Methyltransferase METTL3 Promotes Translation in Human Cancer Cells. *Molecular cell*, *62*(3), 335-345. https://doi.org/10.1016/j.molcel.2016.03.021

Lin, X., Chai, G., Wu, Y., Li, J., Chen, F., Liu, J., Luo, G., Tauler, J., Du, J., Lin, S., He, C., & Wang, H. (2019). RNA m6A methylation regulates the epithelial mesenchymal transition of cancer cells and translation of Snail. *Nature Communications*, *10*(1), 2065. https://doi.org/10.1038/s41467-019-09865-9

Lin, Z., Niu, Y., Wan, A., Chen, D., Liang, H., Chen, X., Sun, L., Zhan, S., Chen, L., Cheng, C., Zhang, X., Bu, X., He, W., & Wan, G. (2020). RNA m^6A methylation regulates sorafenib resistance in liver cancer through FOXO3-mediated autophagy. *The EMBO journal*, *39*(12), e103181-e103181. https://doi.org/10.15252/embj.2019103181

Lito, P., Rosen, N., & Solit, D. B. (2013). Tumor adaptation and resistance to RAF inhibitors. *Nat Med*, *19*(11), 1401-1409. https://doi.org/10.1038/nm.3392

Liu, J., Yue, Y., Han, D., Wang, X., Fu, Y., Zhang, L., Jia, G., Yu, M., Lu, Z., Deng, X., Dai, Q., Chen, W., & He, C. (2014). A METTL3–METTL14 complex mediates mammalian nuclear RNA N6-adenosine methylation. *Nature Chemical Biology*, *10*(2), 93-95. https://doi.org/10.1038/nchembio.1432

Liu, N., Dai, Q., Zheng, G., He, C., Parisien, M., & Pan, T. (2015). N6-methyladenosine-dependent RNA structural switches regulate RNA–protein interactions. *Nature*, *518*(7540), 560-564. https://doi.org/10.1038/nature14234

Liu, S., Li, Q., Li, G., Zhang, Q., Zhuo, L., Han, X., Zhang, M., Chen, X., Pan, T., Yan, L., Jin, T., Wang, J., Lv, Q., Sui, X., & Xie, T. (2020). The mechanism of m6A methyltransferase METTL3-mediated autophagy in reversing gefitinib resistance in NSCLC cells by β-elemene. *Cell Death & Disease*, *11*(11), 969. https://doi.org/10.1038/s41419-020-03148-8

Liu, X., Gonzalez, G., Dai, X., Miao, W., Yuan, J., Huang, M., Bade, D., Li, L., Sun, Y., & Wang, Y. (2020). Adenylate Kinase 4 Modulates the Resistance of Breast Cancer Cells to Tamoxifen

through an m6A-Based Epitranscriptomic Mechanism. *Molecular Therapy*, *28*(12), 2593-2604. https://doi.org/10.1016/j.ymthe.2020.09.007

Lu, K. P., Finn, G., Lee, T. H., & Nicholson, L. K. (2007). Prolyl cis-trans isomerization as a molecular timer. *Nature Chemical Biology*, *3*(10), 619-629. https://doi.org/10.1038/nchembio.2007.35

Lugowska, I., Koseła-Paterczyk, H., Kozak, K., & Rutkowski, P. (2015). Trametinib: a MEK inhibitor for management of metastatic melanoma. *OncoTargets and therapy*, *8*, 2251-2259. https://doi.org/10.2147/OTT.S72951

Masuda, H., Zhang, D., Bartholomeusz, C., Doihara, H., Hortobagyi, G. N., & Ueno, N. T. (2012). Role of epidermal growth factor receptor in breast cancer. *Breast Cancer Res Treat*, *136*(2), 331-345. https://doi.org/10.1007/s10549-012-2289-9

Mauer, J., Luo, X., Blanjoie, A., Jiao, X., Grozhik, A. V., Patil, D. P., Linder, B., Pickering, B. F., Vasseur, J. J., Chen, Q., Gross, S. S., Elemento, O., Debart, F., Kiledjian, M., & Jaffrey, S. R. (2017). Reversible methylation of m(6)A(m) in the 5' cap controls mRNA stability. *Nature*, *541*(7637), 371-375. https://doi.org/10.1038/nature21022

McCubrey, J. A., Steelman, L. S., Abrams, S. L., Lee, J. T., Chang, F., Bertrand, F. E., Navolanic, P. M., Terrian, D. M., Franklin, R. A., D'Assoro, A. B., Salisbury, J. L., Mazzarino, M. C., Stivala, F., & Libra, M. (2006). Roles of the RAF/MEK/ERK and PI3K/PTEN/AKT pathways in malignant transformation and drug resistance. *Adv Enzyme Regul*, *46*(1), 249-279. https://doi.org/10.1016/j.advenzreg.2006.01.004

Meyer, K. D., Patil, D. P., Zhou, J., Zinoviev, A., Skabkin, M. A., Elemento, O., Pestova, T. V., Qian, S.-B., & Jaffrey, S. R. (2015). 5' UTR m(6)A Promotes Cap-Independent Translation. *Cell*, *163*(4), 999-1010. https://doi.org/10.1016/j.cell.2015.10.012

Meyer, Kate D., Patil, Deepak P., Zhou, J., Zinoviev, A., Skabkin, Maxim A., Elemento, O., Pestova, Tatyana V., Qian, S.-B., & Jaffrey, Samie R. (2015). 5′ UTR m6A Promotes Cap-Independent Translation. *Cell*, *163*(4), 999-1010. https://doi.org/https://doi.org/10.1016/j.cell.2015.10.012

Moriceau, G., Hugo, W., Hong, A., Shi, H., Kong, X., Yu, Clarissa C., Koya, Richard C., Samatar, Ahmed A., Khanlou, N., Braun, J., Ruchalski, K., Seifert, H., Larkin, J., Dahlman, Kimberly B., Johnson, Douglas B., Algazi, A., Sosman, Jeffrey A., Ribas, A., & Lo, Roger S. (2015). Tunable-Combinatorial Mechanisms of Acquired Resistance Limit the Efficacy of BRAF/MEK Cotargeting but Result in Melanoma Drug Addiction. *Cancer Cell*, *27*(2), 240-256. https://doi.org/https://doi.org/10.1016/j.ccell.2014.11.018

Nechama, M., Lin, C.-L., & Richter, J. D. (2013). An Unusual Two-Step Control of CPEB Destruction by Pin1. *Molecular and Cellular Biology*, *33*(1), 48-58. https://doi.org/doi:10.1128/MCB.00904-12

Nechama, M., Uchida, T., Mor Yosef-Levi, I., Silver, J., & Naveh-Many, T. (2009). The peptidyl-prolyl isomerase Pin1 determines parathyroid hormone mRNA levels and stability in rat models of secondary hyperparathyroidism. *The Journal of clinical investigation*, *119*(10), 3102-3114. https://doi.org/10.1172/JCI39522

Nishi, H., Shaytan, A., & Panchenko, A. R. (2014). Physicochemical mechanisms of protein regulation by phosphorylation [Review]. *Frontiers in Genetics*, *5*. https://doi.org/10.3389/fgene.2014.00270

Nyce, J., Leonard, S., Canupp, D., Schulz, S., & Wong, S. (1993). Epigenetic mechanisms of drug resistance: drug-induced DNA hypermethylation and drug resistance. *Proceedings of the National Academy of Sciences of the United States of America*, *90*(7), 2960-2964. https://doi.org/10.1073/pnas.90.7.2960

Pan, Q., Shai, O., Lee, L. J., Frey, B. J., & Blencowe, B. J. (2008). Deep surveying of alternative splicing complexity in the human transcriptome by high-throughput sequencing. *Nat Genet*, *40*(12), 1413-1415. https://doi.org/10.1038/ng.259

Pan, X., Hong, X., Li, S., Meng, P., & Xiao, F. (2021). METTL3 promotes adriamycin resistance in MCF-7 breast cancer cells by accelerating pri-microRNA-221-3p maturation in a m6A-dependent manner. *Experimental & Molecular Medicine*, *53*(1), 91-102. https://doi.org/10.1038/s12276-020-00510-w

Park, O. H., Ha, H., Lee, Y., Boo, S. H., Kwon, D. H., Song, H. K., & Kim, Y. K. (2019). Endoribonucleolytic Cleavage of m6A-Containing RNAs by RNase P/MRP Complex. *Molecular cell*, *74*(3), 494-507.e498. https://doi.org/https://doi.org/10.1016/j.molcel.2019.02.034

Ping, X.-L., Sun, B.-F., Wang, L., Xiao, W., Yang, X., Wang, W.-J., Adhikari, S., Shi, Y., Lv, Y., Chen, Y.-S., Zhao, X., Li, A., Yang, Y., Dahal, U., Lou, X.-M., Liu, X., Huang, J., Yuan, W.-P., Zhu, X.-F., . . . Yang, Y.-G. (2014). Mammalian WTAP is a regulatory subunit of the RNA N6-methyladenosine methyltransferase. *Cell Research*, *24*(2), 177-189. https://doi.org/10.1038/cr.2014.3

Prahallad, A., Sun, C., Huang, S., Di Nicolantonio, F., Salazar, R., Zecchin, D., Beijersbergen, R. L., Bardelli, A., & Bernards, R. (2012). Unresponsiveness of colon cancer to BRAF(V600E) inhibition through feedback activation of EGFR. *Nature*, *483*(7387), 100-103. https://doi.org/10.1038/nature10868

Roost, C., Lynch, S. R., Batista, P. J., Qu, K., Chang, H. Y., & Kool, E. T. (2015). Structure and thermodynamics of N6-methyladenosine in RNA: a spring-loaded base modification. *J Am Chem Soc*, *137*(5), 2107-2115. https://doi.org/10.1021/ja513080v

Roundtree, I. A., Evans, M. E., Pan, T., & He, C. (2017). Dynamic RNA Modifications in Gene Expression Regulation. *Cell*, *169*(7), 1187-1200. https://doi.org/10.1016/j.cell.2017.05.045

Rustighi, A., Zannini, A., Campaner, E., Ciani, Y., Piazza, S., & Del Sal, G. (2017). PIN1 in breast development and cancer: a clinical perspective. *Cell Death & Differentiation*, *24*(2), 200-211. https://doi.org/10.1038/cdd.2016.122

Shen, H., Yang, N., Truskinovsky, A., Chen, Y., Mussell, A. L., Nowak, N. J., Kobzik, L., Frangou, C., & Zhang, J. (2019). Targeting TAZ-Driven Human Breast Cancer by Inhibiting a SKP2-p27 Signaling Axis. *Molecular Cancer Research*, *17*(1), 250-262. https://doi.org/10.1158/1541-7786.Mcr-18-0332

Shen, Z. J., & Malter, J. S. (2015). Regulation of AU-Rich Element RNA Binding Proteins by Phosphorylation and the Prolyl Isomerase Pin1. *Biomolecules*, *5*(2), 412-434. https://doi.org/10.3390/biom5020412

Sullivan, R. J., & Flaherty, K. T. (2011). BRAF in Melanoma: Pathogenesis, Diagnosis, Inhibition, and Resistance. *Journal of skin cancer*, *2011*, 423239-423239. https://doi.org/10.1155/2011/423239

Sun, C., Wang, L., Huang, S., Heynen, G. J., Prahallad, A., Robert, C., Haanen, J., Blank, C., Wesseling, J., Willems, S. M., Zecchin, D., Hobor, S., Bajpe, P. K., Lieftink, C., Mateus, C., Vagner, S., Grernrum, W., Hofland, I., Schlicker, A., . . . Bernards, R. (2014). Reversible and adaptive resistance to BRAF(V600E) inhibition in melanoma. *Nature*, *508*(7494), 118-122. https://doi.org/10.1038/nature13121

Sun, H. L., Zhu, A. C., Gao, Y., Terajima, H., Fei, Q., Liu, S., Zhang, L., Zhang, Z., Harada, B. T., He, Y. Y., Bissonnette, M. B., Hung, M. C., & He, C. (2020). Stabilization of ERK-Phosphorylated METTL3 by USP5 Increases m(6)A Methylation. *Molecular cell*, *80*(4), 633-647.e637. https://doi.org/10.1016/j.molcel.2020.10.026

Taketo, K., Konno, M., Asai, A., Koseki, J., Toratani, M., Satoh, T., Doki, Y., Mori, M., Ishii, H., & Ogawa, K. (2018). The epitranscriptome m6A writer METTL3 promotes chemo- and radioresistance in pancreatic cancer cells. *Int J Oncol*, *52*(2), 621-629. https://doi.org/10.3892/ijo.2017.4219

Thapar, R. (2015). Roles of Prolyl Isomerases in RNA-Mediated Gene Expression. *Biomolecules*, *5*(2), 974-999. https://doi.org/10.3390/biom5020974

Vasan, N., Baselga, J., & Hyman, D. M. (2019). A view on drug resistance in cancer. *Nature*, *575*(7782), 299-309. https://doi.org/10.1038/s41586-019-1730-1

Villanueva, J., Vultur, A., & Herlyn, M. (2011). Resistance to BRAF Inhibitors: Unraveling Mechanisms and Future Treatment Options. *Cancer Research*, *71*(23), 7137-7140. https://doi.org/10.1158/0008-5472.Can-11-1243

Visvanathan, A., Patil, V., Arora, A., Hegde, A. S., Arivazhagan, A., Santosh, V., & Somasundaram, K. (2018). Essential role of METTL3-mediated m(6)A modification in glioma stem-like cells maintenance and radioresistance. *Oncogene*, *37*(4), 522-533. https://doi.org/10.1038/onc.2017.351

Vu, L. P., Pickering, B. F., Cheng, Y., Zaccara, S., Nguyen, D., Minuesa, G., Chou, T., Chow, A., Saletore, Y., MacKay, M., Schulman, J., Famulare, C., Patel, M., Klimek, V. M., Garrett-Bakelman, F. E., Melnick, A., Carroll, M., Mason, C. E., Jaffrey, S. R., & Kharas, M. G. (2017). The N(6)-methyladenosine (m(6)A)-forming enzyme METTL3 controls myeloid differentiation of normal hematopoietic and leukemia cells. *Nature medicine*, *23*(11), 1369-1376. https://doi.org/10.1038/nm.4416

Wan, W., Ao, X., Chen, Q., Yu, Y., Ao, L., Xing, W., Guo, W., Wu, X., Pu, C., Hu, X., Li, Z., Yao, M., Luo, D., & Xu, X. (2022). METTL3/IGF2BP3 axis inhibits tumor immune surveillance by upregulating N6-methyladenosine modification of PD-L1 mRNA in breast cancer. *Molecular Cancer*, *21*(1), 60. https://doi.org/10.1186/s12943-021-01447-y

Wang, H., Xu, B., & Shi, J. (2020). N6-methyladenosine METTL3 promotes the breast cancer progression via targeting Bcl-2. *Gene*, *722*, 144076. https://doi.org/10.1016/j.gene.2019.144076

Wang, P., Doxtader, K. A., & Nam, Y. (2016). Structural Basis for Cooperative Function of Mettl3 and Mettl14 Methyltransferases. *Molecular cell*, *63*(2), 306-317. https://doi.org/10.1016/j.molcel.2016.05.041

Wang, S., Lv, W., Li, T., Zhang, S., Wang, H., Li, X., Wang, L., Ma, D., Zang, Y., Shen, J., Xu, Y., & Wei, W. (2022). Dynamic regulation and functions of mRNA m6A modification. *Cancer Cell International*, *22*(1), 48. https://doi.org/10.1186/s12935-022-02452-x

Wang, X., Feng, J., Xue, Y., Guan, Z., Zhang, D., Liu, Z., Gong, Z., Wang, Q., Huang, J., Tang, C., Zou, T., & Yin, P. (2016). Structural basis of N6-adenosine methylation by the METTL3–METTL14 complex. *Nature*, *534*(7608), 575-578. https://doi.org/10.1038/nature18298

Wang, X., Lu, Z., Gomez, A., Hon, G. C., Yue, Y., Han, D., Fu, Y., Parisien, M., Dai, Q., Jia, G., Ren, B., Pan, T., & He, C. (2014). N6-methyladenosine-dependent regulation of messenger RNA stability. *Nature*, *505*(7481), 117-120. https://doi.org/10.1038/nature12730

Wang, X., Zhao, B. S., Roundtree, I. A., Lu, Z., Han, D., Ma, H., Weng, X., Chen, K., Shi, H., & He, C. (2015). N(6)-methyladenosine Modulates Messenger RNA Translation Efficiency. *Cell*, *161*(6), 1388-1399. https://doi.org/10.1016/j.cell.2015.05.014

Wei, J., Yin, Y., Zhou, J., Chen, H., Peng, J., Yang, J., & Tang, Y. (2020). METTL3 potentiates resistance to cisplatin through m(6) A modification of TFAP2C in seminoma. *Journal of cellular and molecular medicine*, *24*(19), 11366-11380. https://doi.org/10.1111/jcmm.15738

Wei, S., Kozono, S., Kats, L., Nechama, M., Li, W., Guarnerio, J., Luo, M., You, M. H., Yao, Y., Kondo, A., Hu, H., Bozkurt, G., Moerke, N. J., Cao, S., Reschke, M., Chen, C. H., Rego, E. M., Lo-Coco, F., Cantley, L. C., . . . Lu, K. P. (2015). Active Pin1 is a key target of all-trans retinoic acid in acute promyelocytic leukemia and breast cancer. *Nat Med*, *21*(5), 457-466. https://doi.org/10.1038/nm.3839

Westmark, P. R., Westmark, C. J., Wang, S., Levenson, J., O'Riordan, K. J., Burger, C., & Malter, J. S. (2010). Pin1 and PKMzeta sequentially control dendritic protein synthesis. *Sci Signal*, *3*(112), ra18. https://doi.org/10.1126/scisignal.2000451

Wiener, D., & Schwartz, S. (2021). The epitranscriptome beyond m6A. *Nature Reviews Genetics*, *22*(2), 119-131. https://doi.org/10.1038/s41576-020-00295-8

Wu, L., Wu, D., Ning, J., Liu, W., & Zhang, D. (2019). Changes of N6-methyladenosine modulators promote breast cancer progression. *BMC Cancer*, *19*(1), 326. https://doi.org/10.1186/s12885-019-5538-z

Xiang, M., Liu, W., Tian, W., You, A., & Deng, D. (2020). RNA N-6-methyladenosine enzymes and resistance of cancer cells to chemotherapy and radiotherapy. *Epigenomics*, *12*(9), 801-809. https://doi.org/10.2217/epi-2019-0358

Xiao, W., Adhikari, S., Dahal, U., Chen, Y.-S., Hao, Y.-J., Sun, B.-F., Sun, H.-Y., Li, A., Ping, X.-L., Lai, W.-Y., Wang, X., Ma, H.-L., Huang, C.-M., Yang, Y., Huang, N., Jiang, G.-B., Wang, H.-L., Zhou, Q., Wang, X.-J., . . . Yang, Y.-G. (2016). Nuclear m6A Reader YTHDC1 Regulates mRNA Splicing. *Molecular cell*, *61*(4), 507-519. https://doi.org/https://doi.org/10.1016/j.molcel.2016.01.012

Xu, J., Chen, Q., Tian, K., Liang, R., Chen, T., Gong, A., Mathy, N. W., Yu, T., & Chen, X. (2020). m6A methyltransferase METTL3 maintains colon cancer tumorigenicity by suppressing SOCS2 to promote cell proliferation. *Oncol Rep*, *44*(3), 973-986. https://doi.org/10.3892/or.2020.7665

Yang, S., Wei, J., Cui, Y.-H., Park, G., Shah, P., Deng, Y., Aplin, A. E., Lu, Z., Hwang, S., He, C., & He, Y.-Y. (2019). m6A mRNA demethylase FTO regulates melanoma tumorigenicity and

response to anti-PD-1 blockade. *Nature Communications*, *10*(1), 2782. https://doi.org/10.1038/s41467-019-10669-0

Yankova, E., Blackaby, W., Albertella, M., Rak, J., De Braekeleer, E., Tsagkogeorga, G., Pilka, E. S., Aspris, D., Leggate, D., Hendrick, A. G., Webster, N. A., Andrews, B., Fosbeary, R., Guest, P., Irigoyen, N., Eleftheriou, M., Gozdecka, M., Dias, J. M. L., Bannister, A. J., . . . Kouzarides, T. (2021). Small-molecule inhibition of METTL3 as a strategy against myeloid leukaemia. *Nature*, *593*(7860), 597-601. https://doi.org/10.1038/s41586-021-03536-w

Zaccara, S., Ries, R. J., & Jaffrey, S. R. (2019). Reading, writing and erasing mRNA methylation. *Nature Reviews Molecular Cell Biology*, *20*(10), 608-624. https://doi.org/10.1038/s41580-019-0168-5

Zeng, C., Huang, W., Li, Y., & Weng, H. (2020). Roles of METTL3 in cancer: mechanisms and therapeutic targeting. *Journal of Hematology & Oncology*, *13*(1), 117. https://doi.org/10.1186/s13045-020-00951-w

Zhao, Y., Ge, C. C., Wang, J., Wu, X. X., Li, X. M., Li, W., Wang, S. S., Liu, T., Hou, J. Z., Sun, H., Fang, D., & Xie, S. Q. (2017). MEK inhibitor, PD98059, promotes breast cancer cell migration by inducing β-catenin nuclear accumulation. *Oncol Rep*, *38*(5), 3055-3063. https://doi.org/10.3892/or.2017.5955

Zheng, W., Dong, X., Zhao, Y., Wang, S., Jiang, H., Zhang, M., Zheng, X., & Gu, M. (2019). Multiple Functions and Mechanisms Underlying the Role of METTL3 in Human Cancers [Review]. *Frontiers in Oncology*, *9*(1403). https://doi.org/10.3389/fonc.2019.01403

Zhou, K. I., Shi, H., Lyu, R., Wylder, A. C., Matuszek, Ż., Pan, J. N., He, C., Parisien, M., & Pan, T. (2019). Regulation of Co-transcriptional Pre-mRNA Splicing by m(6)A through the Low-Complexity Protein hnRNPG. *Molecular cell*, *76*(1), 70-81.e79. https://doi.org/10.1016/j.molcel.2019.07.005

ABSTRACT

Studies on the role of N6-adenosine methyltransferase METTL3 as a critical regulator of tumorigenesis and targeted drug resistance

By Poshan Yugal Bhattarai

Advisor: Prof. Choi Hong Seok, Ph.D.

Department of Pharmacy,

Graduate School of Chosun University

Methyltransferase-like 3 (METTL3) is the catalytic subunit of the N^6-adenosine methyltransferase complex responsible for the N^6-methyladenosine (m^6A) modification of mRNA in mammalian cells. The expression of METTL3 is increased in several cancers; however, the underlying mechanisms that regulate METTL3 expression are unclear. We explored the regulatory roles of peptidyl-prolyl *cis-trans* isomerase NIMA-interacting 1 (PIN1) in METTL3 stability and the m^6A modification of mRNA. PIN1 interacted with METTL3 and prevented its ubiquitin-dependent proteasomal and lysosomal degradation. PIN1-stabilized METTL3 increased the m^6A modification of *TAZ* and epidermal growth factor receptor (*EGFR)* mRNA, resulting in efficient translation. Knocking out PIN1 reduced polysome assembly and TAZ and EGFR mRNA in polysome fractions. Furthermore, inhibiting the MEK1/2 kinases and PIN1 reduced the m^6A-dependent translation of *TAZ* and *EGFR* via the destabilization of METTL3, thereby inhibiting breast cancer cell proliferation and the induction of cell cycle arrest at the G0/G1 phases. The METTL3 knockout further reduced the colony formation induced by

overexpressing PIN1 in MCF7 cells. In an orthotopic mouse model, the enhanced growth of tumors formed in PIN1-overexpressing 4T1 cells was suppressed by the knockout of METTL3, supporting the positive role of PIN1 in METTL3-induced tumorigenesis. In the clinical context, PIN1 and METTL3 expression were significantly increased in breast tumors compared to normal tissues. METTL3 expression increased with tumor progression and was positively correlated with PIN1 expression in breast cancer tissues. Taken together, our data highlight the regulatory role of PIN1 in mRNA translation and suggest that the PIN1/METTL3 axis may be an alternative therapeutic target for breast cancer.

In a different clinical setting, acquired resistance often limits the therapeutic efficacy of the BFAF (V600E) kinase inhibitor PLX4032 in patients with advanced melanoma. Epitranscriptomic modification of mRNAs by N^6-methyl adenosine (m^6A) modification contributes to melanoma pathogenesis; however, its role in acquired PLX4032 resistance remains unexplored. Here, we showed that m^6A methyltransferase METTL3 expression is upregulated in A375R cells, a PLX4032-resistant subline of A375 melanoma cells, compared with the parental cells. Moreover, METTL3 increased the m^6A modification of epidermal growth factor receptor (EGFR) mRNA in A375R cells, which promoted its translation efficiency. In turn, increased EGFR expression facilitated rebound activation of the RAF/MEK/ERK pathway in A375R cells, inducing PLX4032 resistance. In contrast, the knockout of METTL3 in A375R cells reduced EGFR expression and restored PLX4032 sensitivity. PLX4032 treatment following METTL3 knockout induced apoptosis and reduced colony formation in A375R cells and reduced A375R cell-derived tumor growth in BALB/c nude mice. These findings indicate that METTL3 promotes rebound activation of the RAF/MEK/ERK pathway through EGFR upregulation and highlight a critical role for METTL3-induced m^6A modification in acquired PLX4032 resistance in melanoma.

ACKNOWLEDGEMENT

First of all, I would like to express sincere gratitude to my advisor Prof. Hong Seok Choi for his continuous support, inspiration, and encouragement. I had joined the pharmaceutical biochemistry lab as an amateur scientist, but professor provided an atmosphere in which I could transform myself into a skilled researcher.

I'm also thankful to my mentor Dr. Garam Kim. She always helped me to solve the problems in research, and move forward. More than just a mentor, she was a friend and family in South Korea. Similarly, I'm very much thankful to my colleague and spouse Muna Poudel for her support in research as well as in life. I'd also like to acknowledge the support of our lab members: Pratikshya Shrestha and Hyelim kang.

Finally, I'm thankful to my parents, brother, and in-laws for their constant support and encouragement.